

The Effects of Particulate Matter on Global Crop Yields

This thesis is submitted for the degree of Doctor of Philosophy

MICHAEL CHARLES WOLFFE, BSC, MRES, PGCE

Lancaster Environment Centre
LANCASTER UNIVERSITY

Abstract

Particulate Matter (PM) is understood to harm human health, but little research has assessed its impact on crop yields. Emerging evidence suggests PM may have a sizeable effect on crops. PM reduces yields through indirect and direct mechanisms. In the indirect mechanism, airborne PM intercepts incoming photosynthetically active radiation (PAR) through absorption or scattering. In the direct mechanism, PM deposition on crop surfaces directly blocks PAR transmission.

Using the JULES-crop model, this thesis finds PM reduces maize yield by 3.5% on the North China Plains (NCP) via the indirect mechanism. PM deposition is responsible for a further 2.4% maize yield loss in the same area, with rice and wheat crops less affected at 2.0% and 0.3% average yield losses, respectively. India is also particularly affected by PM deposition, with average maize, rice, and wheat losses of 1.2, 0.7, and 0.3%. Specific locations suffer losses as high as 8%, attributable to a combination of meteorological factors, the black carbon content of bulk PM, and crop-specific factors. Despite these high local impacts, average global cereal crop yield losses to PM deposition circa 1%.

The timing of PM perturbations within the crop development cycle also affects yield outcomes. The combined effects of the direct and indirect mechanisms are additive, and most negatively affect crop yields during the early reproductive stage for maize and wheat, and the early vegetative stage for rice. Uncontrolled future PM emissions are found to have particularly substantial effects on crop yields in India, with expected losses of up to 20% on the Indo-Gangetic Plain. The thesis also explores the effects of PM timing in relation to crop development stage, and how this may predict future crop yield losses attributable to PM pollution.

Overall, this work highlights the role of airborne PM in limiting PAR availability for photosynthesis, particularly in highly polluted areas of China and India. The effects of PM deposition on cereal crop yields are quantified here for the first time, and are noted as potentially limiting future food supply in India. Identifying the potential impacts of PM highlights the urgency of PM emission reductions for policy makers. The thesis contributes to our understanding of the impacts of PM pollution on food supply, and highlights the need for further experimental studies to better comprehend the scale of threat that this pollution may pose in the future.

Table of Contents

Abstract	1
Table of Contents	2
List of Figures and Tables	5
Acknowledgements	9
Author's Declaration	10
Chapter 1: Introduction	11
1.1 Global Food Security	11
1.2 Particulate Matter Composition.....	12
1.3 Mechanisms for PM Impacts on Crops	18
1.3.1 Indirect Mechanism	18
1.3.2 Direct Mechanism.....	22
1.4 Examples of PM sources and distribution in China and India.....	29
1.4.1 China.....	30
1.4.2 India	34
1.5 Crop modelling	36
1.6 Aims of this thesis	39
Chapter 2: Temporal variability in the impacts of particulate matter on crop yields on the North China Plain.....	42
Contribution statement:	42
Graphical Abstract:.....	42
Abstract 44	
2.1 Introduction.....	45
2.2 Materials and Methods	49
2.2.1 Model Set-up.....	49
2.2.2 BASE simulation.....	50
2.2.3 Driving Factors for Changes in SW and Diffuse Radiation.....	53
2.2.4 Sensitivity at Different Development Stages	53

2.2.5 Impact of City Radiation Profiles on Yields	54
2.3 Results	55
2.3.1 Aerosol Optical Depth (AOD) Results	55
2.3.2 The BASE Simulation	56
2.3.3 Sensitivity at Different Development Stages	62
2.3.4 Impact of City Radiation Profiles on Yields	62
2.4 Discussion	66
2.4.1 PM Influences Maize Yields.....	66
2.4.2 Radiation from Comparable Cities Alters Maize Yields	68
2.4.3 How PM might Change Radiation in the Future	69
2.4.4 Comparison to Previous Studies.....	70
2.4.5 Uncertainties and the Future of Maize Yields on the NCP	71
Chapter 3: Quantifying the Impacts of Particulate Matter Deposition on Global Cereal Yields	74
Contribution statement:	74
Abstract	75
3.1 Introduction.....	76
3.2 Materials and Methods	78
3.2.1 Model Parameterisation.....	78
3.2.2 Model Description.....	79
3.2.3 Simulations	85
3.3.3 Results	87
3.3.3.1 Indian Agricultural Research Institute (IARI) point simulations	87
3.3.3.2 Global Simulations.....	88
3.4 Discussion	99
3.4.1 Which world regions are most affected by PM deposition?	99
3.4.2 Factors governing the magnitude of PM deposition crop losses	99
3.4.3 Why are different crops so differently affected?	101
3.4.5 How substantial might the losses be in the future?	102
3.4.6 Limitations and future work.....	103

3.5 Conclusion.....	105
Acknowledgements	106
Chapter 4: The Impact of PM on Cereal Yields Depends on Crop Development Stage	107
Contribution statement:	107
Abstract	108
4.1 Introduction.....	109
4.2 Materials & Methods.....	112
4.2.1 Model Parameterisation.....	112
4.2.2 Development Stage Perturbed simulations	114
4.2.3 Radiation and Deposition Perturbations.....	115
4.3 Results	117
4.3.1 Direct Effect of PM	118
4.3.3 Total Effect of PM.....	122
4.4 Discussion.....	125
4.4.4 Limitations and further work.....	128
Chapter 5: Conclusions	130
5.1 The diffuse light fertilisation effect.....	130
5.2 PM deposition effects on crop yield	131
5.3 How the timing of PM perturbations within a crop development cycle affects yields	132
5.4 Future work	133
References	139

List of Figures and Tables

Table 1.1 Description of primary PM components considered in this thesis, including sources, residence time within the atmosphere, physical and optical properties, and resulting effects on surface radiation.....	13
Figure 1.1 Illustration of PAR interception by PM, where a) no PM intercepts incoming PAR, and b) where PAR is backscattered by PM, absorbed by airborne PM, or transmitted through the PM cloud as diffuse radiation which is intercepted at lower canopy layers. Different coloured circles represent different sizes and species of PM.	21
Figure 1.2. Illustration of the removal of PM from a leaf surface. a) A leaf with few adaxial microstructural features does not retain PM when wind blows across its surface as the adhesion forces are weak. b) A leaf of the same area with more adaxial microstructural features retains more PM under the same wind. This is due to greater adhesive forces between deposited PM and the leaf surface.....	25
Figure 1.3 a) Incoming PAR is reflected or absorbed by PM on the adaxis, thus reducing the amount of PAR available for photosynthesis by the affected plant. b) i) Under normal circumstances, the plant leaf undergoes gas exchange, with water vapour evaporating from stomata and carbon dioxide taken into the leaf interior for photosynthesis. However, ii) if the stomata are blocked this cannot occur, reducing photosynthesis rates and trapping heat within the leaf interior.....	27
Figure 1.4. Illustrations of (a) the Chinese and (b) Indian model domains used throughout this thesis, with cropped area highlighted in green, and average pm flux to the surface for crop growing seasons between 2015-2020 ($\text{mg m}^{-2} \text{h}^{-1}$) shown as orange contours.	30
Graphical Abstract	43
Figure 2.1. i) Maize yield versus BASE average hourly SW in grid cells with saturated soil, ii) BASE average hourly diffuse fraction vs yield in saturated soil grid cells iii) BASE SW vs diffuse fraction for all grid-cells.....	52
Table 2.1. Summary of key model results from simulations. Average yield is colour coded such that the average yield for BASE is the midpoint, with 0% change as the mid-point, red for decreasing yield, and blue for increasing. The percentage difference from base is colour .coded 0% difference from BASE as white and the largest difference as the most purple.	58

Figure 2.2. i) Cropped region of the NCP in model, ii) BASE model yield output ($t\ ha^{-1}$), iii) Average Growing Season Day time Hourly SW ($W\ m^{-3}$), iv) Average Growing Season Day Time Hourly Diffuse Fraction.....61

Table 2.2. Indicative values for average SW, diffuse fraction and PM2.5 concentration for NCP study region and for city regions studied. Average hourly SW and diffuse fraction are taken from the climatology (generated from 1979 to 2017 ERA-5 meteorological data) used to drive all city runs for the growing season of modelled maize crop. AOD is an average value, taken from the C3S climate data store meteorological dataset for aerosol optical depth, for the city containing grid cell, for the months April to September (inclusive of growing season), from 1997 to 2010. PM2.5 data is taken from a range of ground-based studies conducted during the timeframe of this modelling study. Though the PM concentrations are not always overlapping in time in many cases, this serves as an indicator of representative values within the period of the climatology.....63

Figure 2.3. (a) Yields ($t\ ha^{-1}$) for city radiation profile simulations (i) BJG_Diff and (ii) BJG_SW_Diff. (b-e) percentage difference between (i) <CITY>_Diff and BJG_Diff, and (ii) <CITY>_SW_Diff and BJG_SW_Diff, for (b) New York, (c) Madrid, (d) Delhi and (e) Cairo..64

Figure 2.4. (a) (i-v) Relationships between SW and Diffuse fraction for each city, with data points in blue and quadratic regression line in orange. (b) Yields for CITY_MOD radiation profile simulation. BJG_Mod_SW and (ii) BJG_Mod_Diff. (c-f) percentage difference between (i) <CITY>_Mod_Diff and BJG-Mod_Diff and (ii) <CITY>_Mod_SW and BJG_Mod_SW, for (c) New York, (d) Madrid, (e) Delhi and (f) Cairo.....66

Figure 2.5. (i) Average monthly diffuse fraction for Beijing, Madrid, New York, Delhi, and Cairo. (ii) Average hourly downward SW radiation per month for Beijing, Madrid, New York, Delhi, and Cairo.....68

Figure 3.1. Illustration of PM being deposited across canopy layers. (a) bulk PM (FT) reaches the upper canopy level (level 0). (b) PM passes through gaps in the previous canopy layer (i-1), and accumulates to the subsequent canopy layer (I). (c) shows this process repeating for further canopy layers until all PM is deposited or all layers are exhausted whereupon remaining PM is presumed to have passed through the entire canopy.....81

Figure 3.2 Illustration of PM deposition workflow within JULES simulations.....83

Figure 3.3. Simulated global yields (t ha⁻¹) for wheat (A,i), maize (A,ii) and rice (A,iii) using average of driving data from 2015-20, and average percentage yield reductions under MERRA-2 PM flux with standard wash off (B,i-iii).....89

Figure 3.4 . Yield reductions for rice over time vs precipitation for rice at a site in China in 2015 under standard wash off, showing percentage yield reduction over time alongside rainfall, when this triggers wash off, and the PM flux over time.....90

Figure 3.5. Average simulated yields (t ha⁻¹) for (a) wheat, (b) maize and (c) rice for 2015-20 in (A) China and (B) India. The first column shows baseline yields in the absence of PM deposition while the remaining columns show average yield reductions from this baseline for MERRA-2 PM flux and (ii) no wash off, (iii) standard wash off and (iv) enhanced wash off .91

Figure 3.6. Distribution of yield reductions for (i) rice, (ii) maize and (iii) wheat on the (A) NCP and (B) IGP with PM deposition rates calculated from MERRA-2 PM concentrations for each of the “no” (blue), “standard” (orange) and “enhanced” (green) wash off regimes described in 2.1.2. Note that the mean value does not reflect the wide variance across each region in terms of yield loss, and that the violin plots have extensive tails highlighting the influence of more extreme local factors.....93

Figure 3.7. The average (i) PM and (ii) BC-only deposition fluxes over (A) China and (B) India for the 2015-2020 growing seasons.....95

Figure 3.8. Average simulated yields (t ha⁻¹) for 2015-20 in (A,i) China and (B,i) India alongside (ii) average yield reductions from this baseline using MERRA-2 BC-only flux and (iii) the percentage of total PM-induced yield reductions due to BC.....96

Figure 3.9 Average simulated yields (t ha⁻¹) for 2015-20 in (A,i) China and (B,i) India alongside percentage yield reductions from this baseline for alternative PM scenarios using (A) Bergin et al (2001) PM flux and (B) Mina et al (2018) PM flux, with (ii) fixed Bergin et al (2001) BC fraction and (iii) spatially varying BC fraction set from 2015-20 average (reductions for locations with successfully completed growing cycles).....97

Figure 3.10. Total PM deposited to each crop during their growing season in China (A,i) and India (B,i), alongside the percentage of that PM which is deposited during the reproductive phase (ii). The figure in each panel shows the domain average PM deposition over the growing season.....98

Figure 4.1. The model domain with a number of major cities labelled to aid interpretation of results - image created using seaborn and matplotlib.....113

Figure 4.2. Distribution of sowing and harvest dates for wheat, maize, and rice across the simulated area.....114

Figure 4.3. Example of the different development stage durations and timings within the year for each crop in a single grid cell at 26.0°N, 76.0°E . The monsoon season is marked with two black lines, with monsoon typically falling between this period.115

Table 4.1. Summary of the different variables used in each simulation117

Figure 4.4. The baseline yields for wheat (a,i) maize (b,i) and rice (c,i) across the study area, annotated with the domain mean yield. Below these are the percentage yield losses with the application of PM deposition during the early vegetative stage (ii), late vegetative stage (iii), early reproductive phase (iv) and late reproductive stage (v), annotated with the mean yield reductions for the domain.....120

Figure 4.5. The baseline yields for wheat (a,i) maize (b,i) and rice (c,i) across the study area, annotated with mean yield for the location. Below these are the percentage yield losses experienced across the model domain with the application of PM associated changes to SW and diffuse fraction during the early vegetative stage (ii), late vegetative stage (iii), early reproductive phase (iv) and late reproductive stage (v), annotated with the mean yield change (absolute change taken for simulations with positive and negative changes)....122

Figure 4.6. The baseline yields for wheat (a,i) maize (b,i) and rice (c,i) across the study area, annotated with mean yield for the location. Below these are the percentage yield changes experienced across the model domain with the application of PM associated changes to SW and diffuse fraction during the early vegetative stage (ii), late vegetative stage (iii), early reproductive phase (iv) and late reproductive stage (v), annotated with the median yield reduction's locations with yield losses over 1%.....124

Table 4.2. Percentage yield loss per hour exposure to PM deposition by development stage at exposure.....125

Acknowledgements

I am extremely grateful for the expertise and enthusiastic support of the many people who have helped me on this journey. In particular, I'd like to thank my supervisors. Dr Kirsti Ashworth has been a constant source of advice and motivation, and opened up a wide array of opportunities for me to develop my wider skills. Professor Oliver Wild has been an amazing source of knowledge and expertise throughout the PhD. Both have introduced me to an excellent network of fellow researchers to aid my research and personal development.

I would also like to thank the Royal Society for their funding of this PhD, and enabling me to pursue this interesting and important research for 4 years. Thanks also to those I have worked with at St Helens Council, who have been so supportive throughout the last year whilst I finalised this thesis, vivaed, and went through the corrections process. It's been a pleasure to work with you to build a better future.

Thank you to the wider JULES community who have provided such support and expertise over the years of learning, implementing, and developing this model.

Especially, I would like to thank my amazing wife, Taylor Wolffe. Since we first began dating 15 years ago, you have always been my greatest supporter. Without your patience, support, and understanding, I would never be where I am today, and I am thankful every day to have you in my life. Special thanks also to my Attie pips. Being your Daddy is a joy. You coming into our lives in the middle of this PhD was a delight, and seeing you learn and grow every day was such an inspiration to complete this work. I can't wait to help hide your treasure from Barracudas some more.

Thank you also to my family - my parents, Denise, and John Clarke, and my brothers, Danny and Stephen Clarke, for their loving support over many years, but particularly during this PhD.

Lastly, thank you to all the small creatures who have been a light in my life over these PhD years. Pecan, Pumpkin, Poppy Seed, and Pig will always hold a special place in my heart, and Chu, Moo and Babu, you have been a source of much joy, sorrow, and joy again in my life. And Spud. You are fine.

Author's Declaration

All work contained within this thesis is my own, and has not been submitted elsewhere for the award of a higher degree. Chapter 2 has previously been published in its entirety in *Science of the Total Environment* in 2021, Volume 776, 1 July 2021, 145135, DOI: [10.1016/j.scitotenv.2021.145135](https://doi.org/10.1016/j.scitotenv.2021.145135). The version contained within the thesis is slightly adapted to better fit within the flow of the thesis text.

In all cases, I worked on the conceptualization of the project; the development of the methodology used; the investigation of the research question; formal analysis of all data; interpretation of data; writing of manuscript for supervisor review; co-ordination of co-author feedback. In the case of Chapter 2 I also am lead author for the published manuscript, and carried out the submission and reviewer requested changes.

Chapter 1: Introduction

1.1 Global Food Security

Ten percent of the world's population are undernourished, with over 149 million children below the age of 5 suffering from acute malnutrition (UNICEF, 2021). Global food supply continues to be threatened by an interlinked series of crises, including climate change, soil degradation, and flooding - putting the lives and livelihoods of millions at serious risk. Over 98% of those suffering under- and malnutrition reside in lower- and middle-income countries. Being largely located at mid and low latitudes, these same countries are set to be the most severely impacted by climate driven extreme weather events (IPCC, 2022). They are also the countries in most pressing need of further economic development and often rely on fossil fuel-driven economic growth to achieve this. These countries are at increasing risk of crop failures due to both rising global temperatures and increasing local air pollutant concentrations (IPCC, 2022).

Developing a better understanding of the global threats to food supply is a prerequisite to countering them. Particulate matter (PM) is a key air pollutant which has recently been identified as hazardous to crops, and therefore a potential threat to food supply. Airborne PM affects the light available for crops to use in photosynthesis, potentially reducing crop yields by 5-10% (Greenwald et al., 2006; Zhou et al., 2018). Deposited PM on crop surfaces may further exacerbate yield reductions, causing a further ~5% loss (Mina et al., 2018). Deposited PM also intensifies climate impacts. By coating upper leaf surfaces, leaves are insulated, and stomata are blocked. This traps heat within the leaf whilst reducing transpiration rates, causing the plant to be more susceptible to the effects of heat stress at lower temperatures (Mina et al., 2013). The limited research in this area indicates serious risks to food security in heat stressed areas with large PM concentrations, such as China and India. However, further research is needed to determine the global threat posed by this group of pollutants.

This thesis shows that PM pollution is a potentially significant contributor to crop yield reductions across many parts of the world. Given the increasing trend in PM concentrations for many developing and middle-income countries such as India, this could come to present a substantial threat to regional food security over the coming decades. This thesis aims to highlight the risks posed by PM in highly polluted croplands, and to provide evidence for consideration in mitigation action.

In this work, the indirect and direct effects of particles on crops are explored. The remainder of Chapter 1 describes PM in detail, outlining how PM of differing composition affects crops, and identifying knowledge gaps concerning the effects of PM pollution on global food production and food security. The published paper that forms Chapter 2 of this thesis explores and clarifies the role of airborne PM in reducing crop yields. Chapter 3 presents the first global simulations of the effects of PM deposition on food security. Identifying India and China as the worst affected countries, detailed regional analyses describe the total current effects of PM deposition on yields in these locations, and highlight the deleterious effects of uncontrolled future PM emissions in India. The work within Chapters 2 and 3 identifies the crop development stage during which a crop is exposed to PM pollution-related stressors as a key determinant of their eventual impact on food production. Chapter 4 explores the impact of predicted 2050 levels of PM pollution, alongside a number of other coincident stressors on food production in India, and assesses the importance of development stage dependence for predicted future food supply. Chapter 5 summarises the findings of this thesis, and outlines further work required to better understand the current, and potential future, impacts of PM and other air pollutants on food supply.

1.2 Particulate Matter Composition

Particulate matter (PM) is the term commonly used in atmospheric and air pollution sciences to refer to a highly heterogeneous mixture of aerosolised particles. This work primarily focuses on the total impacts of all PM, the bulk of which is composed of black carbon (BC), organic carbon (OC), sulphates, secondary organic aerosol (SOA), sea salt, and mineral dust - the PM components typically considered in modelling studies. Nitrates are also an important PM component, but are absent from the majority of simulated and measured global PM.

Atmospheric particles are (unequally) distributed across a wide size range (e.g., Khan et al., 2021), but are broadly categorised as PM₁, PM_{2.5} and PM₁₀; that is PM particles with aerodynamic diameters of 1 μm , 2.5 μm or 10 μm respectively (where aerodynamic diameter describes the diameter of an idealised sphere with the density of water, 1g cm^{-3} , that settles in still air at the same velocity as a given PM particle). Anthropogenically generated components are generally relatively fine (PM_{2.5} and smaller; Klimont et al., 2017); those which have previously been found to be most influential on crop losses are described below in Table 1.1.

Pollutant	Primary sources	Physical and optical properties	Impacts on environment and crops
Black Carbon (BC)	<ul style="list-style-type: none"> • Fossil fuel combustion, forestry, and transportation infrastructure¹. 	<ul style="list-style-type: none"> • Aerosolised BC is typically unreactive. • Consists of graphite like chains of elemental carbon. • Forms large, agglomerated particles with other aerosol species^{2,3}. • Highly thermally stable. • Highly light absorbing at visible wavelengths, including PAR⁴. • BC, including soot, remains airborne for 4-12 days^{5,6}. 	<ul style="list-style-type: none"> • Heats atmosphere by absorbing light and re-emitting as infrared. • Directly reduces available PAR for crop photosynthesis. • BC is responsible for a majority of PM light absorption^{7,8}.

<p>Organic Carbon (OC)</p>	<ul style="list-style-type: none"> • Fossil fuel combustion, forestry, transportation, and industry. • Main contributor to production of secondary organic aerosol (SOA). • Predominates over primary organic aerosol (POA) in all environments⁹. 	<ul style="list-style-type: none"> • OC species are mainly composed of carbon, but also contain other chemical elements. • ~80% of OC species are semi-volatile¹⁰. • Rarely found as primary particles, due to volatility and reactivity. • Resident in atmosphere for 1 day in urban environments and 5-10 days in sub-urban environment¹¹. 	<ul style="list-style-type: none"> • OC molecules are generally light scattering. • By scattering incoming solar radiation, OC increases the fraction of diffuse light at the surface. This increases photosynthesis rates in some plant species.
----------------------------	-----------------------------------------------------------------------------------------------------------------------------------------------------------------------------------------------------------------------------------------------------------------------------------------------	--------------------------------------------------------------------------------------------------------------------------------------------------------------------------------------------------------------------------------------------------------------------------------------------------------------------------------------------------------------------------------------------------------------	---------------------------------------------------------------------------------------------------------------------------------------------------------------------------------------------------------------------------------------------------------------------------

<p>Sulphates</p>	<ul style="list-style-type: none"> • Reactive sulphate ions are created by burning fossil fuels. • These react with other chemical species to form secondary sulphate pollution. 	<ul style="list-style-type: none"> • SO_x is the primary source of sulphate ions in the atmosphere, which can react with water to form sulphuric acid (leading to acid rain¹³), or with ammonia ions to generate ammonium sulphate particles. • These chemical species have high albedo and are therefore highly light scattering. • The residency time for tropospheric sulphates lies in the range of 3-9 days¹⁴, long enough to reach regions distant from their source. 	<ul style="list-style-type: none"> • Generally light scattering particles, that reduce the levels of PAR at the earth's surface, both directly^{15,16} and indirectly (through cloud seeding)¹⁷. • This reduces the direct PAR available for photosynthesis in crops, but increases the proportion of diffuse radiation at the surface.
------------------	----------------------------------------------------------------------------------------------------------------------------------------------------------------------------------------------------------	--------------------------------------------------------------------------------------------------------------------------------------------------------------------------------------------------------------------------------------------------------------------------------------------------------------------------------------------------------------------------------------------------------------------------------------------------------------------------------------------------------------------------------------------------------	------------------------------------------------------------------------------------------------------------------------------------------------------------------------------------------------------------------------------------------------------------------------------------------------------------------------------------------------------------------------------------

<p>Nitrates</p>	<ul style="list-style-type: none"> • Reactive nitrogen oxides (NO_x) are generated through burning of fossil fuels¹⁸. • These react with other chemical species to form secondary nitrate pollution. 	<ul style="list-style-type: none"> • Highly light scattering PM species that directly scatter solar radiation. • Most reflective under high relative humidity¹⁹. • Critical for formation of secondary organic aerosol (SOA). • The reaction of nitrate ions with water vapour creates an acid (nitric acid, HNO₃) producing acid rain. • Nitrates reside in the atmosphere for 3-9 days, similar to sulphates²⁰. 	<ul style="list-style-type: none"> • Highly light scattering, reducing total PAR at the surface for crop photosynthesis, but increasing the proportion of diffuse light. • Few major atmospheric aerosol models include nitrogenous compounds due to difficulties in simulating the behaviour of these compounds. • This is a major source of uncertainty in the total effects of PM on a global scale.
-----------------	---------------------------------------------------------------------------------------------------------------------------------------------------------------------------------------------------------------------------------------------------	-------------------------------------------------------------------------------------------------------------------------------------------------------------------------------------------------------------------------------------------------------------------------------------------------------------------------------------------------------------------------------------------------------------------------------------------------------------------------------------------------------	------------------------------------------------------------------------------------------------------------------------------------------------------------------------------------------------------------------------------------------------------------------------------------------------------------------------------------------------------------------------------------------------------------------------------------------

<p>Secondary Organic Aerosol (SOA)</p>	<ul style="list-style-type: none"> • Formed when reactive oxygen species (ROS) oxidise organic molecules. • Primary organic PM is one source of organic precursor, but a vast majority of organic precursor comes from the release of biogenic volatile organic chemicals (BVOCs, at least 2.4Pg per year¹). 	<ul style="list-style-type: none"> • An extremely diverse set of particles. • Most SOA particles have a high albedo¹. 	<ul style="list-style-type: none"> • SOA species are typically light reflecting and scattering, contributing to reduced PAR, but increased diffuse fraction, at the Earth's surface.
----------------------------------------	-------------------------------------------------------------------------------------------------------------------------------------------------------------------------------------------------------------------------------------------------------------------------------------------------------------------------------------------------	----------------------------------------------------------------------------------------------------------------------------------------------------------	-----------------------------------------------------------------------------------------------------------------------------------------------------------------------------------------------------

Table 1.1 Description of primary PM components considered in this thesis, including sources, residence time within the atmosphere, physical and optical properties, and resulting effects on surface radiation.

References: 1. Briggs et al., 2016, 2. Peng et al., 2016, 3. Y. Zhang et al., 2016; Dalirian et al., 2018, 4. Steinfeld, 2012, 5. Lindberg and Garten, 6. 1988, Cape et al., 2012, 7. Costabile et al., 2013, 8. Kirchstetter et al., 2004, 9. Wu, Wu, and Yu, 2018, 10. Textor et al., 2006, 11. Petzold et al., 2013, 12. Malm et al., 2003, 13. Lindberg and Garten, 1988, 14. Steinfeld, 2012, 15. Langner et al., 1992, 16. Haywood and Shine, 1997, 17. Charlson et al., 1992, 18. Charlson et al., 1992, 19. van Donkelaar et al., 2016, 20. Burney and Ramanathan, 2014, 21. Guenther, 2002, 22. Wang et al., 2014, 23. Penner and J.E., 1994, 24. Ortega et al., 2013

1.3 Mechanisms for PM Impacts on Crops

Photosynthetically active radiation (PAR) is a subset of shortwave (SW) radiation with a wavelength of 400-700nm, and is used for photosynthesis by plants and photosynthetic bacteria. In land plants, PAR is intercepted by the chloroplasts in leaves, where its energy is used to fix carbon into a bioavailable form.

When a photon of PAR travels through the atmosphere, it can be intercepted by many particles (e.g., atmospheric gas particles, water droplets, aerosolised dust, etc). Upon interception, these photons are either absorbed or scattered. Because PM is a heterogeneous mixture of particles, the effects of bulk PM on incoming PAR vary spatio-temporally as they depend on a wide range of factors. These include PM composition, concentration, size distribution, and the prevailing meteorology. The net effect of airborne PM on photosynthesis is strongly debated, and is discussed in depth in section 1.3.1.

By contrast, there is a smaller pool of evidence for the effects of deposited PM on plant photosynthesis, but the direction of this effect is clearer. The adherence of deposited aerosol on a plant canopy directly reduces light absorption by coated leaves, reducing photosynthesis rates. Furthermore, it blocks stomata, reducing transpiration, and increasing leaf temperature. This is discussed in detail in section 1.3.2.

1.3.1 Indirect Mechanism

Airborne PM reduces incoming photosynthetically active radiation and diffuses direct light. As discussed in section 1.2.1 and 1.2.2, PM is a highly heterogeneous mixture, with individual components of PM interacting with incoming solar radiation differently. The mass absorption and scattering efficiencies (MAE and MSE respectively) of particles are optical properties that describe the propensity of a particle to absorb or scatter incoming radiation. Beta is the aerosol light upscatter fraction, describing the proportion of radiation impacting a particle which is backscattered rather than scattered forward. These characteristics vary amongst all components of PM. For example, black carbon has a large MAE but negligible MSE, whilst the inverse is true for sulphate particles. These optical properties change with particle water content, shape, size, and chemical composition, and so the optical properties of bulk PM vary spatio-temporally.

This changes the direction and scale of PM impacts on incoming PAR, and thereby indirectly modifies crop yields by changing photosynthesis rates.

Airborne PM further reduces light at the surface through the Twomey effect, where PM alters the albedo of clouds. Airborne PM can act as additional cloud condensation nuclei, thus increasing the size of cloud droplets and increasing the amount of light which is scattered by clouds. The reduced light transmission to the Earth's surface will also reduce photosynthesis rates for plants in affected areas (Lohmann, U., & Feichter, J., 2005).

1.3.1.1 Reductions in total PAR

All PM components reduce the concentration of PAR at the surface, predominantly through absorption of PAR and re-emission as infra-red radiation (Mahowald 2011). Some components, however, have a greater MAE - i.e., they are more efficient absorbers of PAR. As highlighted in section 1.2.1, BC is the most abundant and important light absorbing PM component. Though BC accounts for less than 10% of all aerosol pollution globally (Klimont et al, 2017), in some locations it can account for more than 80% of light absorption at the wavelength of PAR (400-700nm) (López-Caravaca et al. 2022).

Organic carbon also plays a role in reducing PAR at the surface through haze generation. During atmospheric inversion events, aerosols concentrate at a low altitude rather than dissipating (Yin et al., 2015). When this pollution is trapped, organic molecules often act as nucleation centres generating larger PM particles. As this process accelerates, particle density and concentration increase rapidly, with primary emissions over the affected area being added to these growing particles (Guo et al. 2014). As this low-lying PM accumulates, it scatters increasing levels of light away from the Earth's surface over a localised area. Such haze events can cut incoming PAR to the earth's surface by as much as 45% (Aziz et al., 2017). Given the linear relationship between total PAR absorption and crop photosynthesis (Sun, Dongbao, and Qingsuo

Wang, 2018), light absorbing PM exerts a large downward pressure on potential crop yield.

1.3.1.2 Diffuse Radiation

Non-carbonaceous components of PM are less light absorbing and more scattering. By scattering incoming PAR, these PM particles cause solar rays to become less concentrated, spreading ground level irradiance over a greater area. In forest environments, a number of observational (Alton et al., 2007; Gu et al., 2002; Niyogi et al., 2004; Strada et al., 2015) and modelling (Mercado et al., 2009; Rap et al., 2015; Roderick et al., 2001; Xie et al., 2020) studies suggest that such PM pollution may actually increase canopy gross primary production (GPP), i.e., the total carbon fixation undertaken by plants within the canopy. This is attributed to a greater distribution of irradiance throughout the tree canopy, with lower concentrations of PAR at the upper, light-saturated leaf canopy, and higher concentrations at light-poor, lower canopy layers (illustrated in Figure 1.1 below). Changing the geometry of the incoming light in such a way increases total plant GPP, and is called the “diffuse light fertilisation effect” (Kanniah et al., 2012, Williams et al., 2014).

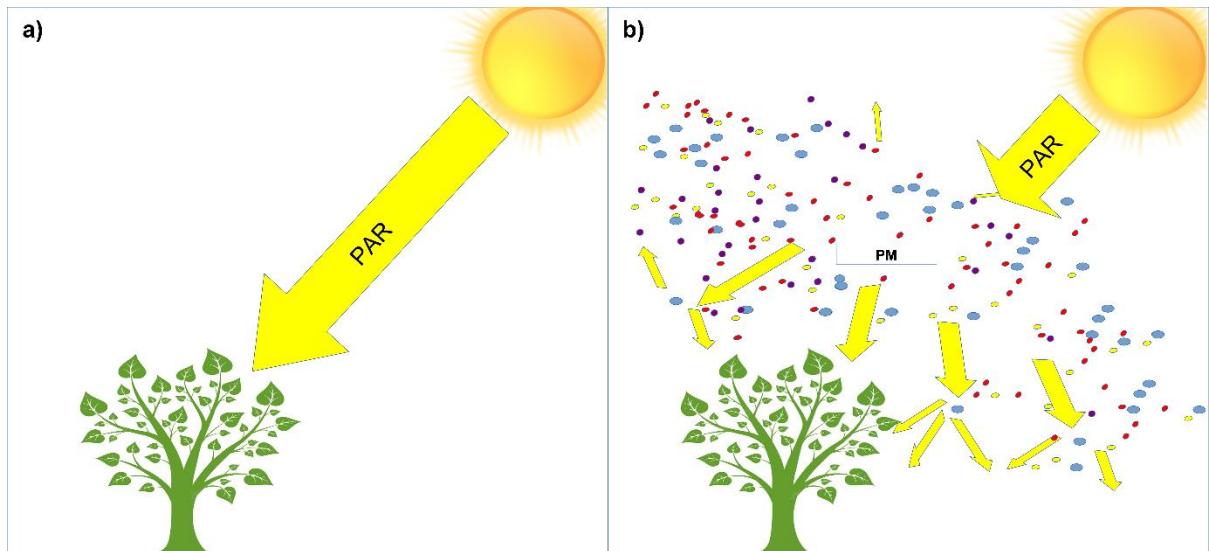


Figure 1.1. Illustration of PAR interception by PM, where a) no PM intercepts incoming PAR, and b) where PAR is backscattered by PM, absorbed by airborne PM, or transmitted through the PM cloud as diffuse radiation which is intercepted at lower canopy layers. Different coloured circles represent different sizes and species of PM.

Although the diffuse light fertilisation effect has been demonstrated in forests (Mercado et al., 2009, Rap et al 2018, Gui et al., 2021), the magnitude of the effect is much less certain over grassland and cropland. Whilst there is a paucity of *in vitro* experimentation, some *in silico* studies have attempted to address this uncertainty. Unfortunately, these studies are thus far inconclusive, with some finding a strong correlation between GPP and diffuse light (Nguy-Robertson et al., 2015), but others finding it to play an insignificant role in crop GPP (Niyogi et al., 2004).

These differences are attributed to the varied canopy architecture between forest, cropland, and grassland pasture. Dense forests with extensive lower canopies benefit greatly from the redistribution of PAR across these canopies, enabling foliage in the lower canopy to access higher levels of PAR and preventing the uppermost layers from over-saturating and “wasting” PAR. This more efficient light use can compensate,

or even overcompensate, for reductions in total irradiance due to PM-scattering of incoming PAR. This effect is much more notable in C3 plants (e.g., trees), as they are more readily light saturated under high levels of direct sunlight. C4 plants, including a large number of grasses and crops (e.g., maize), do not as easily become light-saturated, and are thus more sensitive to reductions in the total level of direct PAR. Research in crop plants specifically is, however, limited and conflicting. Some studies suggest that PM-enhanced diffuse light improves crop productivity (Roderick et al., 2001, Hemming et al., 2008, Cheng et al., 2015, Li and Yang, 2015) and others suggest that the balance of radiation changes reduces yields (Greenwald et al., 2006, Alton et al., 2008, Strada et al., 2015).

1.3.1.3 Total effects

The few published observational studies on the total effects of PM on crop yields suggest that significant crop yield reductions may occur in highly polluted regions. For example, it has been estimated that black carbon and sulphate pollution is responsible for circa 6% yield losses for Indo-Gangetic-Plain wheat over a 30-year period (Auffhammer et al., 2006; Burney and Ramanathan, 2014). If such yield losses are mimicked across the entire of India, that would be equal to 6 Mt of wheat in 2021. This equates to approximately 28 million people's annual caloric intake at 2000 kcal per day (USDA, accessed 01-2023). Given the existing burdens on food security of global heating, soil erosion, and extreme and unpredictable weather, these losses could compound to cause serious food supply issues in the future.

1.3.2 Direct Mechanism

Particulate matter (PM) is not airborne for its entire lifecycle. Eventually it is deposited to the earth's surface, whereupon it may readily adhere to vegetated surfaces. Once adhered, PM reduces the total light reaching the plant surface, blocks

stomata (reducing gas exchange) and increases leaf temperature (Burney & Ramanathan, 2014; Zhou, Chen, & Tian, 2018; Mina et al., 2018; Rai, 2016). The mechanisms (Section 1.3.2.1) and impacts (Section 1.3.2.2) of this are discussed below.

1.3.2.1 Dry deposition and adherence to plant surfaces

Non-gaseous air pollution takes the form of particles or aggregates. Smaller particles in the size range 1-2.5 μm tend to reside in the atmosphere for a period of days to weeks (Gugamsetty et al., 2012, Winiger et al., 2016) and are primarily deposited by impaction (where a particle is unable to follow the streamline of airflow because of an interposed surface). Larger particles, in the range 2.5-10 μm instead reside within the atmosphere for hours-days and are largely deposited by gravitational settling (Gugamsetty et al., 2012). When an atmospheric particle is intercepted by a plant surface, its propensity to adhere depends on key aspects of leaf morphology. Broadleaf tree species, for example, are less efficient at capturing PM than needle leaf trees due to a comparatively lower surface area (Chen et al., 2017). In addition, needle leaf trees tend to have higher wax content in the epidermis which increases PM retention (Steinparzer M., et al., 2023). The orientation of leaves, the number of micron-scale ridges, and the wax content of the leaf cuticle, also dramatically affect adhesion (Weerakkody et al., 2018). Rice and wheat are examples of crop plants with large numbers of micron-scale ridges. Such features likely increase PM retention time, and reduce particle removal (Yang et al., 2021) by providing a greater surface area for adhesion and by mechanical trapping of larger agglomerates. Furthermore, such ridges increase leaf hydrophobicity, reducing PM removal by rainfall.

Deposited PM is removed from the adaxial surface by wind and rainfall. The intensity of rain or wind required to remove PM can vary dramatically between plant species and sub-species (2-3x difference depending on type and density of leaf surface substructures; Wang et al., 2015). Studies regarding this phenomenon mostly focus on urban trees, used to accumulate PM particles in urban environments, thus removing them from the atmosphere (e.g., Xu et al., 2019). The large surface area of tree leaves and their complex, rough surfaces readily retain deposited PM (Han et al 2020). Rainfall

readily reduces the accumulation of water-soluble particles accumulated on tree leaves of all species, with rainfall above 15 mm hr^{-1} observed to remove virtually all PM particles from a range of tree species (Xu et al., 2017). Zhou et al., (2020) found that rainfall above 15 mm hr^{-1} removed roughly 80% of accumulated PM in three different species of wetland grass. However, here the optimum removal intensity was found to be rainfall of 30 mm hr^{-1} . Interestingly, each of the three studied wetland grasses retained a different size distribution of PM. This is believed to be due to the microstructure of the leaf surfaces, with similar results seen in other studies where surface roughness is closely correlated to particle retention (e.g., Weerakkody et al., 2018).

Wind further reduces PM accumulation. Dust accumulation on the flat surface of a solar panel is greatly reduced with exposure to wind with a shear velocity greater than 10 m s^{-1} (Jiang et al., 2018), with all particles above $1 \mu\text{m}$ in diameter re-suspended in the atmosphere. Similarly, at windspeeds of 10 m s^{-1} , PM is readily removed from leaf surfaces (Zheng and Li, 2019). However, at low wind speed, subsurface structures such as micron-sized surface grooves and leaf hairs, alongside increased stomatal density, are negatively correlated with particle removal rates (illustrated in Figure 1.2 below). The overall effects of PM deposition on crop yield, accounting for PM removal by wind or rain, are highly uncertain. In Chapter 3, a model is created to simulate these effects and present the first analysis of this phenomenon at regional and global scale.

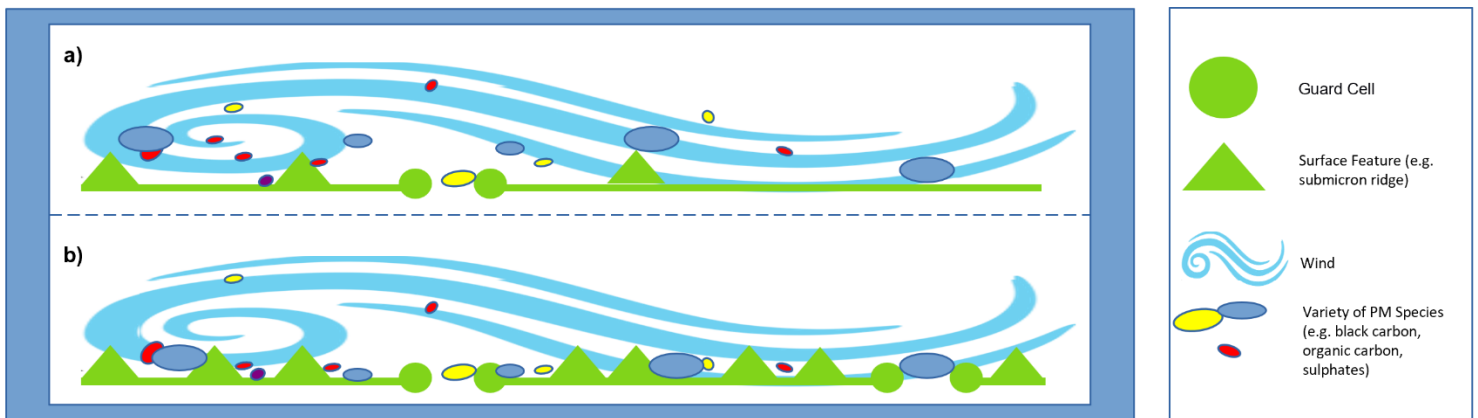


Figure 1.2. *Illustration of the removal of PM from a leaf surface. A) A leaf with few adaxial microstructural features does not retain PM when wind blows across its surface as the adhesion forces are weak. B) A leaf of the same area with more adaxial microstructural features retains more PM under the same wind. This is due to greater adhesive forces between deposited PM and the leaf surface.*

1.3.2.2 How does PM deposition affect crops?

One particularly insightful piece of work on this phenomenon is found in Mina et al, 2018. This work describes a set of pot trials carried out at the Indian Agricultural Research Institute (IARI), where two rice varieties were exposed to ambient, reduced, and enhanced PM concentrations over their growth cycles, and the effects of this exposure quantified. These pot trials found that continual accumulation from atmospheric PM (average PM_{2.5} concentrations of 187 $\mu\text{g m}^{-3}$ and PM₁₀ concentrations of 388.5 $\mu\text{g m}^{-3}$) caused significant reductions in yield of two rice strains: with an average 4% loss of Pusa Basmati and a 7.8% loss of Pusa Sugandh. When removal of PM by rainfall and wind was limited, these losses increased to 7.5% and 14% respectively. This study conducted detailed analysis of the affected crops, identifying the main factors contributing to yield loss as PAR blocking, reduced gas exchange, and leaf temperature increases. The contribution of these effects is also noted as varying substantially between the two studied rice varieties, with differences in

leaf surface features altering how readily PM is removed or retained. Leaf hairs and overall surface area are noted as the main features explaining the volume of PM flux to and from these surfaces. Similarly, the relative leaf sizes and canopy densities are noted as affecting micrometeorology surrounding the crops. This influences the velocity of PM deposition to individual plants.

Crop yield losses occurred because deposited PM physically blocks the interception of PAR by the adaxis. Similar to the PM indirect effect, deposited aerosol absorbs and scatters PAR before it can be intercepted by photoreceptors, reducing the energy available for photosynthesis and carbon fixing. The reduction in photosynthesis was compounded by the blockage of adaxial stomata - reducing gas exchange and further slowing photosynthesis. Finally, the deposited layer of PM acts as an insulator, increasing leaf temperature. Increasing leaf temperature above a crop variety's photosynthetic maximum, will slow or halt photosynthesis (Teixeira et al., 2013). In countries such as India, many crops (for example wheat) are grown at close to the maximum temperature threshold for existing cultivars of a given species. Thus, Indian wheat yields are expected to drop by up to 18.1% from 2020 levels by 2050 due to heat stress (Dubey et al., 2020).

The observations in Mina et al., 2018 are consistent with those made in other plant species (Naidoo et al 2010 and Saxena et al, 2017) and are illustrated below in Figure 1.3.

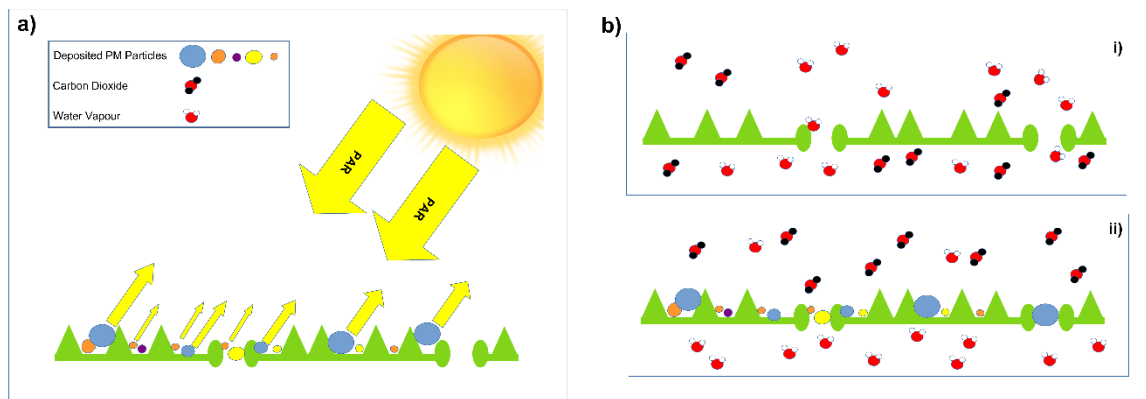


Figure 1.3. a) Incoming PAR is reflected or absorbed by PM on the adaxis, thus reducing the amount of PAR available for photosynthesis by the affected plant. b) i) Under normal circumstances, the plant leaf undergoes gas exchange, with water vapour evaporating from stomata and carbon dioxide taken into the leaf interior for photosynthesis. However, ii) if the stomata are blocked this cannot occur, reducing photosynthesis rates and trapping heat within the leaf interior.

The portion of yield reduction attributable to light interception, stomatal blockage, and leaf temperature increases varies by location, growing conditions, crop management practices, and cultivar, as well as by PM composition and size. The interaction of these variables remains poorly studied. Despite few studies exploring the intricacies of PM impacts on crop yields, extant literature does demonstrate a sizeable negative impact from dust deposition, highlighting PAR interception in particular as contributing to yield losses. As a further example, Hatami et al. (2017; 2018) explored the impact of desert dust on the yields of cowpea (*Vigna unguiculata* L.) and wheat (*Triticum aestivum* L.), finding reductions in grain yield of up to 13.8% and 35.5% respectively. These findings are in line with earlier analyses of the impacts of cement dust on crop yields (Singh et al., 1981; Mishra et al., 1986); where lower yields for affected crops were reported, and reductions in intercepted light for photosynthesis posited as the prime cause. Similarly, Naidoo G. and Chirkoot D. (2004) found that coal dust had a sizeable effect on Mangrove trees (*Avicennia marina*), with up to a 39% reduction in net primary production (NPP) for coal dust-coated leaves. The size

distribution of particles and their composition and optical properties, alongside the characteristics of the affected plant leaves (e.g., stomatal density, wax content, leaf hair coverage etc.) are extremely important to the magnitude of the direct effect, and a better understanding of each of these variables is important to project future impacts from PM deposition. A thorough exploration of parameter space through computer simulations could facilitate this. In a global model, all parameterisations of PM effects will, by necessity, be approximations of the truth at ground-level. However, as long as we are clear about the limitations of large scale modelling studies, they can play an important role in illustrating areas for further inquiry and exploration, and allow the various factors affecting crop yield to be studied in isolation. This dissection promotes greater understanding, and can highlight areas in need of further *in vivo* analysis.

One existing modelling study of particular importance for this thesis was conducted in Bergin et al (2001). This study provides insight into the impacts of the direct effect in an agriculturally important region of China, the Yangtze River Delta. Though a simplistic model (using fixed values for leaf area of simulated crops, a fixed rate of dry deposition from a constant concentration of PM, and ignoring PM removal by wind or rain), this work provides a mathematical framework for describing the effects of deposited PM on PAR transmittance to affected plants. This work estimates a reduction in PAR availability of ~35% for plants in the Yangtze River Delta using a subset of key aerosol parameters. Despite its limitations, and lack of verification *in vivo*, the mathematical underpinnings of this model have been used to calculate reductions in transmitted PAR attributable to deposited PM in a number of publications (Bergin et al., 2017, Li et al., 2020), and provide a mathematical framework on which further study of PM deposition effects can be based.

Possibly the most important effect absent from the Bergin et al. model is PM removal. In Mina et al. (2018), experiments were conducted with either ambient rainfall, enhanced PM removal through leaf washing, or the physical blocking of PM removal. When rain was excluded, yield loss more than doubled from 7% to 15%. Conversely, enhanced rainfall meant losses could be as low as 4%. In Chapter 3, Bergin's model is

adapted to work in a multi-layer crop canopy model with the inclusion of PM removal by wind and rain. This model is then used to recreate the PM deposition associated yield losses seen in Mina et al (2018), providing a first estimate of global yield losses attributable to existing PM deposition for rice, maize, and wheat. Regional studies are then conducted for China and India to further elaborate present, and potential future, food supply disruption owing to PM deposition.

1.4 Examples of PM sources and distribution in China and India

Northern China and Central India are particularly important areas for studying the effects of PM pollution on agricultural activity. Each of these regions contain vital agricultural centres (the North China Plain (NCP), and Indo-Gangetic Plain (IGP), respectively), and have amongst the highest average PM concentrations in the world (average of $108 \mu\text{g m}^{-3}$ for Beijing city region (Zhai et al., 2019), average of $66 \mu\text{g m}^{-3}$ on the IGP (Das, Manob, et al., 2021)). Even greater PM levels are seen at specific sites within these regions. For example, annual average PM_{2.5} concentrations of $135 \mu\text{g m}^{-3}$ were observed in Delhi in 2020 (Singh et al., 2021). By comparison, the average PM concentration in New York was only $12.3 \mu\text{g m}^{-3}$ for the period 2005–2016 (Peltier et al., 2011)). The crop growing areas of China and India are some of the most polluted crop-growing areas in the world, with substantially higher PM pollution than those in Europe or North America (e.g., Nebraska, USA has an average PM_{2.5} concentrations circa $43 \mu\text{g m}^{-3}$ (Statista, 2023)).

PM on the NCP and IGP is generated from a wide array of large point and area sources, particularly transportation infrastructure, energy production, and fertiliser usage (Turpin and Huntzicker, 1991; Yu et al., 2004). Transportation and fossil fuel-based energy production generate large quantities of SO_x and NO_x which are converted to secondary sulphate and nitrate aerosols, as well as primary PM (predominantly black carbon (BC) and organic carbon (OC)).

The airborne concentration of these pollutants, whilst important, only partially explain the impacts of PM on crop yields. As discussed above, the direct effect relies

upon the flux of these particulates to the surface, i.e., the rate at which the particles are deposited. This is illustrated in Fig. 1.4 below, which shows the flux rate for these particles in $\text{mg m}^{-2}\text{h}^{-1}$ for bulk PM across the NCP (panel a) and IGP (panel b) (discussed below in 1.4.1 and 1.4.2).

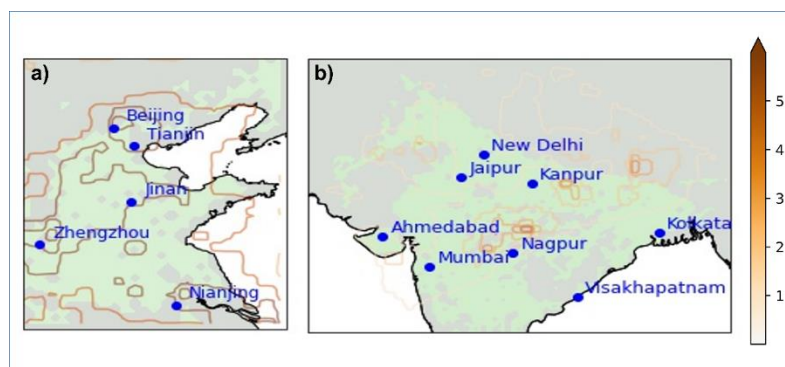


Figure 1.4. Illustrations of the (a) Chinese and (b) Indian model domains used throughout this thesis, with cropped area highlighted in green, and average pm flux to the surface for crop growing seasons between 2015-2020 ($\text{mg m}^{-2} \text{h}^{-1}$) shown as orange contours.

1.4.1 China

China, particularly the North China Plain (NCP) area, is illustrative of the key contributors to regional PM emissions. PM on the NCP is concentrated along a corridor from Beijing and Shanghai (Turpin and Huntzicker, 1991; Yu et al., 2004). Coal power plants have proliferated in this region, producing large quantities of PM (Riuli W. et al., 2019), and acting as major air pollution point sources (Li et al., 2021). These are still relied upon for a majority of Chinese power production, with coal contributing over 57.7% of total energy generation in 2019 (China Statistical Yearbook, 2020), and producing over 23% of all PM (Hua et al., 2016). China's 14th Five Year Plan, unveiled in 2021, included a plan to build and operate at least 100 additional coal plants in the 2020s. Whilst legislation adopted in 2014 has meant that PM emissions from coal plants reduced by 72% between 2014 and 2019 (Tang et al., 2019), adding substantial

numbers of new coal plants will offset these improvements to air quality and worsen regional air pollution.

The PM produced by coal plants is highly heterogeneous in size, varying from large composite particles above 10 μm in diameter, to small soot particles less than 1 μm in diameter (Zhao et al., 2008; Lu, Zhang & Streets, 2011). The chemical makeup however is more homogeneous, with BC (Yang and Chen, 2017) and organic carbon particles making up the bulk of the emitted PM. BC, as stated in Section 1.2.1, is highly light absorbing. Whilst organic carbon is generally more reflective and less light absorbing, organic carbon emitted from coal plants contains a large proportion of brown carbon which is highly light absorbing (Government of the Republic of China, Ministry of Energy, 2012; Yuan et al., 2018). Coal plants are thus a primary source of PAR-absorbing PM particles.

Industrial emissions are also major polluters in the NCP region (Rohde and Muller, 2015), owing to the large regional population and consequent economic activity. Whilst developing technologies have reduced the PM emissions from cement production over recent years (50% reductions in PM_{2.5} produced per kilo of cement between 2010 and 2015 (Liu et al. 2021)) this pollution still contributes significantly to the total atmospheric load of PM across China. In China, cement production is a particularly important industrial source of PM, being responsible for 14% of all PM_{2.5} emissions across the country in 2010 (Zhang et al., 2016; Zhu et al., 2018). One recent study found that cement dust constituted nearly 10% of all PM pollution during springtime in southwestern China (Shi et al., 2021). Together with reducing PAR reaching the surface (Hueglin et al., 2005; Din, Yahya, and Abdullah, 2013), cement dust also contains heavy metals such as lead and cadmium (Penner 1994). Whilst less important in terms of PAR interception, these are extremely detrimental to health outcomes in the immediate vicinity of their production (Wang et al., 2018). Such pollution has previously been shown to dramatically reduce food quality and supply (Qin et al., 2021).

Vehicular exhausts are a similarly significant contributor to PM pollution throughout China (Chen et al., 2009). This is particularly relevant within the Jing-Jin-Ji metropolitan region of the NCP, which includes the megacities of Beijing and Tianjin, and the Hebei region. Greater urbanisation and wealth have necessitated and facilitated increased private vehicle ownership (Yang et al., 2017). Across China, exhaust emissions were reported to account for 12-36% of total NO_x emissions, 10.7% of PM₁₀ and 16.8% of PM_{2.5} in 2011 (Zhang et al., 2016; Zhu et al., 2018), a problem which continues into the present, with the average amount of each pollutant emitted per vehicle remaining near constant between 2011 and 2019 (Wang et al., 2019, Song et al., 2019). The number of personal transportation vehicles and industrial goods vehicles has continued to increase to the present day. Particularly important is the expanding fleet of Chinese heavy duty diesel vehicles currently in use, which contribute significantly to PM emissions, particularly in urban environments (81.92% of emissions in Tianjin, (Song et al., 2018)).

Agricultural and rural regions also contribute to total PM, particularly through fertiliser spraying which generates ammonium (NH₄⁺) ions. This contributes to both primary and secondary aerosol load in the region through reaction of ammonium with organic carbon, driving the formation of secondary organic nitrate aerosol (Schuhmacher, Domingo and Garreta, 2004; Gupta et al., 2012; Abril et al., 2014). The co-location of ammonium emissions with large-scale biomass burning during crop residue combustion further favours the formation of this type of PM. In the winter of 2015, organic carbon accounted for up to 45% of the total PM load in the Beijing-Tianjin-Hebei region, with biomass burning contributing 25% of this total (Wang, Y., et al., 2019). Given that biomass burning is carried out largely in the autumn (Kecorius et al., 2017), this burning has little effect on crops grown early in the season. However, crops like winter wheat, which are sown at this stage, may be affected by this nitrogenous PM pollution.

The final key source of PM in China with an anthropogenic component is mineral dust (Zhang et al., 2010). In East and Northeast China, this is the largest individual

component of PM larger than 2.5 μm (Shen, et al., 2011). Though dust pollution would occur without human intervention, a proportion of mineral dust arises from land use change which drives desertification, increasing opportunities for mineral dust aerosolisation. This dust is predominantly 10 μm in diameter or larger (Meng et al., 2018), rapidly deposited, and has high albedo. Whilst the high albedo leads to a sizeable light scattering effect, this is highly localised given the rapid deposition of such large PM particles (Yao et al., 2016; Li et al., 2019).

Taken together, we see a substantial baseline atmospheric PM load with seasonal variations and spikes driven both by anthropogenic and meteorological effects. PM concentrations peak during the winter when additional energy demand necessitates increased coal plant usage, and are lowest during the summer months when heating based energy demands are the lowest (Xu, J., et al., 2019). Interestingly, however, aerosol optical depth (AOD – a measure of solar beam extinction by dust and haze) is the highest during summer months. This is attributed to the strong hygroscopic growth of aerosol molecules in high humidity – whereby particles agglomerate into larger molecules with higher water content that are more reflective and backscatter light more effectively. This means that AOD generally peaks during the peak development windows for local maize, rice, and spring wheat crops (see Chapter 4, Figure 4.3). The reduction in light availability may substantially impact on crop growth during this period. Conversely, the hygroscopic growth of PM particles during the summer months can be primarily attributed to seasonal monsoon weather patterns. The increased rainfall during these months may also trigger the removal of deposited PM (as discussed above in 1.3.2), and thereby reduce the overall impact of PM. The studies within this thesis seek to further elucidate the relationship between the indirect and direct effects of PM on crops, and how these change under different environmental conditions.

To conclude, over China we see a complex set of interacting PM sources, with BC and brown carbon from fossil fuel combustion being the greatest contributors to reduced surface radiation. Conversely, anthropogenic organic carbon, SOA, nitrates, and sulphates act to form scattering aerosols that increase the proportion of diffuse light.

Understanding the balance of these emissions and effects is therefore critical to estimating the total effect of PM on PAR availability for photosynthesis in this critical growing region. This is studied in further depth in Chapter 2.

1.4.2 India

The Indo Gangetic Plain (IGP) produces 60% of all of India's grainstuff (Indian Council of Agricultural Research). This highly significant region also boasts the highest PM pollution in the Indian Subcontinent, with average PM concentrations in IGP cities greater than $65 \mu\text{g m}^{-3}$ in early 2020, just prior to the Covid-19 pandemic (Das, Manob et al 2021). Fossil fuel usage in India is rapidly increasing, and over recent years has become more tightly coupled to the country's economic growth (Chandran Govindaraju and Tang, 2013; Steckel, Edenhofer and Jakob, 2015). As increasing numbers of power plants are constructed, the lack of restrictions on coal burning on the IGP proximal to the Indian capital of Delhi (Sreenivas and Bhosale, 2013) has contributed to increasing PM concentrations in and around the city.

The pollutant plume across the IGP is generated primarily by the cities within it, and pollution is particularly severe during the winter months, when winter wheat is grown locally, due to the increased heating demand for residential and commercial buildings (Deshmukh, Deb & Mkoma, 2013). Local industrial and energy sectors (10-60% of total PM) alongside local transportation networks (40-50% of total plume) (Jat and Gurjar et al., 2021) contribute the bulk of PM pollution. In Delhi, a majority of vehicular emissions are attributable to heavy-duty goods and trade vehicles (Nagpure et al., 2016), with 57% of vehicular PM attributable to these large vehicles (Jain et al., 2016). The Delhi pollutant plume is particularly important, contributing $40\text{-}150 \mu\text{g m}^{-3}$ of total local PM (Jat and Gurjar 2021).

Since 2001, the proportion of PM₁₀ generated directly by vehicular exhaust emissions has decreased to 14-34%. In parallel, the proportion of vehicular emissions

generated by non-exhaust emissions such as road dust and brake and tyre wear has increased, and now accounts for up to 86% of all PM₁₀ emitted by vehicular activity. This PM likely impacts PAR intensity over the IGP crop growing region, and deposition to crops will likely dramatically limit photosynthesis rates (Hatami et al., 2017). Changes to PM particle source and species over this period may alter the magnitude of this impact – for example, reductions in BC may reduce the amount of PAR absorbed by deposited PM particles.

Agricultural emissions, particularly biomass burning, also contribute to regional PM pollution. These are intermittent events rather than a continuous source of emissions throughout the year, but can create a vast quantity of pollution. For example, a study in Punjab found that biomass burning more than doubled PM concentrations in the area during the autumn months (Singh et al., 2021). These emissions can contribute up to 55% of total PM across the wider IGP during crop residue burning seasons (Ojha et al. 2020). This season primarily takes place across the months of September and October, with winter wheat typically the first grain harvested (Izumi et al. 2019). This likely means that biomass burning occurs during the reproductive phase of rice and maize, with associated PM pollution potentially affecting their yields.

It should also be noted, however, that crop burning predominantly occurs immediately post-monsoon (Sembhi, H., et al., 2020). This annual meteorological feature greatly reduces airborne PM concentrations, acting as one of the prime drivers of intra-annual variation in PM concentration (Sen et al. 2017). The monsoon primarily affects the concentrations of PM₁₀, where ambient PM₁₀ concentrations drop by ~68 $\mu\text{g m}^{-3}$. Conversely, changes to PM_{2.5} concentration are negligible (Mehmood et al., 2020). Conversely, increased fuel burning during the winter, when atmospheric conditions are stagnant and the planetary boundary layer is lower, result in a roughly doubled ratio of PM_{2.5} to PM₁₀ compared to summer months (Sen et al. 2017, Mogno et al., 2021), and overall, substantially higher PM concentrations (~143 $\mu\text{g m}^{-3}$).

Previous research has suggested that environmental perturbations may have the most impact on crop yields during their early reproductive stage, i.e., during some of the highest pollution periods on the IGP. The same magnitude of water stress, for example, was found to be significantly more impactful on rice and wheat yields during flowering than during the crop's vegetative development stage (Farooq et al., 2014; Pinto et al., 2020). Extreme heat is also found to be more impactful during flowering in the early reproductive phase, with wheat yields reduced by up to 45% after exposure, whilst losses were reported to be negligible if the same perturbation was applied later during the reproductive phase (Wollenweber et al., 2003). One pot trial found that combined heat and drought stress during the early wheat reproductive phase was found to reduce yields by 62% more than the same perturbation applied 21 days later (during the late reproductive phase) (Pradhan et al., 2012). The timing of PM associated light perturbations relative to crop development state are discussed throughout this thesis, with model simulation presented here in Chapter 2 (Wolffe et al., 2021) suggesting a greater impact from PM stress on crop yields if it occurs in the early reproductive phase. Chapter 3 examine this same phenomenon for PM deposition, and the work in Chapter 4 is dedicated to establishing the extent and causes of this effect through a range of crop modelling simulations.

1.5 Crop modelling

Crop modelling simulates a crop growth cycle *in silico*, and facilitates a range of experiments, in scale and type, that can be challenging to replicate in the real world. These can then be used to broaden our understanding of a field of study and inform *in vivo* experimentation.

The Joint UK Environment Simulator (JULES) is a standalone land surface model that forms part of the UK Earth System Modelling Project (UKESM). In standalone mode, it simulates processes at the surface when given meteorological

input. Since 2015, JULES has included a dedicated crop model, viz. JULES-crop (Osborne et al., 2015). This model includes four cereal crops (wheat, soya, maize, and rice), the mathematical descriptions of which have each been developed over the intervening years to various degrees (Williams et al., 2017, Mathison et al., 2021).

To be able to calculate crop carbon content in each carbon pool, the model requires a range of meteorological inputs - the most important of these are temperature, short wave radiation, the diffuse fraction of short-wave radiation, and precipitation.

Short wave radiation, combined with soil moisture (a function of precipitation and retained soil moisture from previous prescribed levels or precipitation events) is the main driver of crop size. For global simulations, both values are most often derived from reanalysis datasets – generated from a combination of observational data and infilling with machine learning and simulated data. Whilst this provides the necessary scale of data to generate global projections, it does contain a range of uncertainties that should caution against overinterpretation of results. Data from reanalysis models is only as strong as the machine learning models and simulations which complete in-filling, and these can show small or large deviations against observations - particularly in high resolution work. For example, ERA-5, a well-regarded reanalysis dataset, systematically overestimates the diffuse fraction of shortwave radiation over central China (Jiang et al., 2020).

Shortwave radiation, diffuse fraction, and water availability are used to determine photosynthetic rate, which drives carbon fixation. This model is coupled to a stomatal conductance scheme that represents leaf level transpiration. It should be noted that the canopy photosynthesis model in JULES is extrapolated from leaf level photosynthesis dynamics, then scaled up to whole canopy level. A fixed number of canopy levels can then be specified which interacts with sunfleck penetration (Clark et al., 2011). This is not necessarily reflective of reality, where plant canopies are complex and dynamic structures, but is a necessary simplification to enable large-scale simulations without undue resource requirements.

In JULES-crop, carbon allocation is primarily determined by crop development state, and crop plants develop through a number of stages. These stages are defined within the JULES model via the variable DVI, a measure of crop development, which has a scale running from -2 to +2. A DVI of 0 corresponds to the emergence of the crop. Between 0 and 1, a crop is in the vegetative development stage, corresponding to the period of crop development when fixed carbon is allocated to expansion and growth of leaf, stem, and root components. Between a DVI of 1 and 2, a crop is in its reproductive phase when carbon stores are remobilised, and GPP is dedicated to producing the harvestable fraction of the crop. These stages can be further subdivided into early vegetative (DVI = 0.0-0.5), late vegetative (DVI = 0.5-1.0), early reproductive (DVI = 1.0-1.5) and late reproductive (DVI = 1.5-2.0) phases. When a crop is parameterised, it has a prescribed number of degree days required to move from DVI 0 to 1, and from 1 to 2. Temperature is used to calculate degree days as the model timestep is iterated, and therefore functions as the prime driver of crop development stage. The model captures reality well for large-scale vegetation dynamics, enabling projections of future vegetation responses to temperature changes (e.g., Oliver R, J., et al., 2022).

The length of time each crop resides within a given development stage is based upon unique crop parameters first parameterised in Osborne et al., 2015, and reflects the differing carbon allocation of the programmed species in *in vivo* studies. Carbon is allocated to five carbon pools: leaf carbon, stem carbon, stem reserve carbon, root carbon and harvestable carbon. A crops parameterisation within JULES dictates what proportion of accumulated carbon is apportioned to each of these pools for a given DVI, for example spring wheat will have different portions of carbon allocated to each pool at a given DVI to simulated rice. Whilst these are parameterised based on literature values for carbon accumulation (Osborne, et al., 2015), there is natural variation in the response of crop varieties to these stimuli even within the same species, as was seen in the Mina et al 2018 study discussed in 1.3.2.2. Similarly, crops within JULES are planted with fixed planting densities and canopy distributions over vast geographical

areas. This is not necessarily reflective of reality, and illustrates why *in silico* studies should be backed by robust observational evidence.

JULES-crop has both strengths and weaknesses as a global crop model. Osborne et al. 2015 demonstrates that whilst absolute yield is not always accurate across all crops, interannual variability for maize and rice is well-captured. In particular, Indian rice accurately reflects *in vivo* responses to interannual variations in meteorology. Of the crops examined within this thesis, wheat captures changes in interannual variability least accurately.

Williams et al., 2015, examined the major sources of interannual yield variability within JULES-crop for maize, looking to characterise how simulated crops respond to changes in different environmental stimuli. Changing temperature, precipitation and shortwave radiation whilst leaving all other driving variables constant captures a majority of interannual variation in the model, but precipitation and temperature alone do not. The response of interannual variability in carbon fixation has, however, been substantially tuned since Williams et al., 2015 was published, with recent work from Oliver R. J., et al., 2022 demonstrating an accurate vegetative response to temperature fluctuations which can be used to project the effects of future climate change on global plant growth.

The relative strength of JULES-crop in predicting interannual variability facilitates its use in projecting yield outcomes for the changing light conditions associated with PM pollution (see 1.3.1 above). However, at time of writing, JULES-crop has no facility for simulating the direct effects of PM (see 1.3.2 above). As is discussed below in 1.6, all simulations within this thesis are conducted with a custom branch of JULES-crop, and a number of additions and developments are made to the model to simulate the direct effects of PM.

1.6 Aims of this thesis

This PhD aims to fill a number of knowledge gaps, identified above, surrounding the effects of particulate matter on crops across the globe. Particular focus is paid to China and India, where high levels of historic and current air pollution are found in these country's crop producing regions. The key aims for this thesis are to:

1. Establish the relative effects of PM mediated diffuse light fertilisation effect and reduced total surface irradiance on crop yields.
2. Identify the extent to which PM deposited to crop leaves affects global crop yields.
3. Explain how the interplay of pollutant intensity and pollutant timing within a crop development cycle affect final crop yield.

Chapter 2 of this thesis presents a detailed model-based analysis of the changes in maize yield on the North China Plain given the relationship between aerosol optical depth, PAR intensity, and the proportion of diffuse light. Comparable locations in other world regions which feature large urban agglomerations but have lower aerosol pollution are found to have distributions of direct and diffuse light more beneficial to maize growth, producing greater crop yields. These light profile comparisons strongly indicate that PM over the NCP acts to reduce regional crop yields. Through this work, we work toward aim 1 outlined above, showing that over China, the diffuse light fertilisation effect of PM is outweighed by reductions in PAR. We also indicate that the timing of PM emissions within the crop development cycle is important to the final outcome for yields, contributing towards aim 3.

Chapter 3 describes what are, to the best of my knowledge, the first global simulations of the effects of PM deposition on cereal crop yields. I simulate the extent of crop losses attributable to PM deposition globally from 2015-2020, and explore the potential effects of increasing PM concentrations on future yields. Detailed regional analyses of the North China Plain and Northern India (focusing on the Indo-Gangetic Plain) describe the uncertainties in these simulations, and demonstrate the importance of PM composition for the scale of this effect. This work completes aim 2, identifying that

whilst the global effects of deposited PM on cereal crop yields are small (~1% yield losses), the regional and site level effects can be an order of magnitude greater. Again, we find the timing of PM deposition to be associated with yield outcomes, leading towards aim 3.

Chapter 4 builds on the novel work presented in Chapters 2 and 3, in which the timing of PM pollution relative to crop development status was highlighted as a key driver of yield reductions. Here the effects of a range of environmental perturbations on crop yield across India are simulated. The time-dependence of crop response to PM pollution is assessed and analysed to systematically address aim 3.

Chapter 5 highlights the major findings of Chapters 2 to 4, discusses the limitations of this work, and identifies the most pressing questions remaining around the effects of PM pollution on global food production. The future work needed to address and reduce remaining uncertainty is then described.

Chapter 2: Temporal variability in the impacts of particulate matter on crop yields on the North China Plain

This chapter was published in the journal *Science of the Total Environment* in 2021, Volume 776, 1 July 2021, 145135

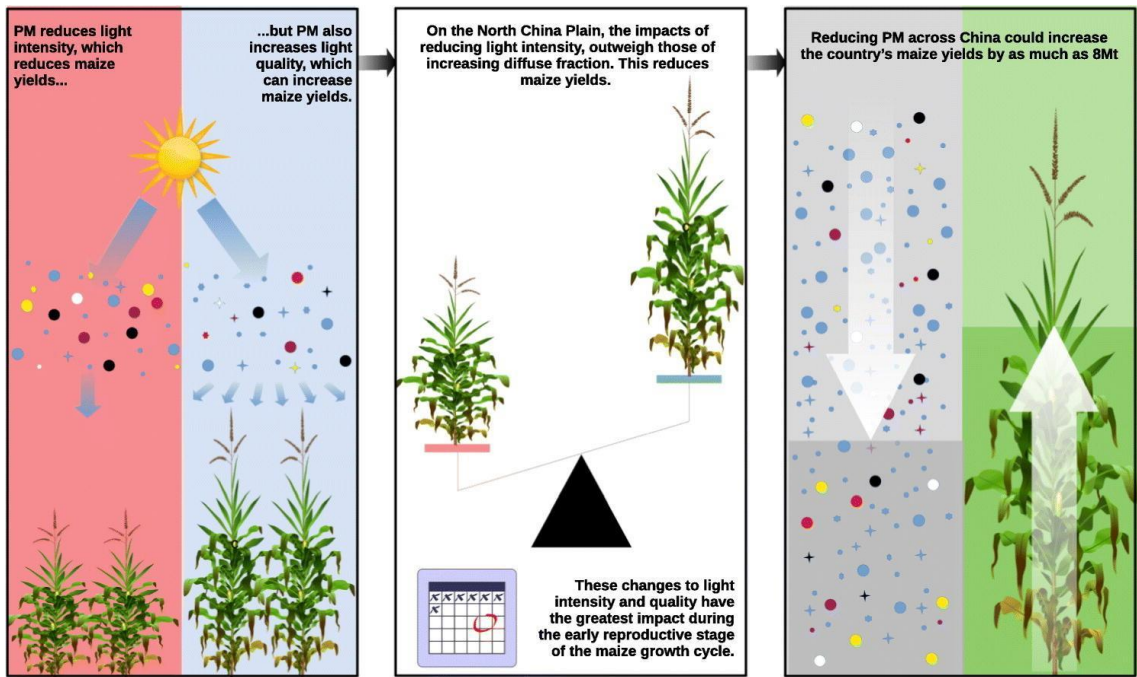
DOI: [10.1016/j.scitotenv.2021.145135](https://doi.org/10.1016/j.scitotenv.2021.145135)

[Slight adaptations have been made to this copy at the behest of examiners.](#)

Contribution statement:

The candidate's contribution was in the: conceptualization of the project; the development of the methodology used; the investigation of the research question; formal analysis of all data; interpretation of data; writing of manuscript for supervisor review; co-ordination of co-author feedback; submission of manuscript.

Graphical Abstract:



Graphical Abstract for published version of Chapter 2

Abstract

The North China Plain (NCP) is a major agricultural region, producing 45% of China's maize. It is also vital to the Chinese economy, encompassing the Beijing-Tianjin-Hebei megacity region. Anthropogenic factors increasingly impact crop yields on the NCP, and globally. Particulate matter (PM) pollution is a significant problem in this region, where annual average PM concentrations over three times the Chinese national air quality standard were recorded for the Beijing-Tianjin-Hebei megacity region between 2013 and 18. PM absorbs light, reducing total shortwave radiation (SW), thereby limiting plant productivity. However, PM also scatters incoming SW, increasing the diffuse fraction, which has been shown to increase growth and biomass assimilation.

The Joint UK Land Environment Simulator (JULES) crop model was used to assess the net impact of these competing changes in light on NCP maize yields. In contrast to some previous analyses, we find that PM-associated decreases in SW outweigh any positive impact on yield from an increasing proportion of diffuse radiation.

Furthermore, carbon allocation to different portions of the growing crop changes during the development cycle. We find significant differences between the effect on final yield of identical changes to diffuse fraction and total SW occurring during different development stages. The greatest simulated yield gains from increased SW and reduced diffuse fraction, consistent with reductions in PM, are observed during the early reproductive stage of development (July–August), when the simulated gain of yield is as much as 12.9% more than in other periods.

To further assess the impact of PM-linked changes in SW and diffuse fraction on NCP crop yields, radiation profiles from different city regions were then applied across the NCP. The changes in SW associated with these city regions could increase maize yields across China by ~8 Mt, or 3% of total yields. This would completely offset China's annual maize imports, increasing both national and global food security.

2.1 Introduction

The North China Plain (NCP) is China's largest agricultural region, accounting for 61% of the country's wheat and 45% of its maize production (National Bureau of Statistics of China, 2008). Today China is a major importer of wheat and maize (FAOSTAT, 2020). Increasing production in the NCP is therefore not only important for local farm economies, but also in reducing pressures on world grain markets. Maize production has risen twelvefold in the NCP over the last 6 decades (Li, 2009) and maize now comprises China's most important feedstock for livestock production (Shihuang and Kaijian, 2010).

Since the 1980s, climate change has begun to impact maize and wheat yields due to rising average temperature, only ameliorated by adoption of new crop varieties and better agronomic practices by producers (Liu et al., 2010, Han et al., 2018). The NCP includes the megacity region of Beijing-Tianjin-Hebei. Air pollution resulting from transportation, energy generation and industry in these major populations centres is known to affect crop yields (Feng et al., 2015; Masutomi et al., 2018). One important component of air pollution is particulate matter (PM), which persists at high concentrations over the NCP. Annual average concentrations of PM_{2.5}, i.e., particles with diameter $\leq 2.5 \mu\text{m}$, of $108 \pm 34 \mu\text{g m}^{-3}$ were recorded in Beijing-Tianjin-Hebei for 2013–18 (Zhai et al., 2019). This far exceeds the international and national air quality guidelines for an average mean concentration of $10 \mu\text{g/m}^{-3}$ (WHO, 2015) and $35 \mu\text{g/m}^{-3}$ (China: Air Quality Standards | Transport Policy, 2013) respectively. Such high levels of PM_{2.5} strongly affect both the intensity of short-wave (SW) radiation and the ratio of diffuse to direct SW radiation reaching the Earth's surface. PM occurs at high concentrations, not just in the NCP, but in many key crop growing regions around the world, particularly in developing nations. For example, the Indo-Gangetic Plain produces ~50% of India's food (Dhillon et al., 2010; Timsina, 2012). However, PM pollution in this region can reach $100 \mu\text{g m}^{-3}$ (Ojha et al., 2020), and is predicted to significantly reduce crop yields (Mina et al., 2018). The global nature of PM pollution, and its ubiquity and

increase in key areas of global crop production has implications for global food security, making it critical to better quantify its impacts on crop yields.

PM is a heterogeneous mix of airborne particles, with highly variable chemical and physical properties. The particle composition, size distribution and altitude of aerosol govern how it interacts with SW radiation. For example, highly light absorbing particles, such as soot and black carbon from combustion of coal for heat in the winter, directly reduce total SW levels at the Earth's surface (Moosmüller et al., 2009; Cohan et al., 2002).

For well managed and watered crops, there is a linear relationship between absorbed SW radiation and crop biomass accumulation (Monteith, 1977; Dohleman and Long, 2009); any reduction in incoming SW will therefore lower production. Reductions, such as those caused by PM, are exacerbated in so-called haze events, where atmospheric inversion results in an accumulation of pollutant at low altitude, strongly reducing surface SW (Aziz et al., 2019). Such haze events are a key cause of reduced visibility and surface SW in the North China Plains (An et al., 2019; Han et al., 2012; Guo et al., 2014). Although most common in December and January 5–6 haze days per month are also observed from April to September, the main period of maize production (Chen and Wang, 2015).

Other PM aerosol components such as sulphate are more reflective (Ramanathan et al., 2001), scattering light instead of absorbing it. Intercepted light may be scattered in all directions by PM, both reducing SW reaching the surface and altering its angular distribution, increasing the proportion which is diffuse (Huang et al., 2014a, Huang et al., 2014b). Well-managed crops will typically form about a dense canopy of 5–7 m² of leaves per m² of ground. Direct beam sunlight is therefore largely intercepted by the uppermost leaves of crop plants, with most leaves below in shade (Wickens and Horn, 1972). In full sunlight, upper leaves intercept more light than they can use in photosynthesis, while photosynthesis is light-limited in the lower canopy (Ort et al., 2015). Diffuse SW reaches the surface from all angles of the hemisphere, enabling it to

penetrate deeper into crop canopies and allowing increased photosynthesis by the light-limited lower leaves. This more even distribution of radiation through the canopy under high levels of diffuse light reduces the risk of oversaturation and thus photo-inhibition in the upper canopy. This redistribution of light to other canopy layers increases radiation use efficiency (RUE) for the plant overall, improving the rates of carbon fixation, net canopy photosynthesis, and hence, gross primary production (GPP) in forest ecosystems (Roderick et al., 2001; Niyogi et al., 2004; Kanniah et al., 2012; Rap et al., 2015) and is known as “diffuse light fertilisation” (Gu et al., 2002).

Variations in PM composition mean that changes in PM concentration do not strictly map to changes in surface radiation. This is compounded by variations in PM size distribution and meteorology which further affect how PM interacts with incoming radiation. Evidence for this can be seen in the widely fluctuating PM concentration over the year on the NCP. As PM concentration increases during the winter and declines in the summer, one would perhaps expect a relatively simple relationship where increased PM concentration directly maps to reduced radiation intensity at the earth's surface. However, aerosol optical depth (AOD), a key measure of the impact of total column aerosol on incoming radiation, peaks instead in late summer (Qu et al., 2016) due to the prevailing meteorological conditions at that time of year. Furthermore, in winter, PM composition becomes increasingly black and organic carbon heavy, as combustion-based power stations increasingly burn coal to provide heating during the winter months. This provides a marked difference in PM composition profile to the summer months when highly reflective nitrate aerosols dominate (Qu et al., 2016), leading to different impacts on surface SW. These factors limit the power of PM concentration alone to explain changes in surface radiation.

Field studies have previously evidenced a positive impact from diffuse light on forest gross primary production. For example, Strada et al., 2015, describe a 13% increase in forest GPP and a 17% increase in cropland GPP under high AOD conditions. Niyogi et al 2004 observed similar, although with the caveat that grassland appeared to suffer a reduction in productivity under high aerosol loads. This has been

replicated in other experimental (Alton et al., 2007; Gu et al., 2002; Cheng et al., 2015; Li and Yang, 2015.) and modelling (Mercado et al., 2009; Rap et al., 2015; Roderick et al., 2001; Xie et al., 2020) studies, providing strong evidence to support an increase in forest productivity, through increased surface diffuse light levels. A smaller number of studies suggest a similar result for crops (However, the magnitude of the benefit from enhanced diffuse light in croplands is disputed. While some studies suggest increased diffuse fraction due to air pollution increases gross primary production of crops (Cheng et al., 2015; Gu et al., 2002; Wang et al., 2015), others have found a reduction in yields (Alton, 2008; Strada et al., 2015). Greenwald et al. (2006), for example, predicted that crop yields may be reduced in a number of locations worldwide due to reductions in total radiation offsetting gains in RUE from a higher diffuse fraction.

A range of factors may account for the varying results in the studies outlined above, and these merit further investigation. One example is that the timing of changes in total SW and diffuse fraction relative to crop development stage may impact yields. Crops progress through a series of characteristic developmental stages; from sowing to vegetative growth, to seed filling to harvest, with carbon allocated in different proportions to different plant functions at each stage. Hence interventions to curb pollution, including PM, may be more or less impactful at different times within the crop life cycle.

Here, the Joint UK Land Environment Simulator-crop (JULES-crop) model is used to explore the effect of PM-mediated changes in light on maize yields across the NCP, and the sensitivity of the crops to the timing of these changes. As discussed above, the interaction of PM with surface radiation is complex, with concentration, composition, and size distribution of the heterogenous mixture of PM particles all contributing to the eventual impacts of PM on surface SW. We therefore study the effects of changes in radiation directly, rather than considering fixed changes in PM concentration to determine how PM-associated changes in total magnitude and temporal variability of SW (light intensity) and diffuse fraction affect maize yields.

Novelly, we conduct a range of sensitivity tests to explore the response of simulated maize yield to changes in total and diffuse SW, such as could result from policy interventions to reduce PM, at different crop development stages. This facilitates understanding of how PM pollution affects yield differently when it occurs at different development stages of our modelled crop. We then use time series of total SW and diffuse fraction from other large global cities with differing PM pollution to investigate the impacts of potential reductions in PM in the Beijing-Tianjin-Hebei region. Measurements of aerosol optical depth (AOD) and total cloud cover are then used to demonstrate that changes in diffuse fraction and total SW are linked to changes in PM. Furthermore, whilst previous authors (e.g., Greenwald et al., 2006) have focused on cloud interactions with light, we use an average climatology to remove interannual variation in cloud cover, allowing us to focus on the influence of PM under more stable cloud conditions. We achieve this by manipulating SW and diffuse fraction, which we have shown to be strongly linked to aerosol optical depth and therefore PM pollution in this region.

This paper therefore aims to explore how radiation profiles associated with levels of PM found in other city regions may affect crop yields on the NCP, and to establish how targeted reductions in PM must take account of the crop life cycle to achieve improvements in yield. Exploration of the developmental state dependence of crop responses to PM linked radiation changes is key to ameliorating the impacts of PM on crop production.

2.2 Materials and Methods

2.2.1 Model Set-up

JULES-crop has been demonstrated to accurately simulate maize yields at several well-characterized sites in the USA (Williams et al., 2017), although it has not previously been tested in the NCP. The study domain (31.0°N, 113.0°E to 43.0°N, 123.0°E) spans a majority of the NCP including the Beijing-Tianjin-Hebei region. The MODIS AQUA-TERRA land cover product MCD12C1 was used to determine the

cropped area of the NCP, which we assumed to be entirely given over to the major summer crop of this region, maize. JULES-crop, within the Joint UK Land Environment Simulator (JULES) model version 5.3 was used to simulate yields across the cropped area (Best et al., 2011; Clark et al., 2011; Osborne et al., 2015). We used the JULES-crop maize parameterization (Williams et al., 2017) with sowing dates taken from Sacks et al. (2010). Crops were assumed to be well irrigated in all simulations. Following the methodologies of Osborne et al. (2015), Williams et al. (2017) and Kimball et al., 2019, we convert the carbon allocated to the harvestable portion of the simulated maize crop to yield (dry t ha^{-1}).

Meteorological data of SW, downward long wave radiation, 2-m air temperature, precipitation, specific humidity, surface pressure and wind speed were taken from ERA-5 (European Reanalysis 5th Generation) for 1981–2017 at an hourly timestep and 0.25° spatial resolution (Copernicus Climate Change Service (C3S), 2017). Diffuse radiation was calculated for each grid cell as the difference between the total and the direct incoming SW radiation at the surface as given by ERA-5. Just over 45% the grid-cells in the domain were assigned as maize using MODIS-terra land fraction products as given by ERA-5.

2.2.2 BASE simulation

A climatological average driving dataset was obtained by calculating the mean of each meteorological variable of the ERA-5 driving data at an hourly timestep for each grid cell for 1981–2017. This was used to generate our baseline simulation (BASE) of maize production across the region. This average climatology reduces interannual variability in SW and diffuse fraction, and allows us to focus on average variations in SW and diffuse fraction and their relationship with one another. Perturbations are thereby compared to a more stable average baseline. Linear and multi-linear regression were used to derive the relationships between simulated yields and meteorological variables, and determine the relationships of diffuse fraction and total SW radiation with one another and with simulated yield.

To assess whether increased diffuse fraction increases maize yield across the NCP independent of changes in SW (as seen in previous studies; Rap et al., 2015; Roderick et al., 2001; Wickens and Horn, 1972), sensitivity tests were conducted in which the diffuse fraction was set to a constant value throughout the year, ranging from 0 and 1, in increments of 0.1. The above sensitivity tests and baseline results were used to generate relationships between total SW, diffuse fraction, and maize yield. These calculated relationships (Fig. 1) greatly informed the experiments detailed below.

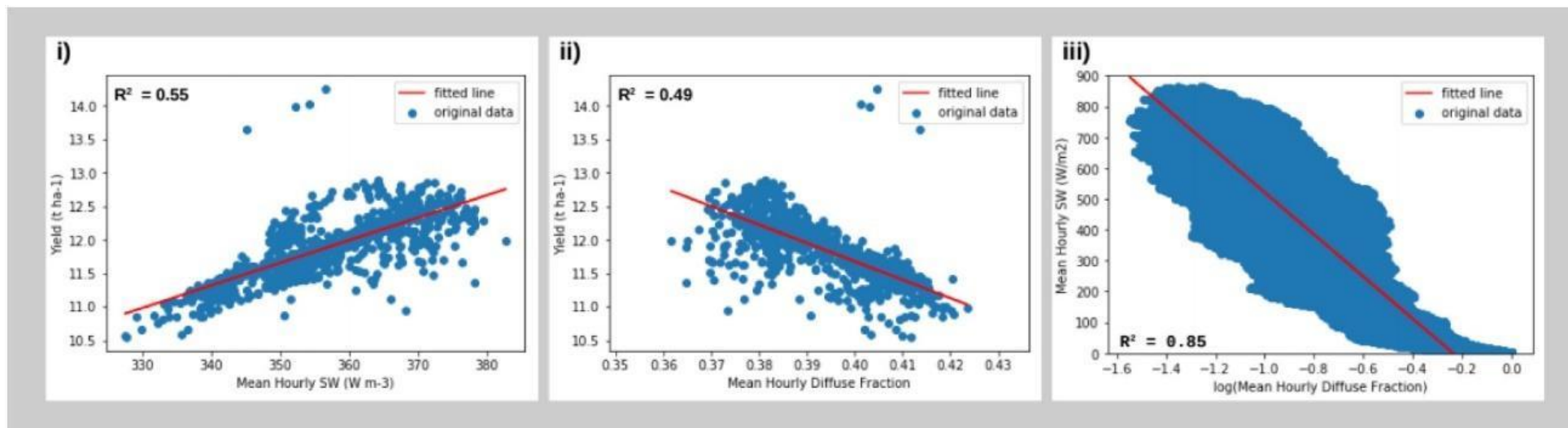


Figure 2.1. i) Maize yield versus BASE average hourly SW in grid cells with saturated soil, ii) BASE average hourly diffuse fraction vs yield in saturated soil grid cells iii) BASE SW vs diffuse fraction.

2.2.3 Driving Factors for Changes in SW and Diffuse Radiation

PM acts on incoming radiation in numerous and complex ways. Changes in concentration alone cannot be used as predictors of changes in radiation. Instead, the influence of PM speciation, size distribution, hygroscopicity and altitude, as well as meteorology must be considered both individually and in combination. Aerosol Optical Depth (AOD) on the other hand, has been demonstrated to be strongly linked to PM concentration (van Donkelaar et al., 2006), whilst also incorporating the interaction of PM and meteorology, thus providing a better indicator of the net impact of PM on surface radiation where concentration alone may lead to erroneous conclusions (Qu et al., 2016). AOD provides a measure of total column PM and its impact upon surface radiation (van Donkelaar et al., 2013; Just et al., 2015; Qu et al., 2016; Qin et al., 2018). Least squares multilinear regression was applied (using the SKLearn python toolkit version 0.23.2) to AOD and total cloud cover (TCC), taken from the C3S meteorological datasets, to assess whether observed changes in SW and diffuse fraction on the NCP are driven by PM, cloud, or both. The inclusion of TCC accounts for the impacts of PM on cloud formation, important given the contribution made by PM to cloud condensation, and thereby indirectly on incoming radiation. Our regression analysis was conducted using growing season average grid cell values of AOD, TCC, mean hourly daytime diffuse fraction for the growing season, mean hourly daytime downward SW radiation for the growing season, and final yield for the years 1997–2010.

2.2.4 Sensitivity at Different Development Stages

Varying meteorology and PM composition over the course of the year alter average total SW and diffuse fraction profiles across the NCP. The maize crop progresses through a series of development stages, characterized by different rates of photosynthesis and carbon allocation between roots, stems, leaves and reproductive structures. The impact of varying profiles of SW and diffuse fraction can therefore affect crop yields differently depending on when during the season perturbations to light occur. We conducted a range of sensitivity tests to assess how the timing of changes to the diffuse fraction and intensity of light relative to crop development stage affects final yield.

Post emergence, the crop develops through the vegetative stage and reproductive stage, each subdivided into early and late in JULES, giving four stages overall. Increased levels of PM during each development stage were simulated by elevating the diffuse fraction of our BASE simulation by 50% for a given stage, and decreased levels of PM by reducing diffuse fraction by 50%. This change was used to illustrate a large scale change to PM concentrations. The relationship shown in Fig. 1. was then used to deduce the total SW for each timestep consistent with the altered diffuse fraction. We refer to total SW modified in this manner as “diffuse-corrected” SW. All other driving variables remain unchanged from BASE. The statistical significance of yield results were determined by related *t*-test using the SciPy Stats module `ttest_rel` function across the cropped area of the model domain.

2.2.5 Impact of City Radiation Profiles on Yields

To investigate timing effects further, and as a proxy for potential future changes in PM concentration and composition, we studied the impacts on NCP crop yields of light profiles from the regions surrounding four global cities (New York, Madrid, Delhi, and Cairo), and one city in the NCP (Beijing).

These cities were chosen for their differing PM profiles and locations. Beijing experiences higher PM_{2.5} pollution ($108 \pm 34 \mu\text{g m}^{-3}$ for 2013–18, Zhai et al., 2019) than Madrid ($12.1 \mu\text{g m}^{-3}$ for the urban background from 2004 to 2009, Karanasiou et al., 2014) and New York ($12.3 \mu\text{g m}^{-3}$ for the period 2005–2016 (Peltier et al., 2011)), but is located at a comparable latitude (Beijing: 39.9°N ; New York: 40.7°N ; Madrid: 40.4°N). Conversely, Delhi experiences seasonally higher levels of PM pollution than Beijing (varying from a minimum concentration of $46 \mu\text{g m}^{-3}$ to a maximum of $279 \mu\text{g m}^{-3}$ over the year; Gorai et al., 2018) but is located at a considerably lower latitude than Beijing. We therefore use Cairo (30.0°N) as a comparator for Delhi (28.7°N) due to its similar latitude but lower PM pollution ($51 \mu\text{g m}^{-3}$ in 2013, Boman et al., 2013). By using two locations with a comparable latitude and maximal possible levels of downward SW flux, we can illustrate how the meteorology and pollution profiles over Delhi city region limit the potential surface SW in the region. Whilst the levels of PM in New York and Madrid are substantially lower than those for Beijing and the NCP, large scale PM reductions across the NCP are likely and possible given the downward trajectory of PM

concentrations over the last 7 years (Statista, 2023). We therefore present this city analysis as a way to explore how SW and diffuse fraction and therefore crop yields could change in the near future. They should be seen as an exploration of possibility space in terms of the outcomes of PM linked changes to SW and diffuse fraction, not an explicit prediction for what the future will definitively look like.

Average hourly diffuse fractions (taken from the 37-year ERA-5 dataset) from each city, were used to drive JULES-Crop over the model domain. The resulting yields on the model domain using SW and diffuse fraction profiles from four global city regions were compared to those obtained using the diffuse fraction for Beijing, and to our climatological average BASE case. Note that these changes are substantially smaller than the 50% changes described above for sensitivity analysis (see Table 2.2 for detail). The climatological average total SW for each city region was then applied in conjunction with the climatological average diffuse fraction time series to simulate the net effects of these different city PM regimes on NCP maize yields.

To disentangle the opposing effects of changes in SW and diffuse fraction on yield, we ran two further simulations for each city to demonstrate: 1) the levels of SW that would be found to occur in each city given the diffuse fraction at that time in the NCP, 2) the potential impacts of an altered relationship between SW and diffuse fraction, which can be partially attributed to changing levels of PM. In the first simulation, the mean diffuse fractions for the NCP domain were applied to each grid cell (as per BASE), with the total SW for that grid cell, derived from the relationship between diffuse and total SW for that city (named CITY_mod_SW simulations). In the second simulation, mean total SW for the NCP domain was applied to each grid cell (as per BASE), and the diffuse fraction for that grid cell was derived from the relationship between diffuse and total SW for that city (CITY_mod_Diff simulations). These simulations superimpose the relationship between SW and diffuse fraction in other city regions over the NCP. As this relationship between total and diffuse SW is strongly linked to levels of cloud and aerosol, it can be considered a proxy to describe the effects of changing profiles of SW and diffuse fraction over the year on the NCP.

2.3 Results

2.3.1 Aerosol Optical Depth (AOD) Results

We found the strongest correlation between changes in AOD and total cloud cover (TCC) with diffuse fraction ($R^2 = 0.90$), whilst changes in AOD and TCC explained just under 40% of variation in total SW. AOD alone was found to explain 80% of changes in diffuse fraction but only 15% of changes in total SW. This suggests that of the variability in SW resulting from changes to cloud and aerosol, an average of 38% comes from aerosol alone (R^2 for aerosol alone divided by R^2 for aerosol + total cloud cover). We conclude that whilst the observed changes in light intensity in the domain are mainly driven by cloud cover, changes to AOD, linked to PM pollution, make a non-negligible contribution to light intensity, and a large contribution to changes in diffuse fraction. Further sensitivity tests presented here, in which we modify light intensity (SW) and/or diffuse fraction, should therefore be seen as an exploration of potential changes in maize yields if PM concentrations were to change across the NCP.

2.3.2 The BASE Simulation

2.3.2.1 Relationships

We found light to be the most critical meteorological variable for predicting simulated maize yield in our baseline simulation (BASE). Yield was positively correlated with mean hourly SW such that a 10% increase in light intensity correlated with an 8% increase in yield ($R^2 = 0.54$, Fig. 1.i). However, we found yield to be negatively correlated with mean hourly diffuse fraction with a 10% increase in diffuse light reducing yield by 9% ($R^2 = 0.49$, Fig. 1.ii). While this may initially appear counterintuitive, it is driven by the strong negative logarithmic relationship between grid cell average total SW and diffuse fraction ($R^2 = 0.85$) for the domain during the growing season (Fig. 1.iii.), therefore reproducing the negative impacts of reduced SW from increased PM cover reported in previous studies (Gu, Wang, Zhuang, & Han, 2018; Zhou et al., 2018). A 10% increase in the mean growing season diffuse fraction (i.e., from 0.49 to 0.54) on the NCP corresponds to a reduction in average SW of 72 W m^{-2} .

The relationship between diffuse fraction and yield was non-linear for constant total SW. Increasing diffuse fraction by 10% relative to the growing season mean increased simulated maize yield by 0.007 t ha^{-1} , while a 10% decrease reduced yield by 0.035 t ha^{-1} . These changes, associated with changing diffuse fraction, represent less than a 0.1% change in yield, whereas a 10% increase in average total SW led to a yield

gain of 1.05 t ha^{-1} , a change 150 times greater. We conclude therefore that the diffuse light fertilisation effect is insignificant in comparison to the effects of reducing total SW.

2.3.2.2 Yields

The average yield predicted across the NCP was $11.9 \pm 0.5 \text{ t ha}^{-1}$, using the 37-year climatological average driving data derived from ERA-5. In 2011, the recorded yield for maize in China was 5.75 t ha^{-1} (Hu and Zimmer, 2013), just under half the modelled yield produced in our BASE simulation. Without irrigation however, the modelled average yield is 6.73 t ha^{-1} . Furthermore, we assume here that maize is grown across all cropped land in the model domain, whereas in reality the most favourable areas for crop production are currently reserved for other crops. This results in a further positive skew of average maize yield in our simulations.

To ensure that light effects are not confounded with other environmental limitations, we continue to apply irrigation in all simulations comparing results against the (irrigated) BASE simulation. The projected yields for all model simulations are shown in Table 2.1. The cropped area and yields for BASE, along with the average SW and diffuse fraction across the domain, are shown in Fig. 2. Table 2.1 provides a reference for the wide range of potential yields that might be expected under the SW and diffuse fraction scenarios explored in this work.

Run #	Name	Average Yield \pm Standard Deviation (kg/m ²)	Percentage Difference from BASE (%)
1	BASE	11.9 \pm 0.5	N/A
2	BASE_Mod	12.4 \pm 0.7	4.9
3	BASE_Diff_0.0	10.2 \pm 0.5	-14.1
4	BASE_Diff_0.1	10.7 \pm 0.5	-9.8
5	BASE_Diff_0.2	11.2 \pm 0.5	-5.9
6	BASE_Diff_0.3	11.6 \pm 0.5	-2.4
7	BASE_Diff_0.4	11.9 \pm 0.5	0.6
8	BASE_Diff_0.5	12.3 \pm 0.5	3.1
9	BASE_Diff_0.6	12.4 \pm 0.5	5.3
10	BASE_Diff_0.7	12.8 \pm 0.5	7.0
11	BASE_Diff_0.8	12.8 \pm 0.5	8.4
12	BASE_Diff_0.9	12.3 \pm 0.5	9.5
13	BASE_Diff_1.0	12.9 \pm 0.5	10.1
14	BJG, Diff	11.9 \pm 0.5	1.1
15	MAD, Diff	11.4 \pm 0.5	-34.2
16	NYC, Diff	11.7 \pm 0.5	7.1
17	DEL, Diff	11.7 \pm 0.5	-17.6
18	CAI, Diff	11.2 \pm 0.5	-31.7
19	BJG_SW, Diff	12.1 \pm 0.4	2.5
20	MAD_SW, Diff	15.2 \pm 1.2	28.9
21	NYC_SW, Diff	12.6 \pm 0.4	5.7
22	DEL_SW, Diff	11.9 \pm 0.5	-0.1
23	CAI_SW, Diff	15.9 \pm 2.1	34.2
24	BJG_Mod_Diff	11.7 \pm 0.5	-1.1
25	MAD_Mod_Diff	11.6 \pm 0.5	-3.0
26	NYC_Mod_Diff	11.7 \pm 0.5	-1.7
27	DEL_Mod_Diff	11.6 \pm 0.5	-3.2
28	CAI_Mod_Diff	11.6 \pm 0.5	-3.2
29	BJG_Mod_SW	11.9 \pm 0.7	1.1
30	MAD_Mod_SW	7.9 \pm 0.7	-34.2
31	NYC_Mod_SW	12.6 \pm 0.5	7.1
32	DEL_Mod_SW	9.8 \pm 0.7	-17.6
33	CAI_Mod_SW	8.1 \pm 0.5	-31.7
34	DEV1_0.5	13.3 \pm 0.9	6.6
35	DEV2_0.5	13.5 \pm 1.4	8.3
36	DEV3_0.5	15.9 \pm 1.4	28.2
37	DEV4_0.5	15.1 \pm 1.2	21.6
38	DEV1_1.5	8.4 \pm 1.2	-33.1
39	DEV2_1.5	8.2 \pm 1.1	-33.5
40	DEV3_1.5	7.9 \pm 0.7	-37.3
41	DEV4_1.5	9.5 \pm 0.9	-24.4

Table 2.1. Summary of key model results from simulations. Average yield is colour coded such that the average yield for BASE is the midpoint, with 0% change as the midpoint, red for decreasing yield, and blue for increasing. The percentage difference from base is colour coded 0% difference from BASE as white and the largest difference as the most purple.

Key:

BASE simulations provide a climatological average for comparison of sensitivity tests to a reasonable baseline scenario.

BASE – a simulation using the climatological average meteorological driving data.

BASE_Diff_x – Uses climatological average meteorological driving data, excepting diffuse fraction, which was set to a fixed fraction (x), e.g., BASE_Diff_0.0 is the BASE simulation but with diffuse fraction set to 0 for the whole run. This baseline scenario provides a benchmark to demonstrate the effects of diffuse fraction modification alone.

BJG, MAD, New York, DEL, CAI – Beijing, Madrid, New York City, Delhi, Cairo.

CITY simulations are used to illustrate potential future scenarios for yield on the NCP with changing SW radiation profiles.

CITY, Diff – As BASE, but with diffuse fraction from CITY across all grid cells for each timestep, e.g., MAD, Diff is the BASE simulation but the diffuse fraction from the Madrid grid cell is applied across the whole area varying with the corresponding timestep through the year.

CITY_SW, Diff – As BASE, but with SW and diffuse fraction from CITY across all grid cells for each timestep, e.g., MAD_SW, Diff is the BASE simulation but the SW and diffuse fraction from the Madrid grid cell is applied across the whole area varying with the corresponding timestep through the year.

CITY_Mod simulations are used to present the relationship between diffuse fraction and SW found at CITY in the context of the NCP as a proxy for the differing conditions and PM profiles found at each CITY region.

CITY_Mod_Diff – As BASE, but with diffuse fraction derived from NCP SW using the relationship between SW and diffuse fraction found at the CITY, e.g., MAD_Mod_Diff is the BASE simulation, but the diffuse fraction derived from the BASE SW using the relationship found between SW and diffuse fraction at the Madrid grid cell.

CITY_Mod_SW – As BASE, but with SW derived from NCP diffuse fraction using the relationship between SW and diffuse fraction found at the CITY, e.g., MAD_Mod_SW is the BASE simulation, but the SWin derived from the BASE diffuse fraction using the relationship found between Swin and diffuse fraction at the Madrid grid cell.

DEV simulations test crop sensitivity to changes in SW and diffuse fraction during different crop development stages.

DEV1, DEV2, DEV3, DEV4 – Early vegetative phase, late vegetative phase, early reproductive phase, late reproductive phase.

DEVZ_0.5 – As BASE, but with diffuse fraction decreased by 50% for development stage Z, with SW set to “diffuse corrected” SW, e.g., in DEV1_0.5 the BASE simulation is used, but when the DVI for developing crop is between 0-0.5 the diffuse fraction is halved, and SW is corrected using the relationship between SW and diffuse fraction observed in Figure 2.1.

DEVZ_1.5 – As BASE, but with diffuse fraction increased by 50% for development stage Z, with SW set to “diffuse corrected” SW, e.g., in DEV1_1.5 the BASE simulation is used, but when the DVI for developing crop is between 0-0.5 the diffuse fraction is increased by 50%, and SW is corrected using the relationship between SW and diffuse fraction observed in Figure 2.1.

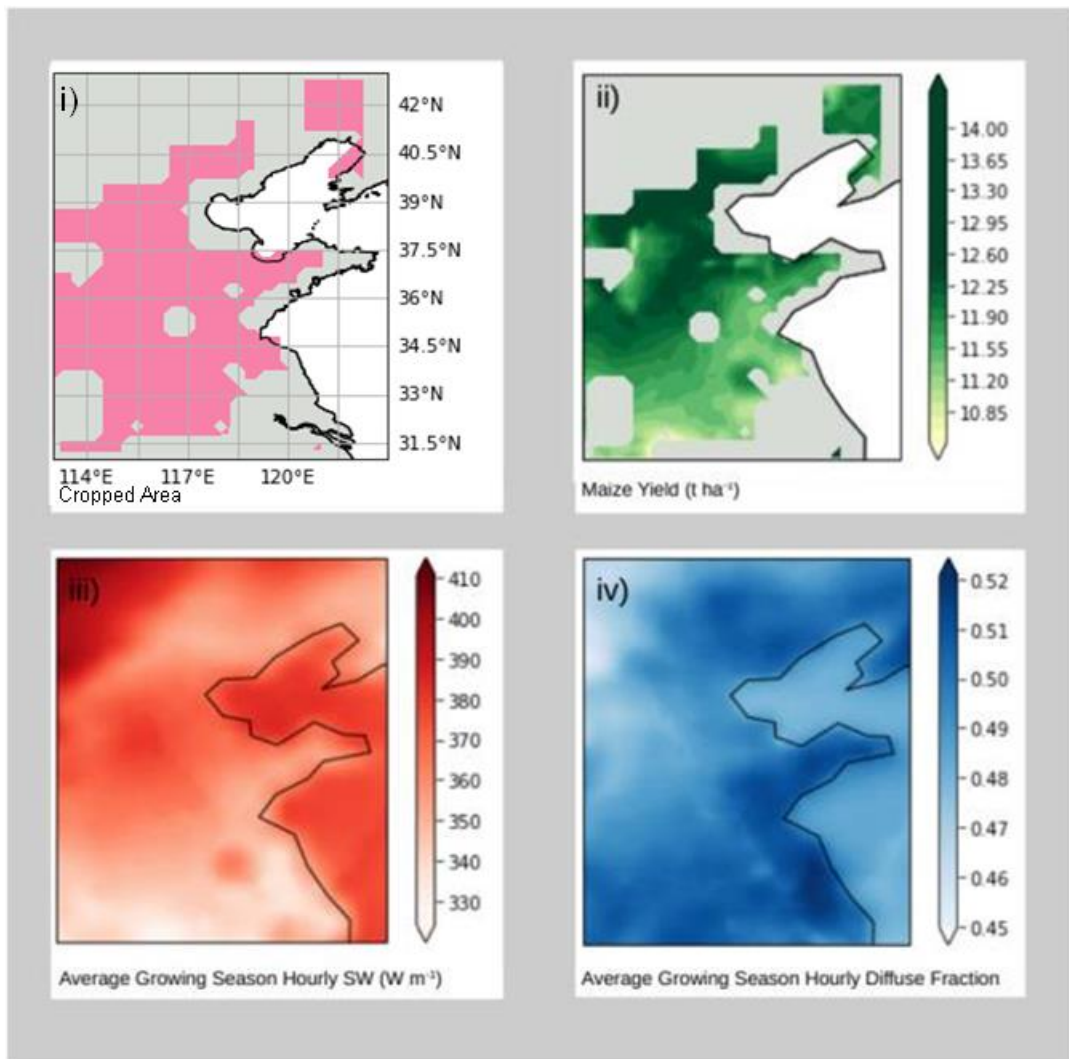


Figure 2.2. *i) Cropped region of the NCP in model, ii) BASE model yield output ($t\ ha^{-1}$), iii) Average Growing Season Day time Hourly \underline{SW} ($W\ m^{-3}$), iv) Average Growing Season Day Time Hourly Diffuse Fraction.*

Spatial variation in maize yield across the NCP in BASE was highly related to the strong negative logarithmic relationship between SW and diffuse fraction. In the BASE_Diff simulations, where diffuse fraction was increased without a change in total SW, maize yield slightly increased due to the diffuse light fertilisation effect, as reported for a variety of crops in previous modelling and observational studies (Mercado et al., 2009; Brodersen and Vogelmann, 2010; Huang et al., 2014a; Rap et al., 2015, Rap et al., 2018; Yue and Unger, 2017). However, as shown in Fig. 1, this relationship is not

observed for our BASE case (Fig. 1.i.). This is due to the observed reduction of SW with increasing diffuse fraction In Fig. 1.iii_

2.3.3 Sensitivity at Different Development Stages

The timing of the changes in SW and diffuse fraction made significant differences to final maize yield. We found maize to be most sensitive to changes in SW intensity and diffuse fraction during the early reproductive stage (DEV3). This stage is when JULES-crop moves utilising carbon for stem and leaf production, and shifts this toward the harvestable portion of the crop. It appears that increased diffuse fraction and reduced SW (representative of an increase in PM concentrations) during this period has the most significant effect, reducing yields by an average 37% compared to BASE (Paired *t*-test, $t = -5.73$, $p = 0.001$). Conversely, reducing diffuse fraction and increasing SW (simulating reduced PM) during DEV3 led to a 28% increase in average yield (Paired *t*-test, $t = -6.46$, $p = 0.001$). Applying the same changes to light intensity (total SW) and diffuse fraction during other development stages had a lower impact. For example, simulating reduced PM during the early vegetative stage (DEV1) increased yields by only 7%, less than one-fifth of the impact for DEV3 (again, the difference here is significant, $t = -5.78$, $p = 0.001$). However, the difference between yields when diffuse fraction is reduced in the early and late reproductive phase was not found to be significant ($t = -2.49$, $p = 0.139$), and neither was the difference between increasing diffuse fraction in the vegetative or early reproductive phase. This indicates that changes in radiation during the early reproductive phase produce the most sizable increases in maize yields, but that increasing ambient SW radiation by reducing the level of PM during the late reproductive phase would also be beneficial.

2.3.4 Impact of City Radiation Profiles on Yields

The global city regions used to simulate crop yields if PM was to change across the NCP, are summarised in Table 2.2 below.

Location	Coordinates	Average Hourly SW (W m-2)	Average Hourly Diffuse Fraction	Average AOD	PM2.5 ($\mu\text{g m}^{-3}$)
NCP ^{1,2}	31.0 N, 113.0E to 43.0 N to 123E	363.5	0.49	0.37	62.5–92.7
Beijing ¹	39.9°N, 116.4°E	365.6	0.51	0.28	108.0
Madrid ³	40.4°N, 3.7°W	453.2	0.37	0.15	12.1
NYC ⁴	40.7°N, 74°W	377.6	0.42	0.20	12.3
Delhi ⁵	28.7°N, 77.1°E	408.5	0.44	0.38	46.0–279.0
Cairo ⁶	30.0°N, 31.2°E	547.8	0.33	0.17	51.0

Table 2.2. Indicative values for average SW, diffuse fraction and PM2.5 concentration for NCP study region and for city regions studied.

Average hourly SW and diffuse fraction are taken from the climatology (generated from 1979 to 2017 ERA-5 meteorological data) used to drive all city runs for the growing season of modelled maize crop.

AOD is an average value, taken from the C3S climate data store meteorological dataset for aerosol optical depth, for the city containing grid cell, for the months April to September (inclusive of growing season), from 1997 to 2010.

PM2.5 data is taken from a range of ground-based studies conducted during the timeframe of this modelling study. Though the PM concentrations are not always overlapping in time in many cases, this serves as an indicator of representative values within the period of the climatology.

1). Yao et al., 2016 (range given for average seasonal values) 2). Zhai et al., 2019, 3). Santurtún et al., 2015, 4). Shmool et al., 2016, 5). Jain et al., 2005, (range given for average seasonal values) 6). Khoder, 2009.

When values of SW and diffuse fraction taken from Beijing city were applied across the domain, yields did not differ significantly from those obtained using SW and diffuse fraction for the whole of the NCP domain. All other city comparison runs

discussed in this section are compared to yields from Beijing (BJG) simulations rather than BASE, because the different spatial distribution of SW and diffuse fraction in BASE would make such comparison inappropriate.

The greatest change from our Beijing-based simulations was found in applying values for Cairo to the NCP. CAI_Diff (i.e. NCP domain SW but Cairo diffuse fraction) simulated yields 34% lower than those of BJD_Diff (Fig. 3.e.i), mostly attributable to average diffuse fraction in Cairo being 35% lower than that in Beijing during the growing season. Application of diffuse fractions from New York, Madrid, and Delhi to the NCP (New_York_Diff, MAD_Diff, DEL_Diff simulations) reduced yields by an average of 1, 5 and 1% respectively due to slightly lower annual average diffuse fractions (0.42, 0.37 and 0.44, respectively) reducing diffuse light fertilisation effects.

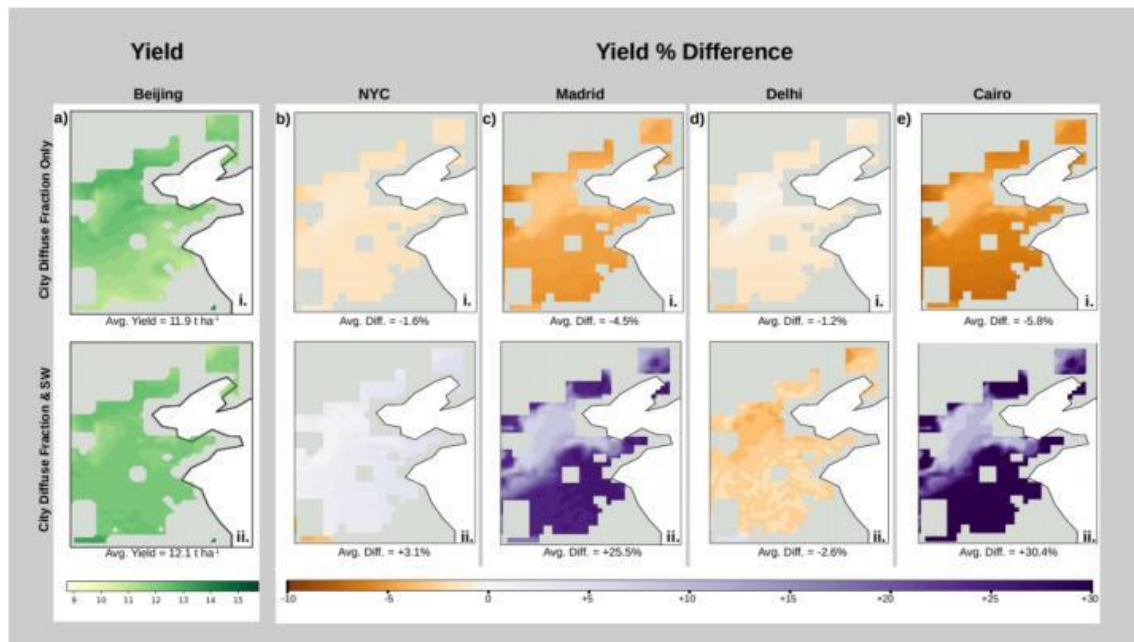


Figure 2.3. (a) Yields ($t\ ha^{-1}$) for city radiation profile simulations (i) BJD_Diff and (ii) BJD_SW_Diff. (b-e) percentage difference between (i) <CITY>_Diff and BJD_Diff, and (ii) <CITY_ SW_Diff and BJD_SW_Diff, for (b) New York, (c) Madrid, (d) Delhi and (e) Cairo.

However, when both diffuse and total SW were modified to reflect the average conditions in each city, the higher average annual SW at New York, Madrid, and Cairo more than compensates for their relatively lower diffuse fraction, with yields increases in

New_York_SW_Diff, MAD_SW_Diff and CAI_SW_Diff simulations by 3%, 26% and 30% respectively (Fig. 3.c,e,ii). Although SW and diffuse fraction are substantially different at Delhi from Beijing, DEL_Diff and DEL_SW_Diff (described in Section 2.5) show little change in yield from BJG_Diff (-1%) and BJG_SW_Diff (-3%) respectively.

Simulations using city-modified diffuse fractions (i.e., those generated using the relationship between total SW and diffuse fraction at each city, Fig. 4.c-f.i.) showed a negligible reduction in yield compared to BJG_mod_Diff (Fig. 4.c-f.ii.). Furthermore, yields simulated using SW derived from the relationships for Madrid, Cairo, and Delhi (Fig. 4.d-f.ii), are lower than those for BJG_mod_SW, with reductions of 35, 32 and 18% respectively. This can be explained in each case by lower total SW in that location for the diffuse fractions found on the NCP. In contrast to the other city regions, modified SW from New York increased yields by an average of 5.9% (Fig. 4.c.ii). as SW in New York is higher for a given diffuse fraction in the NCP.

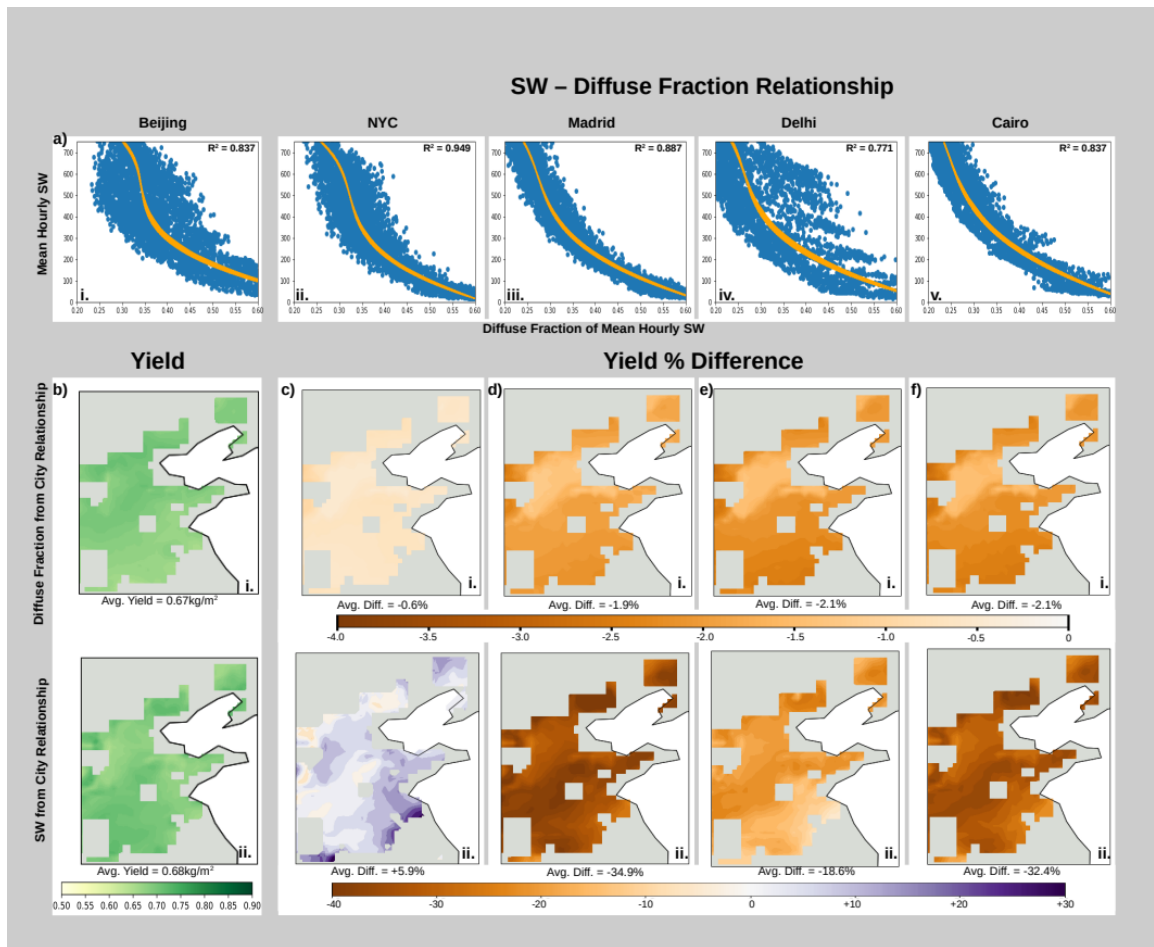


Figure 2.4. (a) (i-v) Relationships between SW and Diffuse fraction for each city, with data points in blue and quadratic regression line in orange. (b) Yields for CITY_MOD radiation profile simulation. BJG_Mod_SW and (ii) BJG_Mod_Diff. (c-f) percentage difference between (i) <CITY>_Mod_Diff and BJG-Mod_Diff and (ii) <CITY>_Mod_SW and BJG_Mod_SW, for (c) New York, (d) Madrid, (e) Delhi and (f) Cairo.

2.4 Discussion

2.4.1 PM Influences Maize Yields

The timing of changes in radiation relative to the developmental stage has the greatest impact during the early reproductive phase. This result has key implications for the nature and timing of emission reductions which may have greatest impact for yield crop yields on the NCP. In line with field observations, the photosynthetic capacity and hence carbon assimilation rate of maize in JULES-crop increases with leaf area during

the vegetative development stage, peaking during the late vegetative stage, and remaining high during the early reproductive stage. However, at the start of the early reproductive phase, the maize plant has matured, and therefore carbon allocation is diverted from stem, leaf, and root to the harvestable portion. Reduced carbon assimilation at this point does not stunt the plant, but instead directly affects the carbon assimilation which would normally be directed toward the harvestable portion. In our analyses, we find that the maize crop is most sensitive to reductions in SW (linked to elevated diffuse fraction) during the early reproductive phase (DEV3_1.5) (see Table 2.1). Similarly, the greatest predicted increase in yield results from reductions in diffuse fraction (i.e., reduced PM) in the early reproductive phase (simulation DEV3_0.5, Table 2.1), which occurs during July in our modelled maize season. As discussed earlier, at this time of year, PM concentration is at a minimum, but AOD reaches a maximum in the NCP due to prevailing meteorology interacting with PM pollution to produce haze (Qu et al., 2016). Whilst this indicates a smaller contribution from AOD to SW variability during this period, our analyses demonstrated that aerosol still contributes 32% of the total variability in SW during the early reproductive phase, i.e., PM still exerts an important influence on SW during this period. The remaining variation not due to cloud and aerosol simply originates from variations in latitude and altitude across the NCP, alongside seasonal variation in incoming radiation. The relatively small change in the AOD – SW relationship between seasons despite large changes in PM concentration and composition highlights the importance of using AOD as a measure of the impact of PM, rather than simply using PM concentration. The complex interplay of PM and meteorology, alongside factors such as PM speciation and size distribution, it impossible to predict how increases or decreases in bulk PM concentration will affect crop yield. PM pollution at a given time of year can thus have a disproportionate impact relative to its concentration. To increase crop yields, then, policymakers should make targeted emission reductions during the early reproductive phase of regional crops when reduced PM concentrations may be expected to have a far greater impact on yields than at other times of year.

PM concentration in the NCP fell by ~30% between 2013 and 2017 (Zhai et al., 2019) following the Chinese Government's introduction of the “Action Plan on the Prevention and Control of Air Pollution” in 2013. Despite these reductions, annual average PM_{2.5} concentrations for the Beijing-Tianjin-Hebei region were still well above

national and international annual mean guidelines of $35 \mu\text{g m}^{-3}$ and $10 \mu\text{g m}^{-3}$ respectively (China: Air Quality Standards | Transport Policy, 2013; WHO, 2015), whilst recurrent haze events remain a pressing issue limiting visibility and reducing total SW at the surface (Guo et al., 2014; An et al., 2019; Zeng et a 2019). Although PM pollution is decreasing on the NCP, our simulations suggest that the relatively high PM concentrations still present will continue to limit potential maize yield. Several factors contribute to the impact of PM on crops, and these are discussed below.

2.4.2 Radiation from Comparable Cities Alters Maize Yields

Average maize yield increased by as much as 29% (Fig. 3b-c, e.ii., Table 2.1) when the climatological average total SW and diffuse fraction at Madrid, New York, or Cairo, which have lower average PM concentrations than Beijing, are applied across the NCP. Conversely, when light conditions from Delhi are applied, average maize yields remain virtually unchanged. We ascribe these effects to the combination of the magnitude and seasonality of changes in SW and diffuse fraction at each city (see Fig. 5 below).

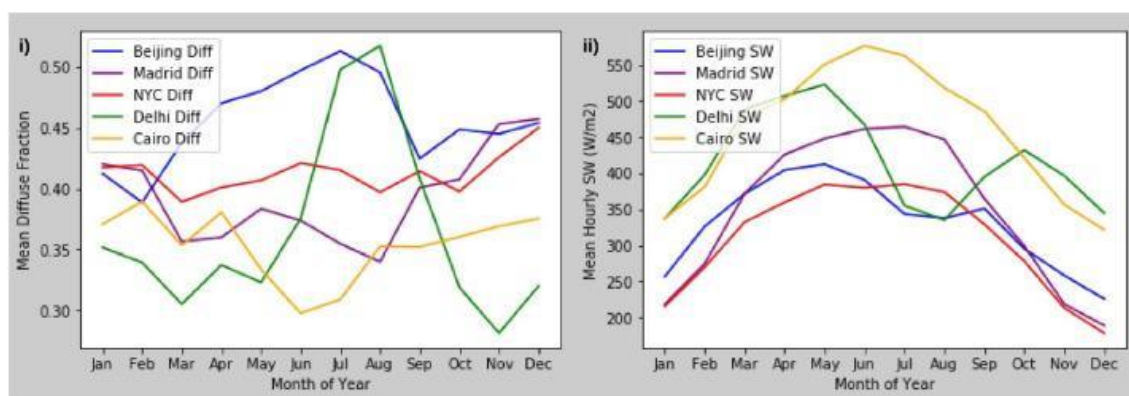


Figure 2.5. (i) Average monthly diffuse fraction for Beijing, Madrid, New York, Delhi, and Cairo. (ii) Average hourly downward SW radiation per month for Beijing, Madrid, New York, Delhi, and Cairo.

Heavy cloud cover associated with the Indian monsoon reduces total SW in Delhi in July and August (Fig. 5.i.). Although partially compensated by a large increase in diffuse fraction, the net effect is still a reduction in maize yields across the NCP. The higher SW and lower diffuse fraction seen during the rest of the year do not fully

compensate the changes in light profile during this critical period. Whilst the changes at Delhi are driven by seasonal increases in cloud cover, modelling studies suggest that despite the increase in wet deposition from increased rainfall in this time period, anthropogenic and natural aerosol do contribute to the reduction in total SW (Kuhlmann and Quaas, 2010). This reduction during the period corresponding to the early and late reproductive phase has a greater impact on maize yield than the higher SW during the rest of the growing season, in line with the results from our development stage simulations. Results presented in the wider literature suggest that reductions in light intensity on the NCP during late summer may result from PM-linked haze events (Chameides et al., 1999; Zhou et al., 2019). Reducing aerosol pollution at this time of year would therefore increase light intensity for crop photosynthesis. Interventions during less developmentally critical stages may have smaller effects than a similar magnitude of intervention carried out during the early crop reproductive stage.

2.4.3 How PM might Change Radiation in the Future

Despite similar annual mean PM concentrations in Madrid and New York (Karanasiou et al., 2014; Peltier et al., 2011), there are large differences in yield between simulations driven with SW and diffuse fraction from Madrid (MAD_Diff_SW) and New York (New_York_Diff_SW). This yield gap is the result of ~20% higher mean SW in Madrid than New York during the growing season (Fig. 5) which is driven by differences in meteorology, including cloud cover, between the two locations. The meteorology of the NCP encourages formation of fog as well as haze, driven by the high relative humidity (Quan et al., 2011; Gao et al., 2015; Yang et al., 2020). Given the higher average ambient SW at Madrid than in the NCP throughout the entire year, it is likely that yield increase is not solely attributable to PM, and that reduced NCP PM concentrations would result in more modest yield gains than those seen in MAD_SW_Diff. Given New York's more comparable SW profile during the growing season, excepting the critical months of July and August, application of New York SW and diffuse fraction (New_York_SW_Diff) may provide a more realistic future scenario for the NCP if July and August AOD could be reduced through reductions in PM concentrations. Though such increases would be relatively small, as differences in daylength and cloud cover have more substantive effects, the 3% rise in yields seen for New_York_SW_Diff would equate to a gain of approximately 8Mt. of maize nationwide,

sufficient to offset the maize annually imported by China (FAOSTAT, 2020), so increasing both national and global food security while increasing economic well-being of NCP farmers.

Contrastingly, if PM pollution intensifies across the NCP during the late vegetative or early reproductive phase, yields may further decline. As seen from simulations using Delhi SW and diffuse fraction, the drop in light intensity during July and August reduces yields, despite a ~ 12% higher average growing season SW in Delhi than Beijing. Although Delhi's annual decrease in light intensity during DEV3 is mainly attributed to cloud cover, two key lessons can be learnt from the case of Delhi. Firstly, if reductions in SW radiation, similar in magnitude to the seasonal reduction in SW seen in Delhi, were to occur in the NCP, it would be detrimental to crop yields in the region. Secondly, although reductions in SW radiation have most impact during DEV3, they also reduce plant growth at other development stages, as found in simulations DEV1_1.5 and DEV2_1.5. It is likely that increasing PM concentrations in Delhi and its surrounding regions have reduced crop yields in the Indo-Gangetic Plain in recent years (Burney and Ramanathan, 2014; Mina et al., 2018). Any reversion to higher PM emissions on the NCP would likely have a similar effect.

Furthermore, the Delhi and New York simulations demonstrate that reductions in PM during the vegetative or late reproductive phases would likely have little impact on yields overall. Increased SW in Delhi, and decreased SW in New York during these time periods does not outweigh the impact of changes in SW during the early reproductive phase. The particular timing of changes in PM then, is especially impactful. Increased total SW during the crop vegetative stage or the late reproductive stage would not be sufficient to significantly increase yields if PM pollution remained high during the early reproductive phase. Similarly, we see in New York that elevated SW during the early reproductive phase may be sufficient to compensate, or even increase, yields if PM remained high at other times of year.

2.4.4 Comparison to Previous Studies

Our results highlight the key role of the timing of changes to PM pollution relative to crop development stage, while adding further evidence to a growing body of research describing the net negative impact of PM pollution upon crop yields. Whilst a number of

modelling studies suggest there exists an optimum diffuse fraction for growth and yield, we do not see this for the range of diffuse fractions realistic of those observed across the NCP. We attribute this to the strength of the non-linear negative relationship between diffuse fraction and total SW, and further link this to changes in AOD and PM.

The timing of changes in PM concentration, size distribution and composition is an understudied aspect of PM impacts on crop yield. We find that the effect from increased SW is greatest during the early reproductive stage, when crops allocate carbon to seed. Our analysis of light profiles from a range of city regions further emphasises the time dependency of PM impacts. This novel analysis stresses the need for targeted intervention by policy makers trying to achieve higher yields by reducing PM, and highlights the necessity of further field studies to characterise PM burden at times of year corresponding with the early reproductive stage for crops in different world regions.

2.4.5 Uncertainties and the Future of Maize Yields on the NCP

Factors other than light intensity and the ratio of diffuse to direct light influence crop production. To remove water stress, a key environmental stressor, as a confounding factor we assumed the region irrigated as reported to be the predominant practice (Yang et al., 2015). This assumption enables us to study light effects in isolation. Additional validation of modelled yields against reported harvests for the NCP would enable maize in JULES-Crop to be parameterised for region-specific maize varieties and agronomic practice, e.g., irrigation regimes and crop losses during harvesting, increasing confidence in our model projections of actual yield. Whilst JULES-crop includes a general parameterisation for crop response to changes in the diffuse fraction of SW radiation, future research is required to establish the specific response of a maize canopy. However, given the dominance of the impact of changes in SW on crop yields over changes in diffuse fraction seen here, we would expect only minor changes in projected crop loss as a result.

Similarly, our analysis relies upon the strength of the reanalysis data provided by ERA-5. Whilst a significant proportion of these data are model- rather than observation-derived, this dataset represents a significant step forward from similar reanalysis datasets (Copernicus Climate Change Service (C3S), 2017; Urraca et al., 2018), and

provides radiation data comparable to satellite retrievals. A recent review identifies an underestimate of diffuse light by ERA-5 compared to some satellite retrievals (Jiang et al., 2020) but the sparse ground measurement sites used within that study demonstrate the need for large-scale reanalysis data to be used for modelling studies addressing a large geographical region. Only two ground stations used by these authors lie within our model domain. Given our use of climatologically averaged data to drive our model, we feel confident that the ERA-5 dataset represents the most useful assessment of surface radiation for our purposes and is suitable for use over the geographical and temporal scales of our simulations.

A positive contribution from diffuse radiation to plant photosynthesis rates has been well documented for tree species (Roderick et al., 2001; Niyogi et al., 2004; Mercado et al., 2009; Kanniah et al., 2012; Rap et al., 2015), but the net impact on crop yields of increased diffuse fraction at the expense of light intensity is less well understood. We find that the decrease in total SW associated with increasing PM concentrations far outweighs any possible fertilisation effect of increased diffuse fraction. Breeding programmes have already delivered substantial increases in leaf angles in the upper canopy of maize, increasing light penetration to the lower canopy such that maize might be expected to benefit less from diffuse light fertilisation than tree species (Hammer et al., 2009; Zhu et al., 2010). We find that the decrease in total SW associated with increasing PM concentrations far outweighs any possible fertilisation effect of increased diffuse fraction. Elevated PM during the early reproductive stage (i.e., flowering and pod filling) would be particularly detrimental to crop development, with a 50% increase in diffuse fraction during this period reducing yield by an average of 37% due to the accompanying reduction in SW. Information on the average timing of this stage could facilitate policy makers to develop air pollution limits that change throughout the year and have a more scientific basis.

Although cloud cover plays a greater role in the attenuation of SW radiation than PM, our analysis of AOD and total cloud cover demonstrates that aerosol contributes a third of the observed change in SW. Our sensitivity analyses based on light intensity and diffuse fraction over New York suggests that an increase in maize yields of up to 3.5% may be realistic for NCP if PM concentrations were to be reduced to those of New York. This will, however, depend on the concomitant changes in particle size and composition,

which further affect the relationship between diffuse fraction and total SW, and which require fuller investigation for future emission reduction scenarios.

One of the largest causes of uncertainty over future maize yields on the NCP is the interaction of PM and ozone pollution. As PM pollution has decreased in the NCP, ozone pollution has increased (Zeng et al., 2019), and while this principally reflects a reduction in NO_x emissions, it has also been partly attributed to increased light intensity increasing the rate of photochemical formation of ozone (Li et al., 2019). Elevated concentrations of ozone were estimated to have decreased maize yields across the USA by ~10% between 1980 and 2011 (McGrath et al., 2015). Yield gains from reductions in PM pollution in the NCP may therefore be offset or outweighed by losses due to rising ozone concentrations, and it will be critical to determine how the two interact. It is imperative that future emissions reduction strategies address PM and ozone pollution together.

Chapter 3: Quantifying the Impacts of Particulate Matter Deposition on Global Cereal Yields

At time of thesis submission, this chapter is in preparation for submission to *Global Change Biology*

Contribution statement:

The candidate's contribution was in the: conceptualization of the project; the development of the methodology used; the investigation of the research question; formal analysis of all data; interpretation of data; writing of manuscript for supervisor review; co-ordination of co-author feedback.

Abstract

Recent field studies have found that Particulate Matter (PM) deposition can threaten cereal crop yields, but the global impact that this has on crop yields is unknown. In this study, we simulate the effects of PM deposition on spring wheat, maize, and rice yields at a global scale using our newly designed and modified version of the Joint UK Land Environment Simulator (JULES) crop model.

We find that PM deposition results in average annual global losses of ~1% for maize and rice, and 0.2% for wheat between 2015-2020, but these losses vary considerably between countries. Crop yields in India and northern China were found to be particularly affected by PM deposition, with average yield losses of up to 2.4% and 1.2% respectively. Individual highly polluted locations in the most productive areas of both countries suffered losses over 8%.

These yield losses have implications for regional food supply. We attribute differences in losses for different species to the relative removal rates of PM from crop leaves, relative exposure during the most sensitive crop development periods, and exposure to particular components of PM. In China and India, we identify black carbon (BC) as a disproportionately impactful component of PM, making up <1% of growing season PM flux, but accounting for up to 56% of yield losses.

We find that if the levels of PM currently found in the most polluted areas of India occurred more widely across the entire nation, then crop yield losses could reach as high as 20%. Our work highlights the need to mitigate aerosol and aerosol precursor emissions before they further impact crop yields in industrialising nations.

3.1 Introduction

Increasing incidence of drought and intense heat threaten human health and crop yields across the globe (IPCC, 2022). Both are driven by global heating, whereby increased levels of CO₂, largely emitted from fossil fuel combustion, increase the ambient temperature through the greenhouse effect. As well as driving climatic change, fossil fuel burning causes severe surface level air pollution events. Primary particulate matter (PM) produced from combustion processes, along with the secondary PM formed as primary PM evolves within the atmosphere, has well-documented effects on human health (see e.g., Kim et al., 2015). Policy makers across the world have therefore taken action to reduce PM concentrations in urban areas. However, very little attention has been paid to the impact of PM pollution on crop yields, despite a number of studies implicating PM pollution in agricultural yield losses across the world (Zhou et al., 2010, Burney et al., 2014, Wolffe et al., 2021).

Most existing research into the impacts of PM on crops has focused on the indirect effects of airborne PM aerosols. By intercepting incoming photosynthetically active radiation (PAR), it is likely that PM limits crop yields in affected areas (Alton, 2008; Greenwald et al., 2006; Niyogi et al., 2004; Strada et al., 2015). One recent study estimated that airborne PM may be responsible for up to 8 Mt (3%) of maize yield losses across China (Wolffe et al., 2021). However, this is not the only mechanism by which PM limits PAR interception by crops. When PM is deposited out of the atmosphere, it can accumulate directly onto leaf surfaces. This creates a physical barrier to PAR interception, which a number of small-scale *in vivo* studies have found to cause yield losses of up to 7% (Hatami et al, 2017, Mina et al., 2018, 2021). However, to the best of our knowledge, the scale of regional and global yield losses directly attributable to PM deposition has not yet been investigated. Evidence is therefore lacking for the sensitivity of key crop species to PM, or what their critical exposure thresholds may be.

One landmark small-scale study into the effect was conducted by Mina et al. (2018). This pot-based trial examined the effect of PM on rice plants on the IGP, where ~50% of all food is produced in India. Levels of PM_{2.5} (PM up to 2.5 µm in diameter) across the IGP are recognised as excessive, and regularly exceed the Indian National Ambient Air Quality Standards for human health of 60 µg m⁻³ in a 24hr period (Mina et al., 2018; U Mina, R Singh, 2013), which is itself well above that set by WHO (5 µg m⁻³).

Mina et al. (2018) reported that high ambient concentrations of PM (88–311 $\mu\text{g m}^{-3}$) during the trial period reduced rice yield by as much as 7%. This study also observed the amplification and reduction of these yield losses under lesser or greater levels of rainfall, as is discussed in Chapter 1, section 1.3.

Field trials in the same area reported an even greater reduction of wheat yield (up to 23%), due to the combined effects of airborne and deposited PM (Sharma et al., 2021). Given India's domestic reliance on food production from the IGP, reductions in yield in this region threaten the national food supply, while improvements in yield could improve food access for millions of people.

Many agricultural areas suffer similar levels of PM pollution. For example, the NCP is one of China's most important crop-growing regions, accounting for 75% of China's maize and 35% of its wheat production (Meng et al., 2012). This area includes the three most highly populated municipalities in China (Shanghai, Beijing, Tianjin) and suffers significant air pollution. PM concentrations are high throughout the year, with annual averages of $108 \pm 34 \mu\text{g m}^{-3}$ recorded for Beijing city region between 2013-2017 (Zhai et al., 2019). While no experimental studies of the impacts of PM on edible crops have been conducted in the region, cotton yields in north-western China were observed to drop 28% due to the deposition of PM₁₀ (PM up to 10 μm in diameter; Zia-Khan et al., 2015). This demonstrates the potential magnitude of the effect of particulate pollution on yields of food and fodder crops.

A modelling approach to this phenomenon can explore these effects at a larger scale. This can provide policy makers with a scale estimate for crop losses to PM deposition, and highlight avenues of future research to the wider scientific community. One modelling study was conducted by Bergin et al. (2001) to examine the impacts of water insoluble PM on crop productivity in the Yangtze River Delta, finding yield reductions of tens of percent. This work provides a useful theoretical mathematical framework for examining this phenomenon, but requires improvements in order to include the effects of soluble PM components, and to work with modern multi-canopy crop models which develop over a full growing cycle.

Our paper builds on these previous studies considerably further to explore the potential magnitude of the impact of PM deposition on crop yield at a global scale. To

simulate these effects, we incorporated PM deposition to leaf surfaces into the Joint UK Land Environment Simulator crop (JULES-crop) model. We applied our model at the location of the *in vivo* study reported by Mina et al (2018) to demonstrate the efficacy of our parameterisation, and assess the accuracy of our model's simulated changes in yield. We then conducted global scale simulations to determine the relative reductions of photosynthesis, carbon accumulation and final yield of three globally important cereal crops: rice, spring wheat and maize due to the deposition of PM_{2.5}.

We further explored the simulated reductions in yields across the worst affected areas of China and India to identify the key factors governing the impact of deposited aerosol on crop productivity. Based on our findings, we suggest further experimental investigations needed to better understand the mechanisms of PM deposition, accumulation, and removal, and to quantify the resultant yield reductions.

3.2 Materials and Methods

3.2.1 Model Parameterisation

All simulations were carried out with a modified version of the Joint UK Land Environment Simulator crop model (JULES-crop) version 5.4. JULES-crop has previously been demonstrated to successfully reproduce maize, rice, and spring wheat crop yields at specific sites. JULES also has skill in reproduction of interannual global yield variability for maize and rice, comparable to the changes in radiation experienced under different PM deposition scenarios. (Mathison et al., 2021; Osborne et al., 2015; Williams et al., 2015, Williams, Harper, et al., 2017). The skill and limitations of JULES in calculating interannual variability is discussed further in Chapter 1, section 1.5. The crop parameters for spring wheat and rice were taken from Osborne et al. (2015), and for maize from Williams et al. (2017).

All simulations were conducted on a 0.25° grid at hourly temporal resolution. Meteorological driving data of downward short-wave radiation, downward long wave radiation, 2 m air temperature, precipitation, specific humidity, surface pressure and windspeed were downloaded from the European Reanalysis 5th Generation (ERA-5) dataset for 2015-2020 at 0.25° spatial resolution and with an hourly timestep (Hersbach et al., 2018). Land cover for all gridded simulations was taken from MODIS AQUA-

TERRA product MCD12C1 at 0.05° resolution and regridded to 0.25°. Crop distribution, irrigation and most likely sowing and harvest dates were taken from Iizumi et al. 2019. This was done following the methodology used in Wolffe et al. (2021) and Osborne et al. (2015). Irrigation is turned on for all cells to remove extraneous variables when studying the impacts of PM on these crops. By including varying soil moisture this would add complexity to the interpretation of these results. This does make our results less comparable to real world yields, but facilitates an easier interpretation of model output.

Unless otherwise noted, PM deposition fluxes were taken from MERRA-2 reanalysis product M2T1NXADG (GMAO 2015) by combining the dry deposition flux of black carbon (BC), organic carbon (OC), sulphates, sea salt, and mineral dust. The sum of these fluxes is referred to as bulk PM throughout the rest of this chapter. Bulk PM was regridded to a 0.25° grid by bilinear interpolation. The fraction of total PM which is BC is taken from the same MERRA-2 reanalysis product. These PM data have been used in a range of studies, and the concentrations and fluxes of PM components independently reviewed and found to be in good agreement with observational data (Qin et al, 2019; Yao et al, 2020).

For this study we incorporate a new module into JULES, describing PM deposition and accumulation to the leaf surface, and the resulting reduction in light transmission and photosynthesis. We apply our modified version of JULES-crop to carry out all simulations in this paper. We describe the details of our new module in Section 2.2 below. The carbon allocated to the harvestable portion of the simulated crop was converted to yield in dry t ha⁻¹ following established methodologies (Kimball et al., 2019; Williams, et al., 2017). Yield losses from PM deposition are evaluated by comparing simulated yields with PM deposition to model yields from identical simulations without PM accumulation switched on.

3.2.2 Model Description

3.2.2.1 Driving data and baseline simulation

We enhanced JULES-crop to include the deposition of PM aerosol to crop canopies, and simulate the resulting reductions in PAR transmission to the leaf surface.

Our methodology is based upon Bergin et al. (2001b), with modifications to account for the accumulation of particles to the surface of crop leaves throughout a 10-layer canopy.

The total mass of aerosol per unit area, $PM_{i,t}$, ($g\ m^{-2}$) accumulated to each canopy layer, i , for $i = 0-10$ (where layer 0 is the top of the canopy), is calculated at each timestep, t , as:

$$PM_{i,t} = PM_{i,t-1} + ((FT_t - \sum_{j=1}^{i-1} FM_{j,t}) / clai_{i,t}) * (LAI_{t-1} / LAI_t) * \Delta t \text{ (Eqn. 1)}$$

where FT_t is the total PM flux to the grid cell for timestep t (or, if unavailable, calculated as the atmospheric concentration multiplied by deposition velocity), $\sum_{j=1}^{i-1} FM_{j,t}$ is the total PM flux for timestep t between canopy layer $i-1$ and the 1st canopy layer ($g\ m^{-2}\ h^{-1}$), $clai_{i,t}$ is the leaf area index of canopy layer i , LAI_t is the total leaf area index of the crop plant at timestep, t , and LAI_{t-1} at the previous timestep. Accumulated PM is assumed to be evenly distributed across all of the leaves within a canopy layer. Whilst this may not be truly reflective of reality given the interaction between local meteorology with the crop canopy, this assumption is required to facilitate model use on the scale required for a global assessment of impacts. Meteorological and deposition variables are not available at a high enough spatial resolution to model this phenomenon at a finer scale. This is illustrated in Figure 3.1

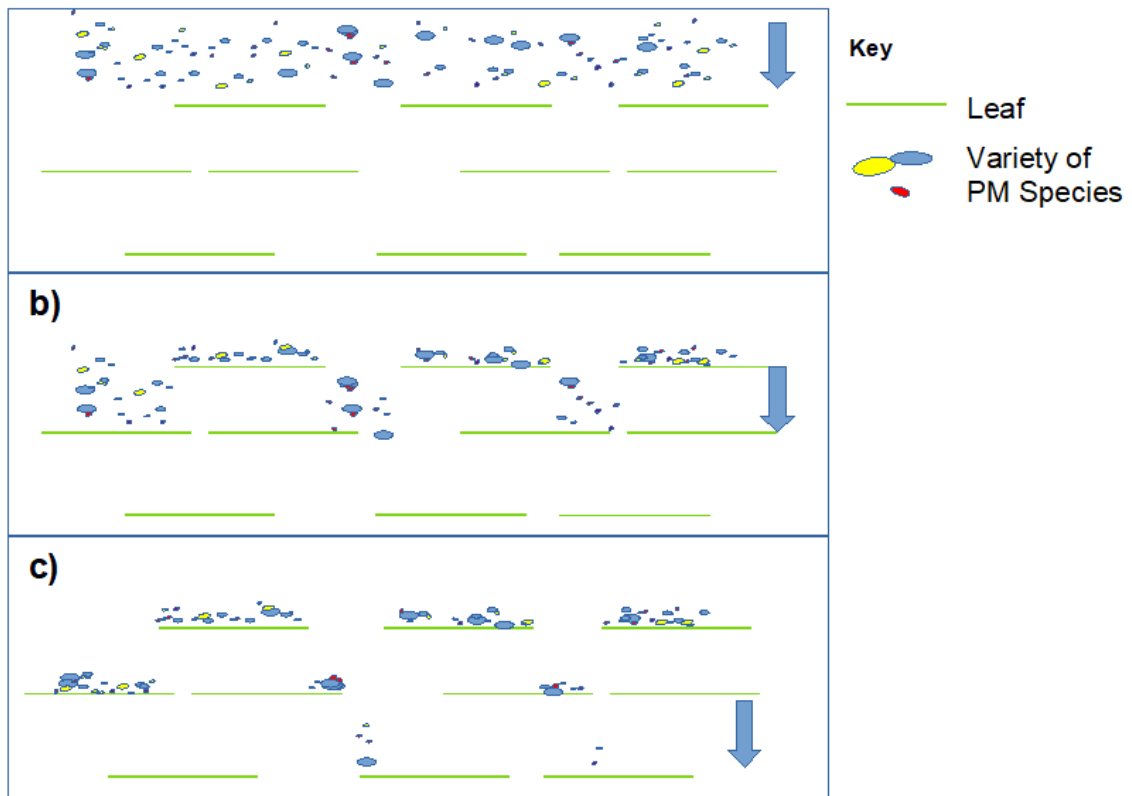


Figure 3.1 Illustration of PM being deposited across canopy layers. (a) bulk PM (FT) reaches the upper canopy level (level 0). (b) PM passes through gaps in the previous canopy layer ($i-1$), and accumulates to the subsequent canopy layer (i). (c) shows this process repeating for further canopy layers until all PM is deposited or all layers are exhausted whereupon remaining PM is presumed to have passed through the entire canopy.

We then calculate T_{PAR} , the fraction of PAR transmitted to the leaf through the layer of deposited PM, based on the mass absorption and mass scattering coefficients of the particles (E_{abs} and E_{scat} respectively) and the fraction of incident radiation which is up-scattered, β . We calculate E_{abs} ($m^2 g^{-1}$) according to:

$$E_{abs} = MF_t \text{ (Eqn 2)}$$

where M is the mass absorption efficiency of black carbon (BC), here taken to be equal to $8.6 m^2 g^{-1}$ (Bergin et al., 2001b, Xu et al., 2002), and F_t the fraction of aerosol that is BC at time t . E_{abs} thus varies both spatially and temporally. BC is thus assumed to embody the totality of light absorbance from deposited PM, as in Bergin et al 2001. This

simplification is used because of the high proportion of bulk PM light absorbance embodied by BC in a number of field studies (Costabile et al., 2013; Kirchstetter et al., 2004, López-Caravaca et al. 2022). Further discussion of the role of BC is seen above in Chapter 1, Table 1.1. $TPAR_{i,t}$ is then calculated as:

$$TPAR_{i,t} = 1 - PM_{i,t} (E_{abs} + E_{scat} \beta) \text{ (Eqn. 3)}$$

We take $E_{scat}=4.0 \text{ m}^{-2} \text{ g}$ and $\beta=0.27$, based on Xu et al. (2002). Canopy layer PAR interception is then integrated by JULES-crop to the whole plant. The workflow of the calculations above is outlined in Figure 3.2 below.

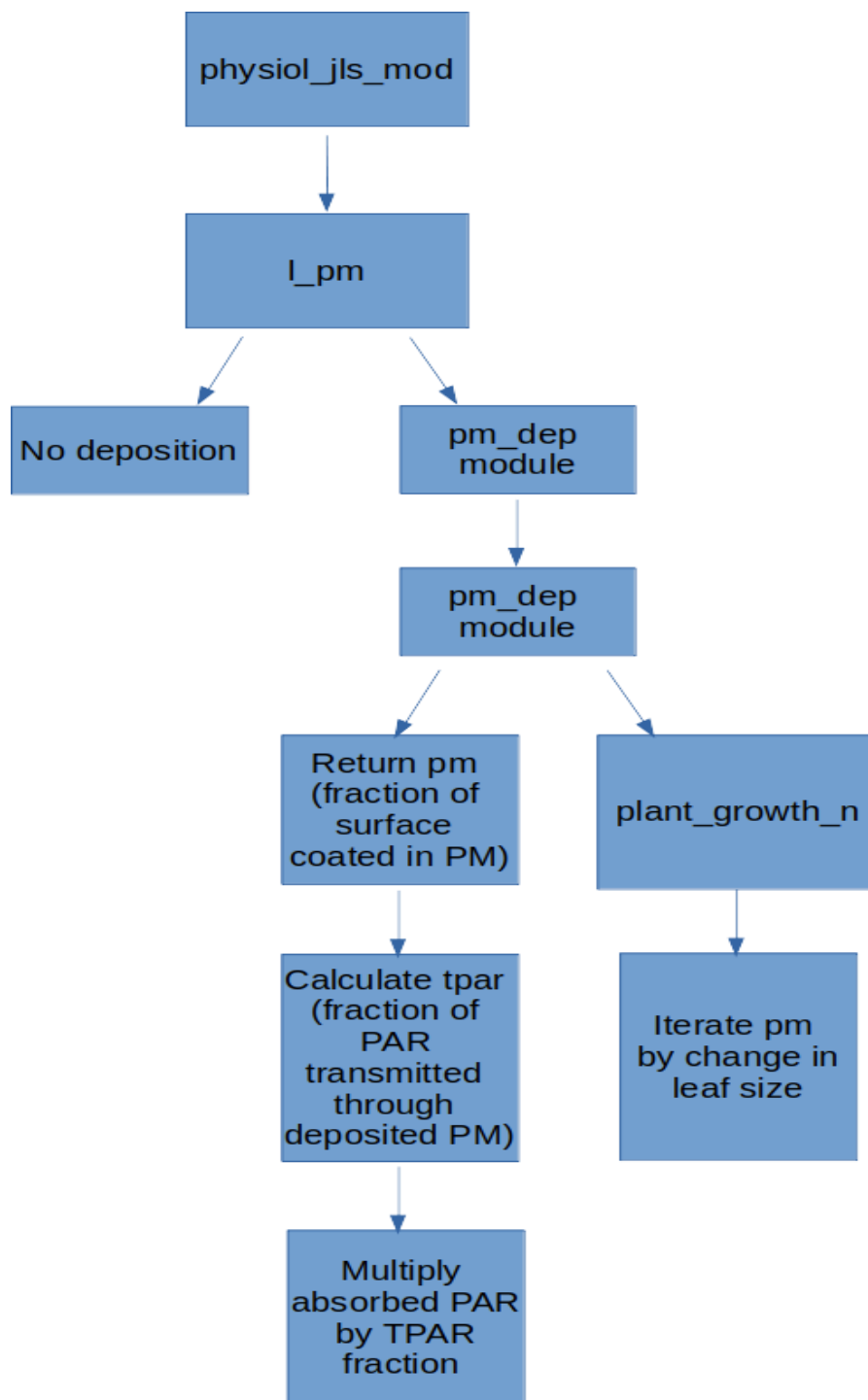


Figure 3.2 *Illustration of PM deposition workflow within JULES simulations.*

It should also be understood that introducing a new driving variable in PM flux introduces new model uncertainties. Simulation outputs are only high quality with high quality input. The MERRA-2 data used to drive these simulations is a well-regarded and

generally well-performing dataset, but it does not always replicate ground-based observations of aerosol optical depth, which are derived from simulated PM concentrations (e.g., Ansari, K., et al., 2023). Given variations between observed and simulated PM concentrations, further validation of the PM flux in MERRA-2 may be necessary to draw more concrete results from the interaction of simulated flux with simulated crops. This source of uncertainty may compound with the existing model uncertainties and simplifications outlined in Section 1.5, and render results less generally applicable to the real world. For example, the crop canopy is assumed to be uniform across large geographical areas and across different crop varieties, and planting density is kept constant across the entire simulated region. This is not true in reality, but is a necessary model simplification to facilitate large scale simulations. Further model improvements to facilitate more detailed site- or region-specific crop parameterisations were beyond the scope of this study, but would be essential for future work which refined this model.

Ideally model findings would be confirmed and validated against further *in vivo* experimentation before applying them to real world policy solutions, but lack of available evidence may preclude this. These results provide an indicative understanding of the potential scale of PM effects, and point the way towards fruitful avenues of potential research rather than acting as a firm projection of future PM impacts.

3.2.2.2 Removal by wind and/or rain

We assume that PM continues to accumulate on leaf surfaces until it is removed by rainfall or high wind. PM removal is here referred to as “wash off”. Few studies have measured or characterised the removal of accumulated PM from crop leaves under different rainfall intensity and duration, or different wind speeds. We explored a range of wash off thresholds and included three alternative scenarios of PM removal in our simulations.

Our “standard wash off” assumes all deposited aerosol with an aerodynamic diameter greater than $0.5 \mu\text{m}$ is removed at rainfall intensity of 5 mm hr^{-1} or higher which occurs for at least 20 minutes, based on studies of trees and wetland grasses (Xu et al., 2017; Yan et al., 2018; Zhou et al., 2020). There is little extant research regarding the removal of aerosol deposited on plant leaves by the wind. However, for flat solar panels, PM_{2.5} and larger particles have been observed to be removed at wind speeds above 5

ms^{-1} . We use a more conservative estimate, of roughly twice the force required for PM removal from a solar panel to account for the relative “stickiness” of foliage. Our standard wash off therefore assumes a windspeed of $>10 \text{ m s}^{-1}$ (Jiang et al., 2018; Zheng & Li, 2019).

We assessed the sensitivity of yields to the wash off thresholds using 1) no wash off and 2) an enhanced wash off. In “no wash off”, there is no removal of PM by wind or rain and PM thus accumulates continuously. This gradually reduces PAR interception to zero for the coated canopy layer. As our standard wash off mode likely underestimates removal rates for less ‘sticky’ foliage, we include “enhanced wash off”, whereby PM is still only removed by windspeeds above 10 m s^{-1} , but we assume that any rainfall event removes all deposited aerosol. Such assumptions facilitate regional and global scale “best-guess” simulations enabling an early approximation of global crop losses from PM deposition. Wash-off effects may vary substantially between varieties of the same species (Mina et al., 2018), and so results using this model should be seen as indicative of the scale of PM deposition impacts rather than a firm real-world estimate.

3.2.3 Simulations

3.2.3.2 Indian Agricultural Research Institute (IARI) Point Simulations

To evaluate our modifications to JULES-crop against an *in vivo* trial studying the effects of PM deposition on crop yield, we ran JULES in single-point mode for the grid cell corresponding to the latitude and longitude (28.64°N , 77.15°E) of the Indian Agricultural Research Institute (IARI) - the location of the study by Mina et al. (2018). No wash off and enhanced wash off were then simulated to generate an upper and lower bound of potential crop losses. All simulated yield losses were then evaluated against those observed in the study reported by Mina et al. (2018). Our simulations are conducted with the same sow and harvest dates as seen in the IARI study, but by virtue of our meteorological data embodying a 0.25×0.25 degree grid cell instead of the point values found at the IARI study site, some differences between simulation and reality are expected. Similarly, our enhanced wash off is driven by a lower threshold for rainfall intensity at which PM is removed – in the Mina et al., 2018 study, this is instead driven by additional manual leaf washing. Lastly, our no-washoff scenario is only a proxy for

Mina's enhanced deposition scenario where rainfall is prevented but windblown PM removal is still likely to occur. Our own simulation does not allow PM removal by any means. Despite these differences, this single site simulation gives a snapshot of the similarities and differences between our own simulated PM deposition and reality, and allows us to baseline how closely our simulated results are likely to be to reality given these caveats.

3.2.3.3 Global Simulations

Global simulations were conducted for an average year using a 6-year meteorological average, defined as the hourly ERA-5 driving data averaged between 2015-2020 for each grid cell across the globe. This aimed to identify the world regions where PM deposition is most detrimental to cereal yields under present day conditions, highlighting areas for further study and of potential importance to policy makers. These simulations use our standard wash off mode. All estimations of average yield for global simulations and regional simulations below exclude grid cells where crops did not pass emergence. As is shown below in Figure 3.6, there are long tails to the yield loss distributions for each simulation. Maximum values for colour bars are set to exclude these outliers.

3.2.3.4 Regional Simulations

The effects of PM on crop yields across the NCP and IGP were then explored in greater depth through a series of sensitivity tests. These simulations estimate upper and lower bounds for crop losses due to PM deposition, and determine the variables contributing most to the uncertainty in our estimated yield reduction. Interannual and spatial variations in yield for each of the three crops are assessed for 2015-2020 for each regional simulation.

Wash Off Sensitivity

We used our three wash off modes to explore the sensitivity of our simulated reduction in yield to our assumptions of wash off thresholds. We repeated our baseline simulations, which applied our standard wash off using two alternatives: no wash off and enhanced wash off as described in Section 2.2.2

PM Speciation Effects

Black Carbon (BC) is the primary light-absorbing component of PM; and is likely to have a disproportionately large impact on yields. To investigate the influence of the proportion of PM that is BC on estimated crop yield reductions we conduct a global simulation in which all aerosol is assumed BC. In this simulation, we set F to 1.0 in Eqn. 3. E_{abs} is thus equal to the mass absorption efficiency of BC, 8.6. We compare the estimated losses to those simulated in the baseline standard wash off scenario.

Alternative PM Scenarios

Substantial increases in PM concentrations are still being recorded in many parts of India (Vohra et al., 2021), and other industrialising nations, e.g., across sub-Saharan Africa (Aliyu et al., 2018). Further simulations were carried out to explore potential crop losses from increased PM levels on the IGP. We apply the high levels of PM observed at IARI (Mina et al., 2018) across the entire IGP, keeping all other driving data as before, and applying the standard wash off mode.

Although PM concentrations have fallen in China over recent years (Zhong et al., 2021) current ambient PM concentrations are approximately equal to those used by Bergin et al. (2001), although current day BC concentrations are less than 1/10th that of the early 2000s. We apply the levels of PM recorded on the Yangtze River Delta (YRD)YRD (Bergin et al., 2001) in our simulations for NCP to demonstrate the evolution of PM deposition related yield losses over the past 20 years. Lastly, we further explore the role of BC in PM deposition impacts by running both our IGP and NCP alternative PM scenarios with a BC fraction of 10%, as was assumed in Bergin et al. (2001).

3.3.3 Results

3.3.3.1 Indian Agricultural Research Institute (IARI) point simulations

Percentage reductions in rice yields simulated at IARI are comparable to those observed for this site in 2015 by Mina et al. (2018). Simulated yield losses reached 21.5% with no wash off, and nearly 20% for “standard” wash off. Mina et al. (2018) reported reductions of 14.9% for PB-1509 rice when rain was excluded from the trial plots, i.e., when no wash off occurred. “Enhanced” wash off, i.e., assuming any rainfall

removed deposited PM from the leaf surfaces entirely, resulted in simulated yield reductions of ~8.7% in line with the 0-11.7% fall recorded by Mina et al. (2018) under their enhanced PM removal conditions. Our standard wash off simulations for IARI appear to somewhat overestimate yield losses compared with observations, but this is most likely attributable to the considerably lower grid-cell average rainfall conditions found in ERA-5 simulations which were used to drive these simulations in JULES-crop (average of 5.5mm rainfall a day), as compared to the highly localised conditions of a small-scale pot plant trial (17mm rainfall a day) (Section 3.1).

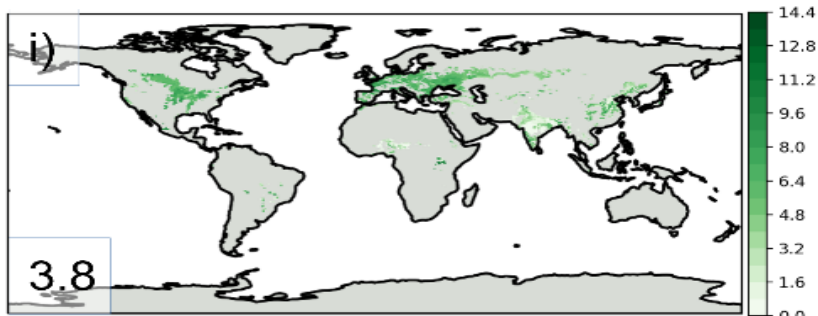
3.3.3.2 Global Simulations

Global simulations using our meteorological average show average global yield reductions of 0.9%, 0.8%, and 0.2% for maize, rice, and wheat respectively (see Figure 3.3 below).

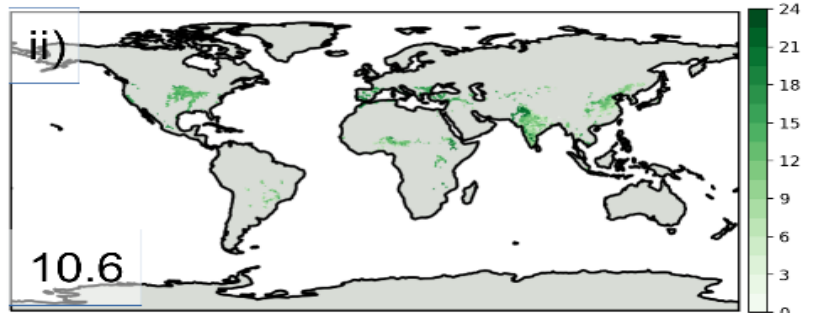
**Crop Yield 2015-20
Average Driving Data
(T Ha⁻¹)**

**Percentage Yield Reduction
under MERRA-2 PM Flux
and Standard Wash Off (%)**

Wheat



Maize



Rice

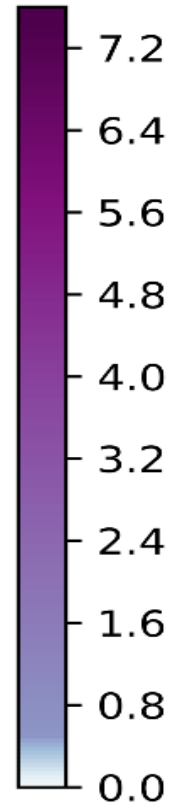
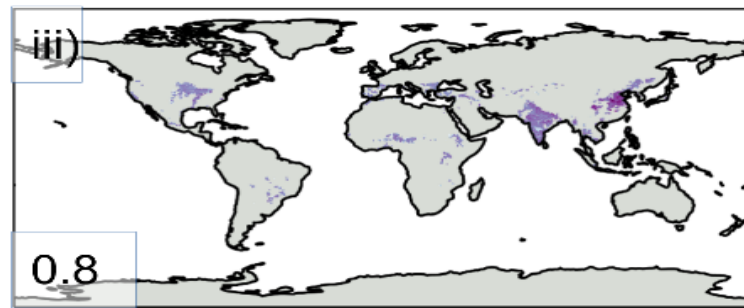
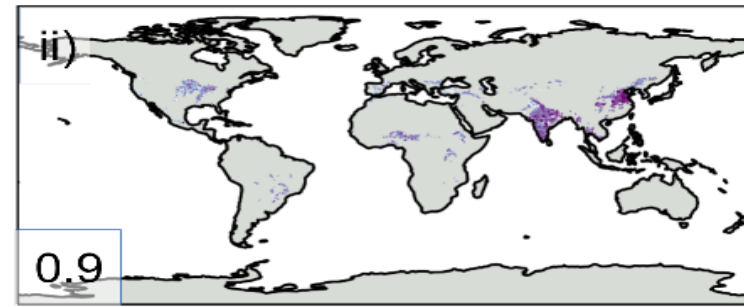
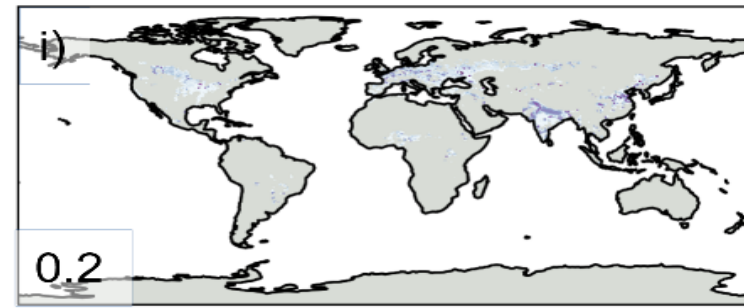
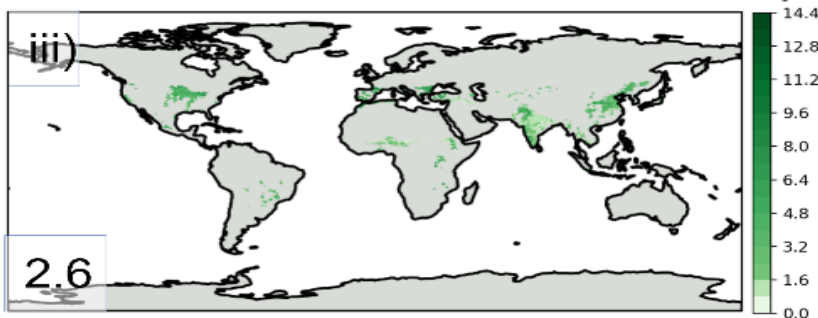


Figure 3.3. Simulated global yields ($t\ ha^{-1}$) for wheat (A,i), maize (A,ii) and rice (A,iii) using average of driving data from 2015-20, and average percentage yield reductions under MERRA-2 PM flux with standard wash off (B,i-iii)

Although these were low, losses in China and India were projected to be much more sizeable: over 8% for maize and rice on the IGP and NCP. This drove us to further investigate the impact of PM deposition in these two regions. Figure 3.4 below illustrates the action of the model at a representative site on the NCP with high levels of PM deposition, demonstrating both PM accumulation and removal alongside the effects of this on accumulated carbon in the harvestable portion. We see that whilst PM is on the leaf surface, we have a growing reduction in accumulated harvestable portion carbon compared to that seen in unaffected crops. When a wash-off event occurs, the harvestable portion begins to recover, until further PM deposition once more reduces carbon accumulation.

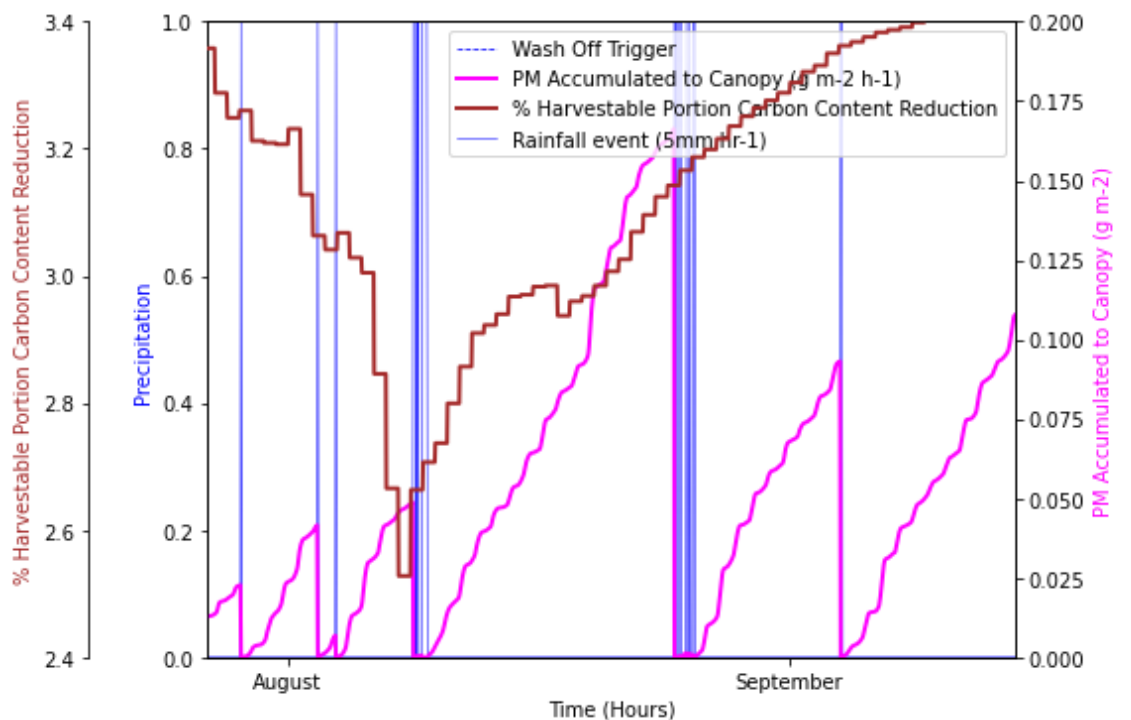
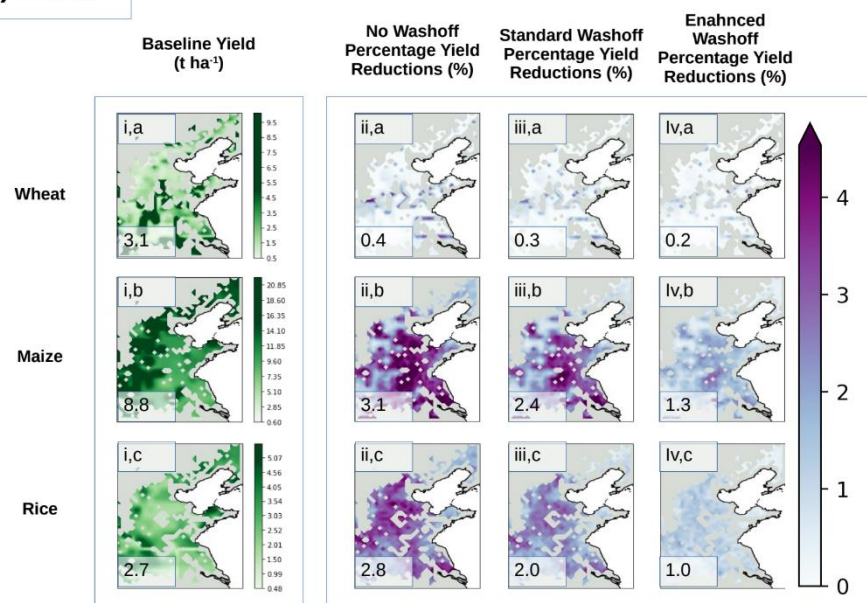


Figure 3.4. Reductions in carbon accumulated to the harvestable portion of a rice crop at a single point for a site in China over its development for 2015 under standard wash off vs precipitation and PM flux. Percentage reduction in carbon accumulated to the harvestable portion of the crop (in red) and accumulation of PM (pink) over time are shown alongside rainfall (blue).

3.3.3.3 Regional Simulations

Baseline Yields

A) China



B) India

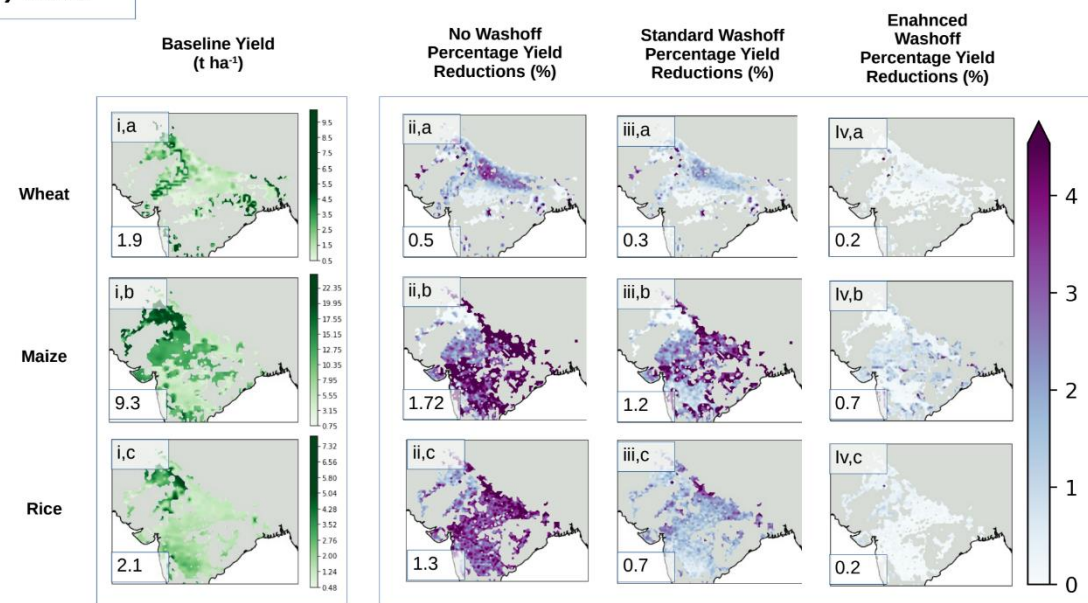


Figure 3.5. Average simulated yields (t ha⁻¹) for (a) wheat, (b) maize and (c) rice for 2015-20 in (A) China and (B) India. The first column shows baseline yields in the absence of PM deposition while the remaining columns show average yield reductions from this baseline for MERRA-2 PM flux and (ii) no wash off, (iii) standard wash off and (iv) enhanced wash off.

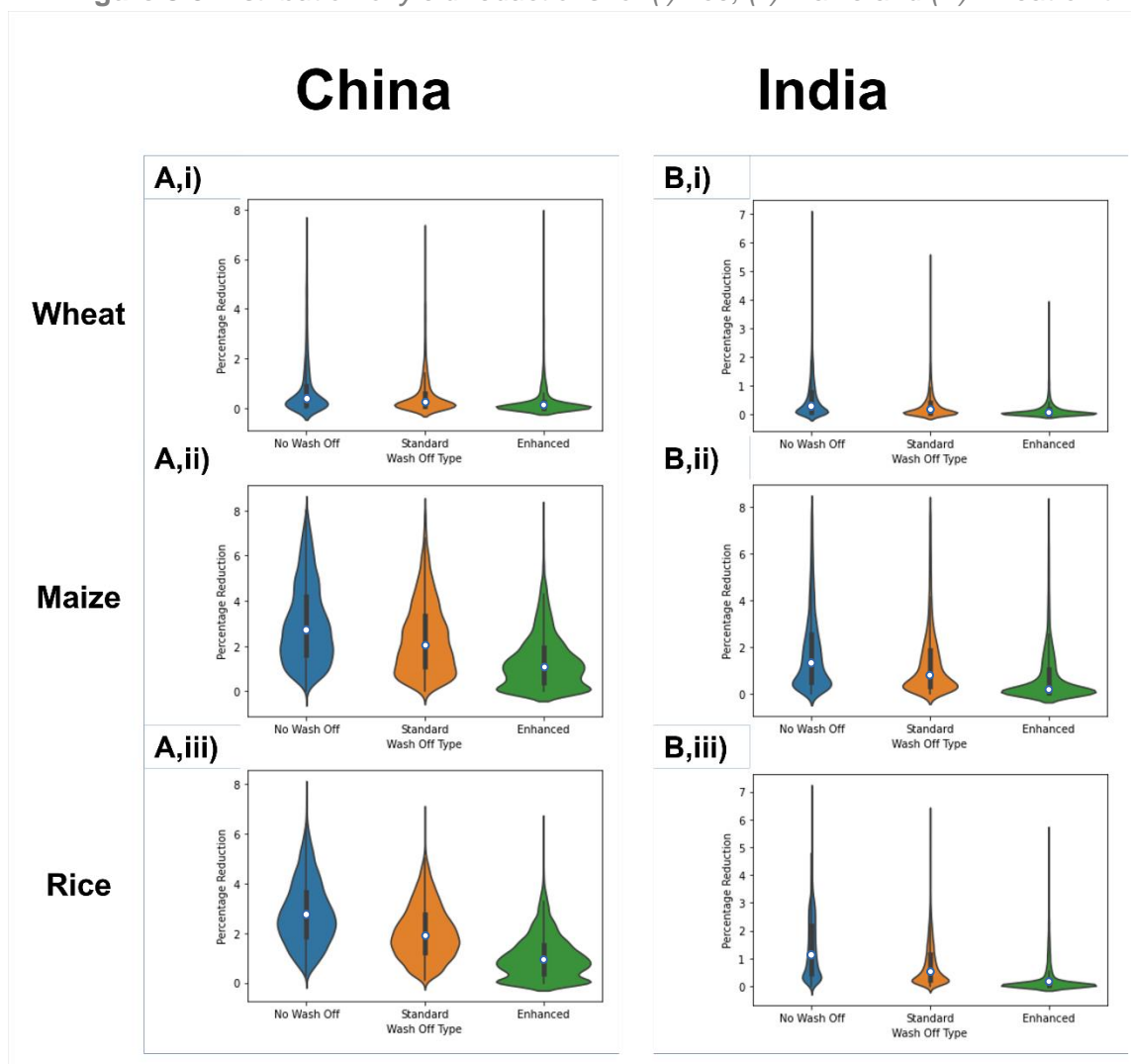
On the NCP, our average simulated yields for wheat (2.8 t ha^{-1}) are lower than the 5.7 t ha^{-1} measured by C. Lu & Fan (2013) whilst our 8.8 t ha^{-1} for maize are somewhat higher than the 5.8 t ha^{-1} reported by Hu & Zimmer (2013). Simulated rice yields (2.7 t ha^{-1}) are considerably lower than the China average of 6.95 t ha^{-1} (Crop Explorer - World Agricultural Production (WAP) Briefs - China and Taiwan).

In India, our simulated 2.1 t ha^{-1} of wheat is lower than the measured 3.5 t ha^{-1} (USDA, Retrieved June 16, 2022) whilst the 9.3 t ha^{-1} for maize is substantially larger than expected, with yields of 3 t ha^{-1} reported (USDA, Retrieved June 16, 2022). Simulated rice yields of 1.8 t ha^{-1} are somewhat below the recorded yields of 2.7 t ha^{-1} (India: Yield of Rice 1991-2021 | Statista).

This paper focuses on the percentage change for yields on the NCP and IGP after a given PM deposition perturbation. The JULES-crop model has some degree of skill in simulating global yields, , but its most important ability for this study is a strength in simulating the interannual variation of crop yields - accurately mapping the percentage changes expected under changing meteorological conditions (Osborne et al., 2015). It performs this task particularly well for rice and maize, though less well for wheat. Due to this performance, a heavier emphasis is given to the simulated outcomes for rice and maize over the minimal changes observed for wheat. For further information about JULES skill in modelling interannual variability, please see Chapter 1, section 1.5.

Here our average yields are within a factor of 2 of actual yields for all simulations, with differences that vary across the model domain. Given the results from previous studies using JULES-crop, and the above results for IARI, we believe that this model can be used to derive a useful first estimate of the potential percentage impact of PM deposition on regional crop yields.

Figure 3.6 Distribution of yield reductions for (i) rice, (ii) maize and (iii) wheat on the (A)



NCP and (B) IGP with PM deposition rates calculated from MERRA-2 PM concentrations for each of the “no” (blue), “standard” (orange) and “enhanced” (green) wash off regimes described in 2.1.2. Note that the mean value does not reflect the wide variance across each region in terms of yield loss, and that the violin plots have extensive tails highlighting the influence of more extreme local factors.

Whilst the average yield reductions shown in Figure 3.6 suggest only modest losses, it should be noted that reductions at some sites reach as high as 6-7 (Figures 3.3A, 3.4A). This is particularly evident for wheat, where despite small yield reductions at a majority of locations, some growing areas exhibit substantial and significant yield reductions of up to 8%. This illustrates the potential regional and global crop yield losses that could occur if PM emissions continue to rise in industrialising countries.

For both China and India, average simulated yield reductions were lowest for wheat. In China, the greatest losses in all wash off scenarios were for rice, whereas in India the greatest losses under standard and enhanced wash off scenarios were simulated for maize. The degree to which a particular crop is affected is attributable to a range of factors, including spatial and temporal variations in PM deposition and wash off events, and differences in the growing cycles of the three crops. These are discussed in detail in Sections 4.2 and 4.3 below.

We further observe that the differences in rainfall threshold between standard and enhanced wash off are particularly important for rice grown in China, and maize grown in India, where they substantially alter the distribution of yield reductions. While the differences in yield reduction between standard and no wash off, enhanced and no wash off, and standard and enhanced wash off may not be sizeable they are statistically significant for all crops (with p-values $\ll 10^{-3}$ for two-sample Kolmogorov-Smirnov (KS) test).

It is also important to note that the average reductions presented here mask large spatial variations across the simulated domains. While this is mostly related to variations in precipitation and wind speed, and hence wash off, there are a number of other potential explanations which we explore in Section 4.3.

BC-Only Simulations

Figure 3.7 illustrates the average PM and BC deposition fluxes derived from MERRA-2 reanalysis over an average growing season. This demonstrates the widespread nature of PM pollution across the model domain.

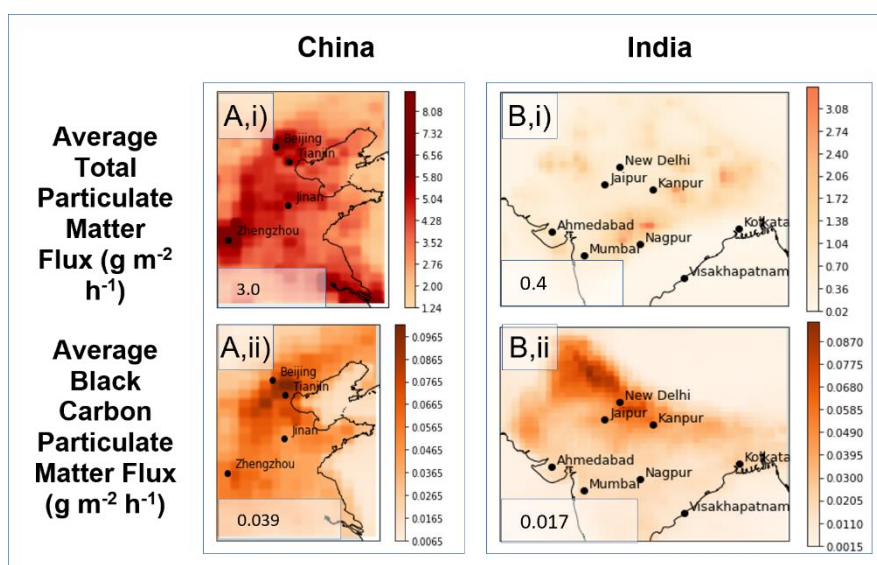


Figure 3.7. The average (i) PM and (ii) BC-only deposition fluxes over (A) China and (B) India for the 2015-2020 growing seasons.

For the average growing season (i.e., average values between sowing date and harvest date for 2015-2020), BC accounts for as much as a quarter of all PM-associated yield reductions across the NCP and over half of the losses on the IGP, despite only accounting for an average of up to 0.77% of total PM across the duration of the crop growing cycles in both domains. The absorption of light by deposited PM substantially outweighs the effects of less light absorbing PM. The effects of light absorbance are hard coded within our model (see equation 3), and are not substantially smaller than the effect of the light scattering part of the deposited PM impact. BC is here apportioned the entire light absorbing capability of deposited PM, but zero scattering fraction. The total effects are therefore heavily dependent on our model. The reasoning for this choice is seen in section 3.2.2.1.

Other light absorbing compounds, such as brown carbon, may also contribute to this fraction of yield reduction and potentially reduce this role for BC in yield reductions. This would not, however, change the total fraction of yield reduction attributable to the relatively small number of highly light absorbing particles found in bulk PM.

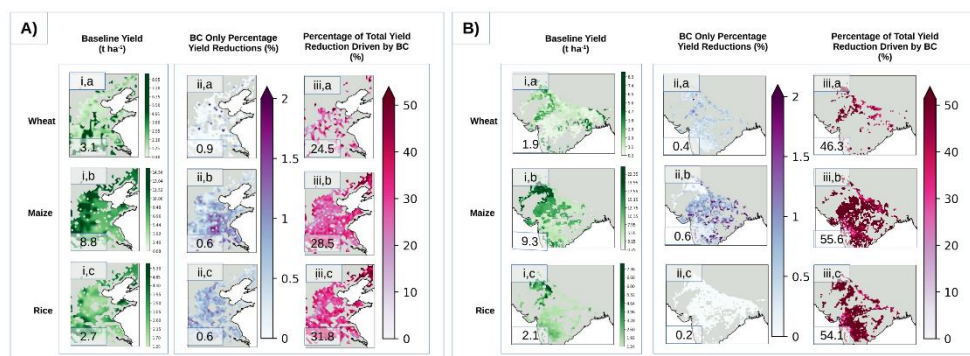


Figure 3.8. Average simulated yields ($t\ ha^{-1}$) for 2015-20 in (A,i) China and (B,i) India alongside (ii) average yield reductions from this baseline using MERRA-2 BC-only flux and (iii) the percentage of total PM-induced yield reductions due to BC.

Alternative PM Scenario

To explore the potential that increasing industrialisation, i.e., higher PM emissions in each of the IGP and NCP, would further limit crop yields in the future, we set PM fluxes to the highest levels recorded by Mina et al. (2018) and the levels used by Bergin et al. (2001), respectively. We kept all driving data other than the PM flux, BC percentage and resulting mass absorption coefficient, E_{abs} (see 2.1.1), unchanged.

For NCP, we set PM fluxes to the historic value of $0.612\ mg\ m^{-2}\ h^{-1}$ reported for the Yangtze River Delta by Bergin et al. (2001). These simulations, without wash off, result in comparable yield reductions to those found in the original regional simulations (see 3.3.1), despite the reductions in PM occurring over recent years in the NCP. If the fraction of BC is further elevated to 10% total PM, as reported in Bergin et al. (2001), then yield reductions are significantly higher than those seen in the present day. When the maximum PM flux recorded at IARI ($17.1\ mg\ m^{-2}\ h^{-1}$) by Mina et al. (2018) is applied to the entire Indian model domain, simulated yield reductions are substantially increased when compared against the baseline figures presented in Figure 3.5. This results in an increase from 1.2% to 11% for maize, 0.7% to 4.5% for rice and 0.3% to 7.1% for wheat (See Figure 3.9 below). Furthermore, if BC is instead set to the much higher levels seen in Bergin et al. (2001), then yield losses for all three cereal crops increase substantially, nearly doubling for maize, tripling for wheat, and quadrupling for

rice. These simulations provide an interesting window to understand the importance of future emission controls, and are further considered below.

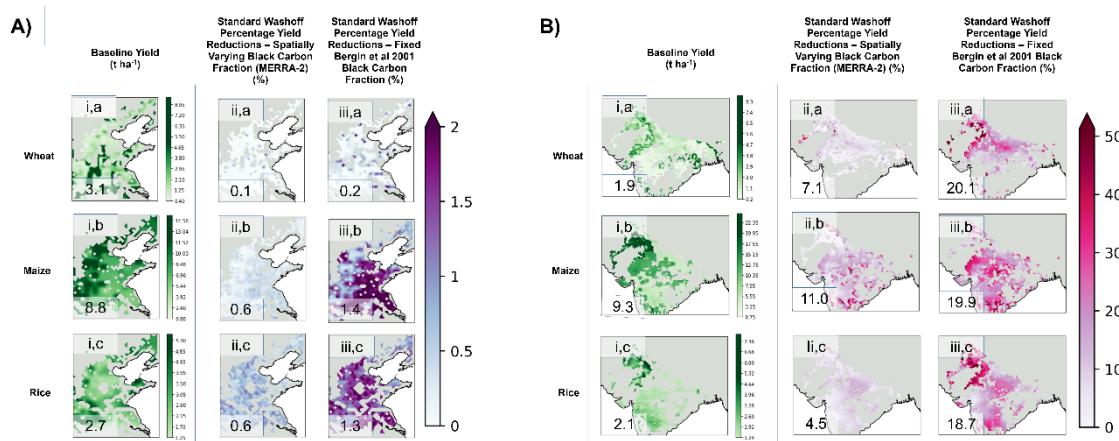


Figure 3.9. Average simulated yields ($t\ ha^{-1}$) for 2015-20 in (A,i) China and (B,i) India alongside percentage yield reductions from this baseline for alternative PM scenarios using (A) Bergin et al (2001) PM flux and (B) Mina et al (2018) PM flux, with (ii) fixed Bergin et al (2001) BC fraction and (iii) spatially varying BC fraction set from 2015-20 average (reductions for locations with successfully completed growing cycles).

PM prevalence during crop development and reproductive phases

Yield reductions resulting from unfavourable environmental conditions depend not only on the magnitude, but also the timing of these conditions (e.g., Pinto et al., 2020; Wolffe et al., 2021; Wollenweber et al., 2003). Here, maize yields are most affected by PM deposition (followed by rice and then wheat) across both domains. However, the total mass of PM, and the percentage, which is BC, deposited to wheat over the growing season is higher than for maize or rice for both India (an average $0.6\ g\ m^{-2}$ compared to $0.3\ g\ m^{-2}$ for maize and $0.1\ g\ m^{-2}$ for rice) and China (an average $2.6\ g\ m^{-2}$ compared to $1.5\ g\ m^{-2}$ for maize and $0.6\ g\ m^{-2}$ for rice).

The effect on yield is associated with the timing of PM deposition to leaves during the crop growing cycle. Experimental data has suggested that crop yields are considerably more sensitive to reduced PAR during the reproductive phase, when crops prioritise the allocation of carbon to the harvestable parts over further leaf, stem, or root

development (Dong et al., 2017; Yang et al., 2020). A crop that accumulates less PM during the reproductive phase is able to allocate a greater proportion of carbon to reproduction, i.e., setting of seeds, the harvestable portion of cereal crops. Figure 3.10 (below) summarises the total mass of PM deposited to each crop over their entire growth cycle, and the fraction of PM deposited during the reproductive phase.

As shown in Figure 3.10, PM deposition across both NCP and IGP is skewed through the crop growing cycles, with Chinese wheat receiving 28.1% of total deposited PM during its reproductive phase, compared to 29.1% for maize and 23.4% for rice. In fact, in India wheat receives an average 14% less PM deposition than maize during their respective reproductive phases. In China, more PM is deposited to wheat during its reproductive phase, but the distribution of wheat across the model domain means that wheat receives significantly higher rainfall in this period than rice, reducing PM accumulation.

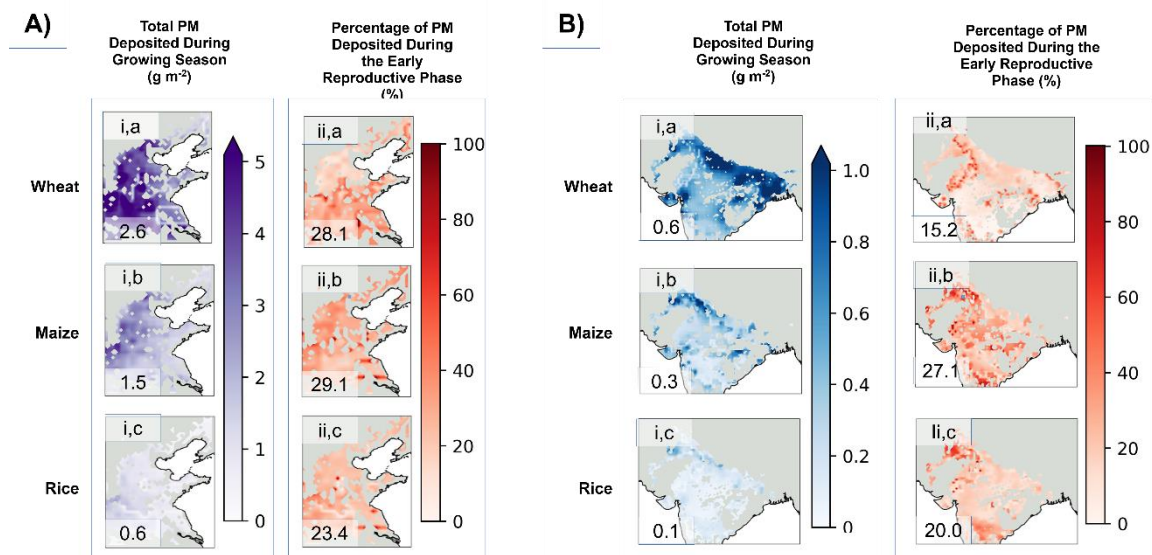


Figure 3.10. Total PM deposited to each crop during their growing season in China (A,i) and India (B,i), alongside the percentage of that PM which is deposited during the reproductive phase (ii). The figure in each panel shows the domain average PM deposition over the growing season

3.4 Discussion

Particulate matter (PM) is a ubiquitous air pollutant well known to affect human health (Kim et al., 2015). It is now increasingly understood to impact crop yields (Alton, 2008; Bergin et al., 2001a; Greenwald et al., 2006; Niyogi et al., 2004; Strada et al., 2015). Deposited PM is responsible for direct reductions in PAR transmission to the leaf surface, and is an important but often overlooked mechanism by which PM affects crop yields. It is vital that we fully understand the threat posed to food supplies by this pollutant so that such risks can be mitigated. Here we clarify the magnitude of yield reductions attributable to PM deposition, and the areas and crops most affected. This highlights the potential extent of the problem and points toward the most important emission-reduction measures required to reduce crop production losses.

3.4.1 Which world regions are most affected by PM deposition?

Global average yield reductions from PM deposition are below 1% (see Fig 2), but substantially larger impacts are observed between and across some key agricultural regions. For example, whilst PM deposition is projected to reduce maize yields over the United States of America by an average 0.39%, in India, average reductions for all crops are just below 1%, and spatial variation is high, with maize yield losses over 8% in highly polluted areas. Similarly, on the NCP average maize yields are reduced by 2.4%, more than double the global average, with peak losses of 8% found near the highly polluted megacities of Shanghai and Zhengzhou. Because of the significantly larger reductions experienced in China and India than elsewhere, further analyses focused on exploring the driving factors contributing to yield losses in these two regions.

3.4.2 Factors governing the magnitude of PM deposition crop losses

The intense economic activity in the North China Plain (NCP) region results in high PM concentrations and, hence, deposition rates. Our simulations suggest the decrease in light reaching the leaf surface due to PM accumulation resulted in average yield reductions of 2.4% for maize, 2.0% for rice and 0.3% for wheat across the NCP between 2015-2020 with these averages masking wide variation (see Figure 3.5). For example, rice yields in some areas close to megacities are reduced by as much as

4.5%, while losses are negligible in the northeast of the simulated area (see Panel Iiic of Figure 3.5A). The scale of yield losses is equally distributed between areas with high and low potential yield, meaning that all areas, whether they have high or low productivity, are equally likely to be affected by PM associated yield reductions.

The IGP in Northern India is also home to large economic and population centres, with high PM emissions from industrial hubs, transportation, and energy infrastructure. Here we see smaller average yield reductions, of 1.2%, 0.7%, and 0.3% for maize, rice, and wheat respectively under our standard wash off regime. However, the spatial variance is large for all crops. Highly polluted locations close to Delhi, Jaipur and Kanpur experiencing losses of up to 8% for rice and maize. Across both IGP and NCP, the spatial variation in losses are attributable to a confluence of local factors including variation in total PM, rainfall, wind speed and BC content.

The BC-only simulations outlined in Section 3.3.2 indicate that BC has a disproportionately high impact on crop yields . However, despite its key influence on the absorption properties of bulk PM, in our global and regional baseline simulations (presented in Sections 3.2 and 3.3) we find that increased BC content is correlated with smaller yield reductions for most crops. This appears to be driven by a negative correlation between average BC content and total PM flux, with higher BC concentrations generally occurring in locations with lower total PM concentrations. The exception to this relationship is Indian maize, where the larger levels of BC in the north of the study area coincide more strongly with the maize than the rice cropped areas (Fig 3.5.B.ii). BC therefore contributes more substantially to maize yield losses here than rice yield losses (See Figs 3.4.B,ii,b and c), with greater maize than rice yield reductions under standard and enhanced wash off regimes (see Fig 3.2.B,ii,b). If applying these results to observed reality, the impact from BC seen here should be interpreted slightly more broadly as representing the broader class of all light absorbing PM particles. These components appear to contribute an outsized impact on total yield reduction in our model, strongly implying that a heavy BC or brown carbon pollution event would limit crop yields. This is important for policy makers to note when permitting the installation of highly polluting industrial or energy generation facilities in close proximity to crop producing areas.

When interpreting these results for all crops, however, the relative skill of JULES in modelling the interannual variation attributable to changes in SW radiation is an important consideration. This skill, or lack thereof, informs the simulated effects of PM

deposition in our model. The parameterisation used here has been seen to capture interannual variation of yields skilfully for Indian rice (Osborne et al., 2015), and further work in recent years on the JULES-crop maize parameterisation has enhanced its performance (Williams et al., 2017). These results are likely to be closest to what would occur *in vivo*. Conversely, spring wheat in particular needs further work to validate these results, performing less well for this task in Osborne et al., 2015. This could partially explain the relative lack of change in wheat yields following PM deposition when compared to the other crops studied. Further experiments are required to tune the model to fully account for the impacts of PM deposition on crop yields.

3.4.3 Why are different crops so differently affected?

The other key driver of different levels of losses between the three cereal crops is the fundamental difference in their growth cycles. The life cycle of a crop species can be separated into three key stages: pre-emergence, vegetative, and reproductive. During the vegetative phase a crop devotes its carbon and energy resources primarily to growth and expansion. By contrast the plant ceases to put energy into growth during the reproductive phase, instead allocating resources to producing the harvestable portion of the crop.

Previous research has suggested that yields from a range of crop plants are most sensitive to environmental stress during the crop reproductive phase. For example, wheat and rice yields have been found to be considerably more affected by water stress during the reproductive phase, possibly due to higher water requirements (Farooq, M., et al., 2014; Pinto et al., 2020). Extreme heat during the early reproductive phase reduces wheat yields by up to 45%, although losses were reported negligible if the same heat event occurs later in the reproductive phase (Wollenweber et al., 2003). One pot trial found that wheat suffered up to 62% greater yield losses when combined heat and drought stress are applied during the early reproductive flowering stage than if these same stresses occur 21 days later during the late reproductive phase (Pradhan et al., 2012). Model simulations by Wolffe et al. (2021) also suggested that PM-associated changes in radiation reaching the canopy most strongly affect maize yields across the NCP when they occur during the reproductive phase.

The absolute and relative lengths and timings of the growth stages vary between rice, maize, and wheat. These, together with the sowing dates and distributions of each crop, govern the total PM deposited to the crop canopy during each growth stage. Figure 3.10 illustrates that rice experiences, on average, lower total PM deposition than either maize or wheat in both NCP and IGP, but that PM deposition is concentrated during its reproductive phase. Rice also spends the least time in the reproductive phase (40%) of the three crops, limiting the opportunity for wash off events to alleviate the rice crop of accumulated PM during this phase, further compounding the effect. In agreement with the research studies highlighted above which examined a range of yield perturbations, we find that PM deposition is most impactful during the early reproductive stage of crop development.

3.4.5 How substantial might the losses be in the future?

The alternative PM scenarios presented in Section 3.3.3 highlight how changes to PM composition and increasing concentration may limit future food production. Over the last 30 years, PM levels across China have changed dramatically. From 1990 to 2013, average PM_{2.5} concentrations increased ~50% (Lu et al., 2020), before declining rapidly. For example, in Beijing these peaked at 102 $\mu\text{g m}^{-3}$ in 2013, before declining to 32 $\mu\text{g m}^{-3}$ in 2022 (Statista, 2023). As a result, the PM fluxes recorded across the YRD in 2001 (0.085 $\mu\text{g m}^{-2}\text{s}^{-1}$) are only marginally higher than those seen across the NCP from 2015-2020. If PM fluxes were on par with those seen in the Yangtze River Delta in 2001 but with present-day BC concentrations, yield losses for maize, rice and wheat would be up to 75% smaller. However, with the BC concentration measured in YRD in 2001, yield reductions for both wheat and maize would only be 35-62% lower than in the present. This highlights both the work remaining in terms of reducing bulk PM concentration on the NCP, and the extent to which PM chemical composition can change the impacts of PM upon crop yields.

However, if PM levels were to increase across the entirety of the IGP to those observed at IARI by Mina et al. (2018), maize yields would fall by 11%, and rice by 4.5%. As crops from the IGP feed ~40% of India's population, i.e., ~550 million people, the implications of losses of such magnitude would be serious indeed. Furthermore, crop exports from India are an important part of the regional and global economy. In summer 2023, India banned the export of rice due to climate change driven yield losses. Compounding such losses through increased PM pollution could further destabilise the regional food supply. Furthermore, if the BC component increased to ~10% of total PM,

i.e., to levels observed in the YRD circa 2001, our simulations suggest cereal crop failures would reach as much as 20.1% across the Indian subcontinent. Under the most severe future climate scenarios (SSP3 7.0), PM concentrations across South Asia, including India, are expected to increase by an average $13 \mu\text{g m}^{-3}$ by 2050 (Shim et al., 2021). India in particular is expected to suffer substantial PM pollution, with estimated increases of 67% for PM_{2.5} by 2050 (Pommier et al., 2018). It is vital therefore to understand the effects of PM deposition on IGP crop yields, to anticipate potential future losses to this increased air pollution.

3.4.6 Limitations and future work

Our simulations demonstrate that PM deposition makes a non-negligible contribution to global crop yield losses, and highlights the risk posed by potential future increases in PM pollution. Although such losses appear modest on a global scale, regional impacts are more substantive with average reductions of up to 2.5% for rice across China, and as much as 8% in specific locations in China and India.

However, these results hinge on a number of modelling limitations, and are a simplification of the reality experienced by crops *in vivo*. For example, the driving data used here is reanalysis data, derived from a combination of measurements and model interpolation. Whilst ERA-5 is a well-respected dataset which accurately captures many variables, a recent review identified that ERA-5 may systematically underestimate diffuse light compared to satellite retrievals (Jiang et al., 2020). Our use of a climatological average dataset may smooth aberrant years, and give a strong average picture of the changes driven by PM deposition, but it likely also includes some measure of systematic bias in absolute crop-yield that could lead to differences between actual and simulated crop yield responses. Similar systematic error may occur within the simulated PM flux datasets, though, again, we are more interested here in identifying the scale of possible change in crop yields from a given deposition flux, than in the absolute yield change found for a specific year. It is for further *in vivo* experiments to determine whether the scale of yield losses projected here are found *in situ* for real crop plants.

While our simulations explore the potential range of losses due to PM deposition, we acknowledge the considerable uncertainties in our estimates due to the paucity of measurements for key parameters. The effects of PM deposition are likely to vary also by cultivar, as well as species and stress, as demonstrated for rice by Mina et al. (2018),

and previously for other air pollutants, e.g., ozone (Osborne et al., 2016, Pleijel et al., 2019). The rates of PM flux are strongly dependent on leaf morphology (e.g., wax content, leaf hair density, stomatal density) which varies substantially between plant species and cultivar (Dzierzanowski et al., 2011; Hirano et al., 1995; Motai et al., 2018; Wang et al., 2015). Furthermore, the structure and density of the crop canopy affects canopy space aerodynamics and, hence, the rate of PM deposition via gravitational settling, and wet and dry deposition. A more granular parameterisation of variations in leaf morphology and canopy structure for different crop varieties across time and space, would enable better parameterisation of the accumulation and retention of PM on crop surfaces.

Other observed and theoretical effects of deposited PM have not been included here as they remain largely speculative. Further experimental evidence is required, for example, of the reduction in yield due to limitations in gas exchange arising from PM blocking, or directly damaging, stomata (Hatami et al., 2017; Mina et al., 2018; Mina, Singh, 2013; Zia-Khan et al., 2015). Reduced evapotranspiration under warming climates may increase leaf temperature beyond the optimal for efficient photosynthetic processes, and thereby reduce growth. Similarly, our model makes a number of simplifications - the model assumes that PM is evenly distributed across a given canopy layer, and makes no account of the effects of changing PM thickness within the canopy. This could lead to an overestimate of the average effect of PM deposition but an underestimate of the effect at specific highly polluted sites. Similarly, we ignore the light absorbing component of PM particles outside of black carbon, when brown and organic carbon can make a substantial contribution to light attenuation. We also assume a rigid canopy distribution and cropping density for each crop, and variations in these will have real world impacts on how readily deposited particles can be removed by wind or rain.

Furthermore, we also ignore the effects of airborne PM on incoming PAR for this study, choosing to focus purely on deposited PM as an underexplored perturbation of crop yields. By excluding this phenomenon here, we do not capture the full extent of PM associated yield reductions within this paper, only this specific aspect. One recent modelling study estimated yield losses for maize on the NCP of ~3% from light perturbations attributable to airborne PM (Wolffe et al, 2021). Combining these losses with those attributable to deposition would give maize yield reductions of ~5% over the NCP, a sizeable total impact. The interactions between the direct and indirect effects of PM should be considered in further research.

Lastly, interactions between PM and ozone pollution remain a major source of uncertainty. Tropospheric ozone is a well-known phytotoxin and is highly deleterious to crop growth and yields (e.g., McGrath et al., 2015; Mills et al., 2018). One recent study found deposited PM to reduce ozone absorption through stomatal blockage (Sharma et al., 2021), and airborne PM has been demonstrated to reduce ozone pollution by taking up free radicals involved in ozone formation (Ivatt, Evans, and Lewis., 2022). As PM emissions and concentrations have declined in China post-2013, ozone levels and associated crop losses have increased, a synergy expected to continue in the near future. Further observational studies are therefore required to examine the relationship between PM-induced changes in radiation intensity and quality, PM deposition, ozone formation, and subsequent crop losses.

3.5 Conclusion

Our simulations show that PM deposition to leaf surfaces reduces PAR transmission, and on average, causes small but significant yield losses for all crops. More substantive localised losses for rice and maize are seen in the key crop-growing regions of North-Eastern China and Northern India. As PM emissions increase in developing nations, it is important to further our understanding of how this pollutant may disrupt future food supply in these often food-insecure areas.

However, our simulations also demonstrate that further research is required to better understand the role of ambient weather in reducing PM accumulation on crop leaves through wash off. Ideally a range of *in vivo* studies would be conducted to identify the extent to which each of the crops simulated here respond to PM deposition fluxes in the field. These could then be utilised to tune our modelling results, and ensure greater confidence in regional and global yield loss projections.

Furthermore, our model would then be extended, to include the effects of deposited PM on stomatal conductance and leaf temperature, and to investigate the interaction of ozone and deposited PM. The response of different rice, maize, and wheat cultivars to PM must also be explored to ensure a fuller understanding of how PM may affect global crop yields.

Acknowledgements

M. Wolffe is grateful to the Royal Society of London for funding his PhD Studentship (RGF\EA\180129). K. Ashworth is a Royal Society Dorothy Hodgkin Fellow and thanks the Royal Society of London for their support and funding (DH150070).

Hersbach et al., (2018) was downloaded from the Copernicus Climate Change Service (C3S) Climate Data Store.

The results contain modified Copernicus Climate Change Service information 2020. Neither the European Commission nor ECMWF is responsible for any use that may be made of the Copernicus information or data it contains.

Chapter 4: The Impact of PM on Cereal Yields Depends on Crop Development Stage

Contribution statement:

The candidate's contribution was in the: conceptualization of the project; the development of the methodology used; the investigation of the research question; formal analysis of all data; interpretation of data; writing of manuscript for supervisor review.

Abstract

Particulate matter (PM) is a pollutant of potential concern for food production, and crops on the Indo-Gangetic Plains of India experience uniquely high peak PM concentrations. However, PM composition and concentration are highly seasonal on the Indian subcontinent, subjecting crops to varying concentrations of varied PM components across their growth cycles. The timing of an environmental perturbation within a crop's development cycle can significantly alter how they affect final yield, and this work explores how the impact of PM pollution can change throughout a crop's development cycle. The JULES-crop model is used here to simulate the impacts of PM on Indian wheat, maize, and rice throughout their lifecycles.

When combined, deposited and airborne PM were found to affect maize and rice yields most substantially during their late vegetative stage. However, the sign of change was not consistent across the simulated crop. On average, maize yields changed by 15.3% with early vegetative stage PM exposure, whilst rice yields changed by 32.6%. However, for rice, yields increased across the entire model area, whilst maize experienced losses in central and southern India, but yield increases in the north. Splitting PM deposition and light effects, we find average losses of -1.2% and -0.8% for deposition alone and average changes of 14.5% and 33.5% for light alone in maize and rice respectively.

For wheat, exposure to PM during the early vegetative stage was substantially more impactful. When PM deposition and light effects are combined the magnitude and scale of change varies drastically across the simulated area, up to a maximum of +119% and minimum of -88%. However, given the length of the wheat early vegetative stage, the greatest impact per unit time of PM exposure comes during the late reproductive stage.

We recommend that further *in vivo* research be conducted to validate model outputs, and advise agronomists to examine how the sowing and harvest dates of sensitive crops may coincide with high pollution events.

4.1 Introduction

Over 50% of all human caloric intake is accounted for by wheat, rice, and maize (OECD, 2021), making them critical for the global food supply. During their growth cycle, these crops progress through a number of development stages between sowing and harvest, and exhibit differing sensitivity to environmental stimuli during each stage.

During the vegetative stage, crops emerge and allocate accumulating biomass to expanded roots, leaves and stems, and temperature sensitivity at this stage is often higher than later in development. For example, maize is known to be particularly susceptible to colder temperatures during this development stage (Hatfield et al., 2015). This additional susceptibility to one environmental stimulus at a particular development stage raises the question as to whether other stressors would also have more effect on final yield if applied at this point.

During the later stages of development, carbon allocation shifts from leaf and stem growth toward the reproductive organs. In this stage, crops produce flowers and, upon pollination, the seeds, and any supporting growth structures such as husk leaves in corn or wheat. This is referred to as the reproductive stage. Wheat and rice crops are particularly susceptible to water stress during this stage due to increased water demands during flowering (Wollenweber et al., 2003; Farooq et al., 2014; Pinto et al., 2020). Similarly, extreme heat reduces wheat yields by 45% more when it occurs during the late vegetative or early reproductive stage compared to the late reproductive stage (Wollenweber et al., 2003). One explanation given for this phenomena is that earlier extreme weather events stunt early crop growth, resulting in fewer flowers surviving to maturity, and consequently fewer mature seed heads (Farooq et al., 2014). In a changing climate, new crop varieties are needed to survive extreme weather patterns and changing ecologies (Acevedo et al., 2020). It is necessary to better understand how different stressors affect crop yield at different development stages to ensure maximal crop yields in the future. In doing so, farming practice and cultivar selection can change to facilitate planting and development of crops in ways that minimise exposure to environmental perturbations.

The Indian subcontinent is particularly likely to suffer ill effects of climate change, with increases in extreme weather events expected to reduce cereal crop yields by 9% over the next 30 years (IPCC, 2022). Carbon dioxide from fossil fuel combustion is

responsible for most of the warming, but this is not the only combustion product which may limit regional food supply.

Particulate matter (PM) is an important air pollutant, produced from combustion alongside a range of other processes (see Introduction, Table 1.1). PM constitutes a mixture of different particles, with a large size and species distribution. These particles have been studied extensively in relation to human health (see e.g., Wang et al., 2015). In particular, PM_{2.5}, i.e., PM particles which have an aerodynamic diameter smaller than 2.5µm, have been recognised as a significant public health risk, and linked to myriad human diseases from bronchitis to Alzheimer's disease in a range of studies (see e.g., Kim et al., 2015). Focus on this pollutant by policy makers has led to significant reductions in PM across Europe, America and much of China (Hammer et al., 2020). However, PM pollution is tightly linked to industrial activity and economic development, and concentrations are currently increasing in many developing economies (Kaur & Pandey, 2021). This is particularly evident in India, where PM levels are extremely high. For example, whilst the WHO recommends average annual exposures of no more than 5 µg m⁻³ (reduced from 10 µg m⁻³ as the risks become more evident) to minimise human health impacts, the most populous cities on the Indo Gangetic Plain (IGP) experienced average concentrations above 65 µg m⁻³ for the first three months of 2020 (Das, Manob et al 2021) and hourly concentrations can still reach as high as 98 µg m⁻³ in Delhi, the largest city within this region (PIB Delhi, 2023).

As well as being a vital population centre, the IGP is critical to India's food supply, providing food for ~40% of the country's population (AgMIP, accessed 01-10-2022). Some research suggests that PM is not only detrimental to human health, but may play a role in reducing regional crop yields (Alton, 2008; Greenwald et al., 2006; Niyogi et al., 2004; Strada et al., 2015, Mina et al., 2018, Wolffe et al., 2021 (Chapter 2)). Significant crop losses in this region would be extremely hazardous to the region's food supply. Further examination of the role of PM in reducing crop yields is therefore vital, especially given the increasing PM concentrations across much of the globe (Hammer et al., 2020).

Whilst a number of researchers have begun to investigate the role of PM in crop health, the existing literature is somewhat conflicting. This is partly due to the heterogeneity in distribution and properties of different PM particles. Some, such as black carbon (BC), are highly light absorbing, reducing the amount of photosynthetically active radiation (PAR) which is able to reach the planet's surface (Lohmann, U., &

Feichter, J., 2005). Given the strong linear relationship between PAR exposure and photosynthesis rates (Sun, Dongbao, and Qingsuo Wang. 2018), less PAR reaching a leaf canopy will ultimately reduce crop yields (Brocklehurst et al., 1978; Li et al., 2010; Sridevi & Chellamuthu.2015; Tsimba et al., 2013).

However, some PM particles such as sulphates are more likely to scatter incoming PAR photons than absorb them. When PAR is scattered it reaches the surface in a more diffuse pattern than would otherwise be the case, and this diffuse light can penetrate deeper into plant canopies than direct light (Li et al., 2015). This can increase radiation use efficiency (RUE), with dark under-canopies increasing their photosynthesis rate at the meagre expense of lowering light-intensity at the already light-saturated upper canopies. A number of *in vivo* (Alton et al., 2007; Gu et al., 2002; Niyogi et al., 2004; Strada et al., 2015) and *in silico* (Mercado et al., 2009; Rap et al., 2015; Roderick et al., 2001; Xie et al., 2020) studies have therefore suggested a 'diffuse light fertilisation effect', whereby PM-induced changes in PAR raise RUE and drive an overall increase in photosynthetic rates and gross primary production (GPP; total carbon fixation by an ecosystem in a given time period). However, other studies suggest that this is only the case for forest ecosystems, whereas the more open canopy structure of crops means that yield gains from the diffuse light fertilisation effect are smaller, and offset by reductions in total PAR (e.g., Cheng et al., 2015, Wolffe et al., 2021).

Furthermore, the effects of airborne PM are compounded by PM deposition to crop surfaces. Field experiments have shown that rice yields can be reduced by up to 7% (Mina et al., 2018) due to PM deposition to leaf surfaces, an effect attributed to the synergistic effects of the direct interception of incoming PAR, and blockage of stomata leading to increases in leaf temperature above the photosynthetic optimum (Hatami et al., 2017, Mina U., Singh, R., 2013). The important Mina et al., 2018 study is described in further detail in Chapter 1, section 1.3.2.2 and 1.5, and in Chapter 3, section 3.1. However, despite a few high quality pot and field trials, the overall impacts of PM deposition to crop surfaces has been poorly studied, with very few researchers considering the effects of this phenomenon (Hatami et al., 2017, Mina U., Singh, R., 2013, 2018, Zia-Khan S, et al., 2015).

Given the extent of PM pollution over the Indian subcontinent (Gorai et al., 2018; Gupta & Kumar, 2006), its status as a centre for PM deposition impact research (e.g., Shim et al., 2021; Mina & Sigh, 2013), and the likely impacts of climate change over the subcontinent (IPCC 2022), India presents a unique location where the differential effects

of PM on crops at different development stages may be uniquely important. This paper uses the Indian subcontinent as a test location to examine how the timing of PM perturbations relative to crop development stage affects regional crop yields. We apply a modified version of the JULES-crop model (see Chapter 3, section 3.2) to understand and assess the impacts of PM pollution at different development stages for spring wheat, maize, and rice. This work highlights the importance of understanding the complex interactions between crop development cycles and their environment, and demonstrates the strengths and limitations of a model-based approach to this question.

4.2 Materials & Methods

4.2.1 Model Parameterisation

The Joint UK Land Environment Simulator (JULES) is an established tool for studying crop yields at single sites (Williams et al., 2017; Kimball et al., 2019; Wolffe et al., 2021), and for simulating the global scale variability in crop yields attributable to changing meteorological conditions (Osborne et al., 2015). The modified JULES-crop v1.5.4 described in Wolffe et al. (2023; in preparation, see Chapter 3) is used for all model simulations described in this paper utilising the “standard wash off mode”. The skill of the JULES-crop model in evaluating the effects of changing meteorology on crop yields is a particular strength of the model (Osborne et al., 2015, Williams et al., 2017, see Chapter 1, section 1.5 for detailed discussion) making it suitable for the purposes of this research. The version used here includes PM deposition to crop leaves, and a parameterisation of the impact of deposited PM on photosynthesis and productivity. This enable us to estimate the impacts of future PM deposition on crop yields at different crop development stages (Wolffe et al., 2023; in preparation, see Chapter 3).

All simulations are conducted on a $0.25^\circ \times 0.25^\circ$ grid for a model domain extending from 15.0°N , 66.0°E to 36.0°N , 93.0°E . This region (shown below in Figure 4.1) captures Northern India and extends to parts of Pakistan and Nepal in order to encompass the full extent of the IGP. Hourly average climatology for the years 2015-2020 (including direct and diffuse shortwave radiation, long wave radiation, 2-m air temperature, windspeed, surface pressure, specific humidity, and precipitation) is taken from the ERA-5 reanalysis dataset (Hersbach et al., 2018). Land cover for all simulations was taken from MODIS AQUA-TERRA product MCD12C1 at 0.05° resolution and regridded to 0.25° .

As in Chapter 3, PM deposition fluxes were taken from MERRA-2 reanalysis product M2T1NXADG (GMAO 2015) by combining the dry deposition flux of black carbon (BC), organic carbon (OC), sulphates, sea salt, and mineral dust. The sum of PM component fluxes is what is meant by PM deposition throughout the experimental methods section. Bulk PM was regridded to a 0.25° grid by bilinear interpolation. The fraction of total PM which is BC is taken from the same MERRA-2 reanalysis product, and is used to derive Eabs - see Chapter 3 Section 2. An average year for this data was constructed in the same manner as for the meteorological driving data from ERA-5.

Crop distribution and most likely sowing and harvest dates were taken from Iizumi et al. (2019) for the years 2015-20 and average values for each timepoint calculated for each grid cell, as described in more detail in Wolffe et al. (2021; See Chapter 2). Yields are calculated from the total carbon allocated to the harvestable portion of the crop at the end of the crop development cycle, which is converted to dry t ha⁻¹ following the methodology outlined in Williams, et al. (2017). Percentage yield changes for perturbed simulations are calculated relative to the yield of a baseline simulation in which PM deposition is set to zero.

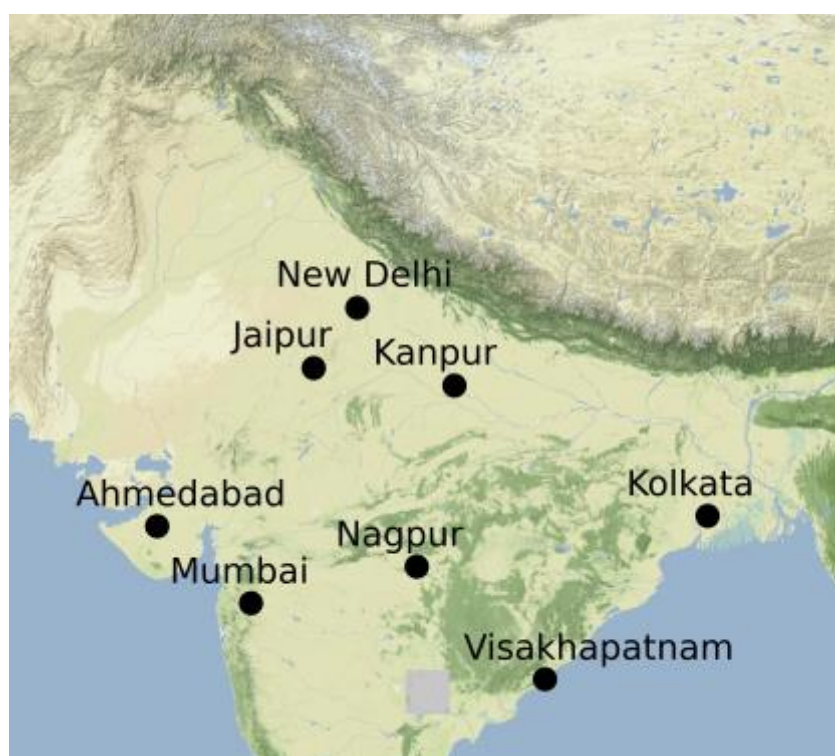


Figure 4.1. *The model domain with a number of major cities labelled to aid interpretation of results - image created using seaborn and matplotlib.*

4.2.2 Development Stage Perturbed simulations

In addition to the baseline simulation described above, a series of perturbation simulations are conducted in which PM concentrations vary during different development stages. As described in Chapter 1, section 1.5, these development stages are defined within the JULES model via the variable DVI, a measure of crop development, using a scale running from -2 to +2. A DVI of 0 corresponds to the emergence of the crop. Between 0 and 1, a crop is in the vegetative development stage, corresponding to the time a crop spends allocating fixed carbon to expansion and growth of leaf, stem, and root components. Between a DVI of 1 and 2, a crop is in its reproductive phase when carbon stores are remobilised, and GPP is dedicated toward producing the harvestable fraction of the crop. These stages are further subdivided here into early vegetative (DVI = 0.0-0.5), late vegetative (DVI = 0.5-1.0), early reproductive (DVI = 1.0-1.5) and late reproductive (DVI = 1.5-2.0).

The relative duration of each development stage varies both between crop species, and by growing location within the model domain (due to ambient meteorological conditions and varying sowing and harvest dates). See Figure 4.2 below for a breakdown of the distribution of sowing and harvest dates, and 4.3 for an example of the growth cycle for each of the three crops in a single grid cell where all three are grown at different times of year and for different durations.

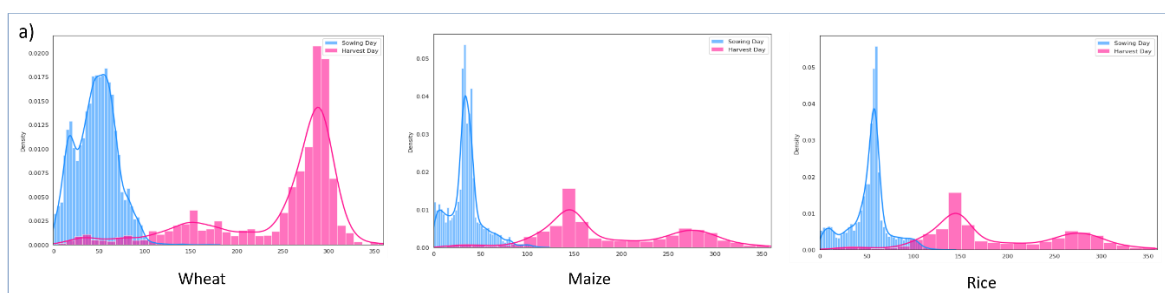


Figure 4.2. Distribution of sowing and harvest dates for wheat, maize, and rice across the simulated area.

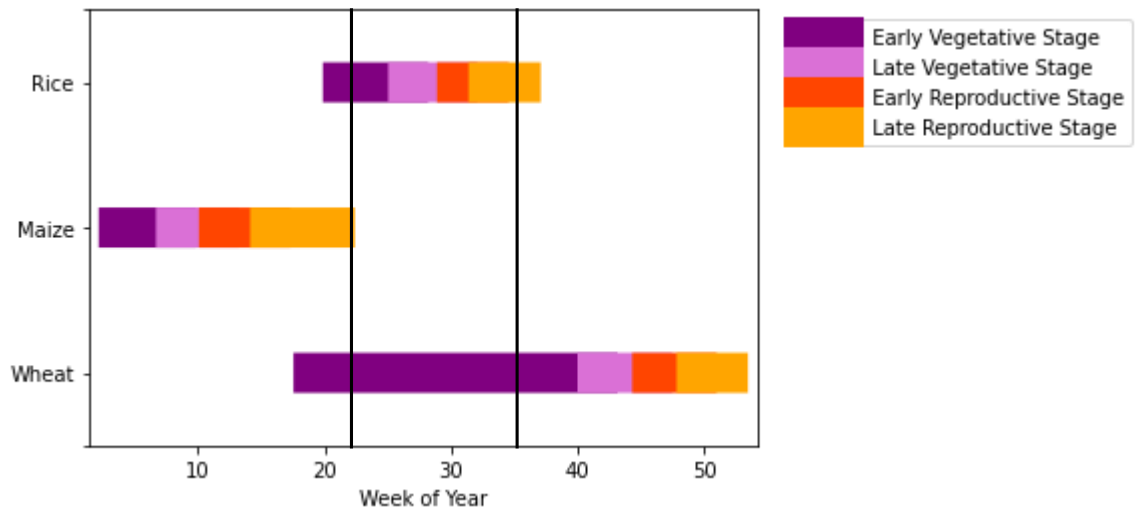


Figure 4.3. Example of the different development stage durations and timings within the year for each crop in a single grid cell at 26.0°N, 76.0°E . The monsoon season is marked with two black lines, with monsoon typically falling between this period.

4.2.3 Radiation and Deposition Perturbations

In perturbed scenarios, an average year is still calculated for all non-perturbed meteorological driving variables (long-wave radiation, precipitation, windspeed, surface pressure, 2m temperature and specific humidity) using ERA-5 driving data at a 0.25°x 0.25° grid resolution.

To obtain a value for a semi-realistic worst-case scenario for PM fluxes in perturbed simulations, data were taken from AerChemMIP. This is a model intercomparison project which investigates future climate and aerosol concentrations and fluxes under climate scenarios compatible with the IPCC Shared Socioeconomic Pathways (SSPs; IPCC 2022; Collins J, Lamarque J, Schulz et al., 2017). We use simulated aerosol fluxes for 2050 calculated as sum of black carbon, organic carbon, sulphate, sea salt and dry dust deposition using SSP3-7.0 (a high emissions future simulated by the NorESM2-LM model (Norwegian Climate Centre, 2020) over the model domain. To reduce variance over the simulated domain and remove extraneous variables, the spatio-temporal average PM flux was used across all grid cells between the earliest sowing date and latest harvest date (0.173 mg m⁻³ h⁻¹). This is a substantial

level of PM deposition, in line with that used in Bergin et al. 2001, and similar to the present day PM fluxes on the NCP.

A constant mass absorption coefficient of 0.259 was calculated following the methodology in Chapter 3 Equation 2, using the spatio-temporal average black carbon concentration. For each perturbation simulation, this 2050 average PM flux was applied for the entirety of a given development stage. PM deposition for the rest of the simulation set to zero as per the baseline simulation described in Section 2.1.

Linear regressions were then determined between PM flux and shortwave radiation (SW; $R^2=0.63$) and PM flux and diffuse fraction ($R^2=0.73$) for the 2015-20 average driving dataset. These relationships were used to deduce average day time values of SW and diffuse fraction given the 2050 level PM flux (in a similar manner to Wolffe et al., 2021, see Chapter 2). As in Chapter 2, sections 2.4-2.5, SW (224.14 W m^{-2}) and diffuse fraction (0.45) are applied during daylight hours for each grid cell for each of the development stages. This fixed SW flux is clearly a substantial reduction in total SW which may limit the growth of some crops and overestimate the effect of airborne PM on crop yields. However, the fixed value facilitates ready comparison across the entire simulated region, and allows comparison of the simulated gains/losses with those seen in Chapter 2. By removing the variation in SW across timesteps and across grid cells, we can compare results regionally and remove extraneous variables when attempting to determine a percentage change.

In a final set of perturbation simulations, airborne and deposited PM effects are applied simultaneously during each development stage in turn. The resulting crop losses demonstrate the potential total effects of PM on crop yield. Model output is used to explore whether light and deposition effects are synergistic, and is used to assess whether the combinatorial effect is greater at one development stage than another. The range of perturbations used within this study are highlighted in Table 4.1 below.

Variables	Baseline Simulation	Development Stage Perturbed Simulations
Total SW Radiation	Hourly average climatology for the years 2015-2020 from ERA-5	Hourly average climatology for the years 2015-2020 from ERA-5, then 224.14 W m ⁻² during perturbed development stage.
Diffuse Fraction of SW Radiation	Hourly average climatology for the years 2015-2020 from ERA-5	Hourly average climatology for the years 2015-2020 from ERA-5, then 0.45 during perturbed development stage.
Particulate Matter Flux	No particulate matter flux	0.173 mg m ⁻³ h ⁻¹ during perturbed development stage.
Other Meteorology (Long wave radiation, 2-m air temperature, windspeed, surface pressure, specific humidity, and precipitation)	Hourly average climatology for the years 2015-2020 from ERA-5	Hourly average climatology for the years 2015-2020 from ERA-5
Crop Distribution and most likely Sow Date	lizumi et al. (2019) for the years 2015-2020 and average values for each timepoint calculated for each grid cell, as described in more detail in Wolffe et al. (2021; See Chapter 2).	lizumi et al. (2019) for the years 2015-20 and average values for each timepoint calculated for each grid cell, as described in more detail in Wolffe et al. (2021; See Chapter 2).

Table 4.1 Summary of the different variables used in each simulation.

4.3 Results

Simulated crop yields for an average year vary somewhat from observed results over the simulated area. Average wheat yields of 1.3 t ha⁻¹ of wheat are substantially lower than the measured 3.5 t ha⁻¹ observed in 2021 (USDA, Retrieved June 16, 2022), and simulated rice yields of 1.7 t ha⁻¹ are also below the recorded yields of 3.4 t ha⁻¹ in

2021 (India: Yield of Rice 1991-2021 | Statista). These yields are closer to those observed in 2015, the earliest timepoint used in calculating our average year, when rice yields were 2.4 t ha⁻¹ (India: Yield of Rice 1991-2021 | Statista) and wheat yields were 2.8 t ha⁻¹ (India: Yield of Wheat 1991-2021 | Statista), though still not close to the observed value. It should also be noted that annual yield figures for wheat include winter wheat, whereas our simulations only include spring wheat. Conversely, our simulations produce a maize yield of 8.8 t ha⁻¹ which is much larger than the reported yield of 3 t ha⁻¹ in 2021 (USDA, Retrieved June 16, 2022). These results are comparable to those seen in Osborne et al., 2015, where maize routinely overestimates yield, but rice and wheat yield are below expected values. This is seen despite the improvements to the maize model carried out by Williams et al., 2017, where maize yields were tuned to match those observed in a range of Fluxnet sites in Nebraska, USA. The differences here may originate from differences in crop variety or farming practices between areas where the model was tuned and the simulated region, and further model tuning is needed to generate yields that are closer to observed reality.

However, absolute yield is not the focus for this study. This work aims to study percentage changes in yields of wheat, rice, and maize under different PM scenarios. The most similar analogy to this is modelling interannual variation, whereby JULES-crop is tasked with capturing how different meteorological conditions translate to a percentage change in end-point yield. JULES-crop is more skilled in simulating this phenomenon than simulating absolute yield, especially for rice and maize, (Osborne, et al., 2015). Wheat is the weakest performing of the three crops for this purpose, so more caution should be applied when interpreting results for this species. Model artefacts are an important consideration when interpreting results.

Despite these caveats, we believe that JULES-Crop is an appropriate tool for beginning to investigate this research question. Further *in vivo* experimentation and model validation is, however, essential to consolidating our understanding of the effects of PM on regional crop yields. Further detail of the strengths and weaknesses of JULES-crop is included in Chapter 1, section 1.5.

4.3.1 Direct Effect of PM

Total yield losses from exposure to PM deposition are significantly different for each PM perturbation, with wheat crops consistently the most affected (losses of up to 28% relative to the baseline simulation). Maize and rice appear considerably less affected (maximum yield losses of 1.2% and 0.8% respectively). There are small (~1%) but significant ($p < 0.05$) differences in the effects of deposited PM applied at different stages of crop development for wheat, and significant and sizable percentage differences in yield reductions for maize and rice (one order of magnitude difference, see Figure. 4.4) between PM deposition occurring at different development stages.

For maize and rice, yield losses due to PM deposition during the early vegetative stage are circa an order of magnitude greater than those seen during other development stages. For wheat, although yield reductions are also highest for PM events during the early vegetative stage, there is only an average 0.2% difference in impact between simulated yields for each of the development stage perturbations.

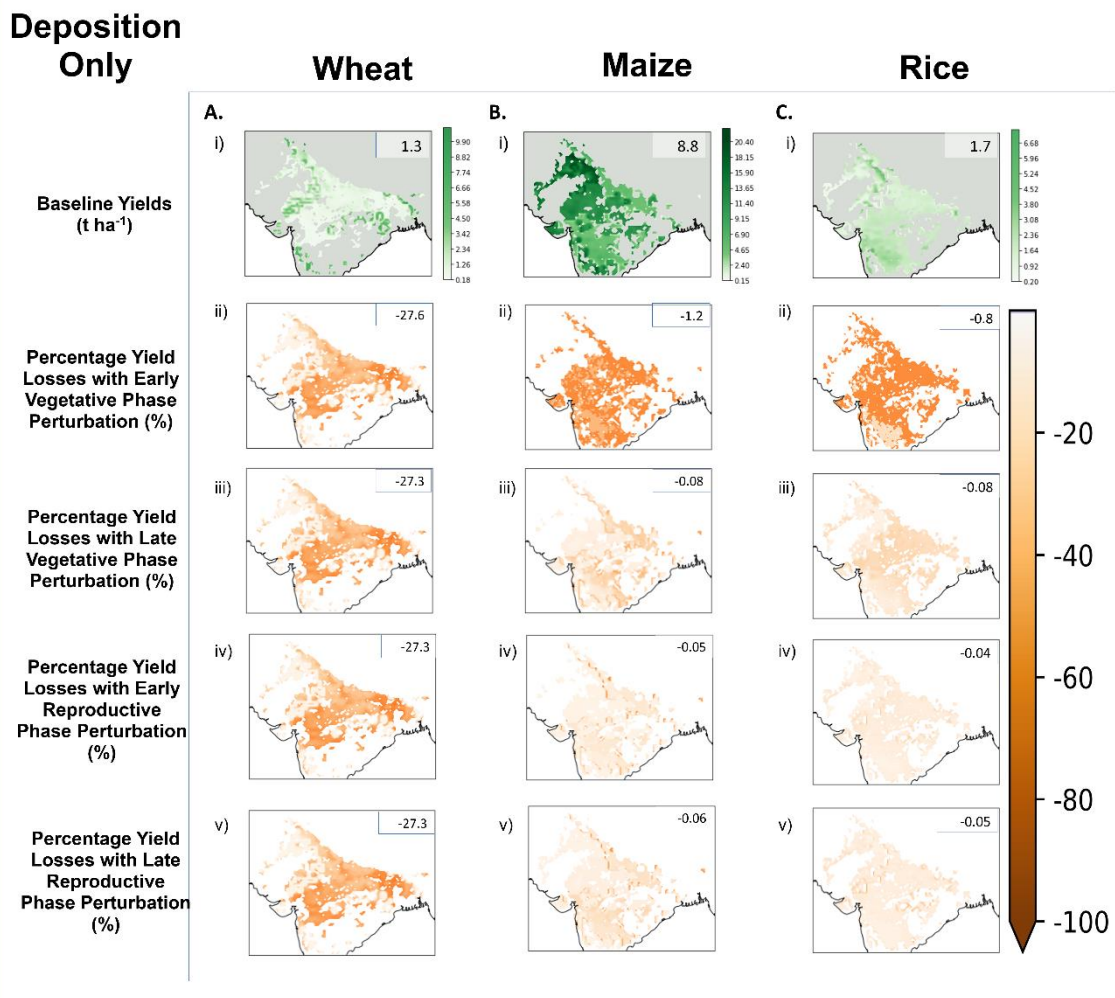


Figure 4.4. The baseline yields for wheat (a,i) maize (b,i) and rice (c,i) across the study area, annotated with the domain mean yield. Below these are the percentage yield losses with the application of PM deposition during the early vegetative stage (ii), late vegetative stage (iii), early reproductive phase (iv) and late reproductive stage (v), annotated with the mean yield reductions for the domain.

4.3.2 Indirect Effect of PM

PM-related light perturbations result in a yield increase in maize and rice crops for the majority of grid cell locations within the model domain. These effects appear counterintuitive given average SW radiation reaching the top of the crop canopy is reduced across all grid cells. However, as shown in Wolfe et al. (2021) the increase in

diffuse fraction (here ~80%) above the average value outweigh the effects of reduced SW for maize and rice in a majority of simulated locations (see Figure 4.5.B and 4.5.C below). Whilst this is an artificially high diffuse fraction for any area, this serves to illustrate the potential for a relationship between diffuse fraction and light intensity whereby the diffuse light fertilisation effect is highly beneficial (as observed in a number of field studies, e.g., Niyogi et al., 2004; Strada et al., 2015). Again, the greatest effects from PM perturbation are observed for changes in light during the early vegetative phase. This implies that at high levels of diffuse light fertilisation, early crop growth or stunting is more impactful for end-point yield than alterations to carbon assimilation during the early reproductive phase when seed setting occurs.

For wheat, the changes to the light profile result in sizable yield decreases across much of the model domain (Figure 4.5.A). The magnitude of these changes is also in excess of the changes in maize and rice yield for all perturbations. This is discussed in greater detail in section 4.1.2 below. Interestingly, this is considerably different to the results seen in Chapter 3, where wheat was least affected by PM deposition. There are a number of potential reasons for this result discussed in detail in 4.4.1 and 4.4.2, however when interpreting these results, it should be noted that the parameterisation of this crop is the weakest of the three studied (Osborne et al., 2015).

Also note that the direction of change is different between different grid cells. This is partially due to the artificial nature of the simulations conducted here. As SW and diffuse fraction are set to a fixed value, this represents an increase from the average baseline value experienced for some grid-cells, and a decrease for others. The absolute change will vary across the region, and therefore alter the direction of effect. For example, one grid cell may experience an increase in average diffuse fraction whilst another experiences a decrease. This will clearly cause a change in the diffuse light fertilisation effect between these grid cells. The purpose of these simulations and using a fixed value is to gauge the development stage where the greatest change occurs, not to identify the actual scale of impact in the real world.

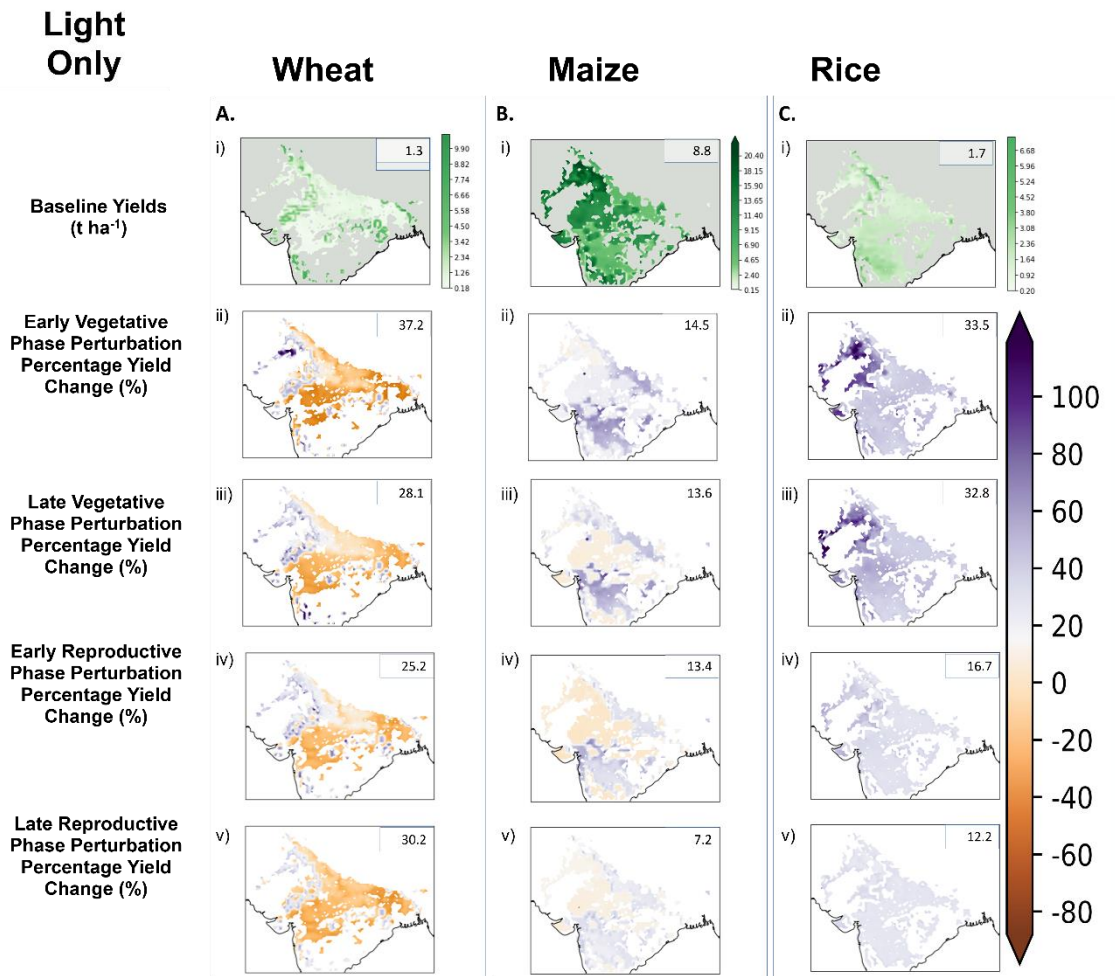


Figure 4.5. The baseline yields for wheat (a,i) maize (b,i) and rice (c,i) across the study area, annotated with mean yield for the location. Below these are the percentage yield losses experienced across the model domain with the application of PM associated changes to SW and diffuse fraction during the early vegetative stage (ii), late vegetative stage (iii), early reproductive phase (iv) and late reproductive stage (v), annotated with the mean yield change (absolute change taken for simulations with positive and negative changes).

4.3.3 Total Effect of PM

The cumulative effects of combined changes in PM deposition and radiation are shown below in Figure 4.6, and appear approximately additive. The small yield decreases for maize and rice due to deposition are outweighed by the yield gains arising from an increase in diffuse fraction, and in spite of the slight decrease in average SW in

the simulated area. For wheat, however, we see that the combined negative impacts of deposition and light changes are little different to the effects of light alone. This is simply because incoming PAR has been perturbed to such an extent, that further deposited PM is not having a substantial impact on light penetration to the crops. However, *in vivo*, these combined effects may instead trigger the early onset of crop senescence, substantially reducing yields.

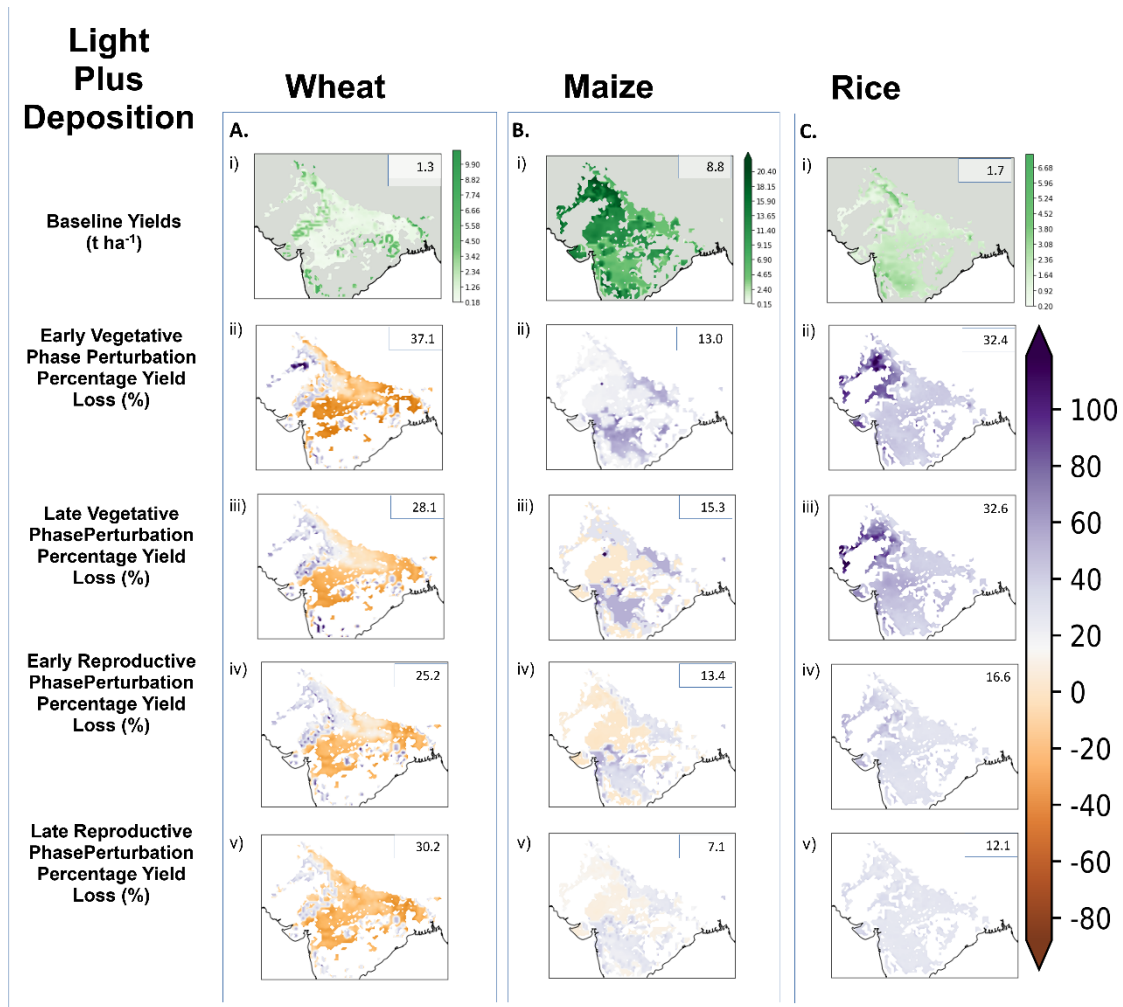


Figure 4.6. *The baseline yields for wheat (a,i) maize (b,i) and rice (c,i) across the study area, annotated with mean yield for the location. Below these are the percentage yield changes experienced across the model domain with the application of PM associated changes to SW and diffuse fraction during the early vegetative stage (ii), late vegetative stage (iii), early reproductive phase (iv) and late reproductive stage (v), annotated with the median yield reduction's locations with yield losses over 1%.*

4.3.4 Development stage dependence - Model Findings

We find that the largest changes in yield for all three crops occur when PM deposition, or PM associated light perturbations occur during their early vegetative stage. However, when both deposition and light perturbations are applied, the early vegetative stage remains most affected for wheat, but the late vegetative phase is most critical for rice and maize. This cannot solely be attributed to the length of time each crop spends in each development stage. For example, simulated wheat spends an average of 65% of its life cycle in the early vegetative stage, but for deposition only simulations, the wheat crop on average only suffers 0.3% greater yield losses from early vegetative stage perturbations than any other perturbation (27.6% vs 27.3%). Conversely, simulated maize spends an average of only 31% of its life cycle in the early vegetative stage, but including PM deposition during this development stage causes 17 times the yield reduction of the next greatest yield reductions, which occur during the late vegetative stage. If the yield reduction for each perturbation is weighted by the average length of time each crop is exposed to a PM perturbation, we see that the most impactful development stage perturbation for wheat (as % yield change per hour of PM deposition) is the late reproductive stage because of the much shorter period spent in this development stage. For maize and rice, the early vegetative stage still remains most impactful. See Table 4.2 below for a full breakdown of the percentage yield change per hour of PM deposition at each development stage.

Development Stage	Wheat	Maize	Rice
Early Vegetative Stage	-0.0203%	-0.0051%	-0.0024%
Late Vegetative Stage	-0.0565%	-0.0003%	-0.0003%
Early Reproductive	-0.1869%	-0.0002%	-0.0002%

Stage			
Late Reproductive Stage	-0.5216%	-0.0002%	-0.0002%

Table 4.2. Percentage yield loss per hour exposure to PM deposition by development stage at exposure

When interpreting our yield losses, the reader should understand that all losses are driven by a reduced carbon assimilation to the harvestable portion of the crop during the early reproductive stage. In maize and rice, the early stunting of the crop means that the plant is smaller during this early reproductive stage, and thus carries out less photosynthesis. This reduces carbon assimilation during this period. Here we observe that simulated early stunting is more impactful than any effect of PM later in the development cycle.

Wheat appears to be much more significantly affected at all development stages than rice or maize, although this should be couched in an understanding that JULES likely has less skill in simulating the effects of PM on wheat than maize or rice. The result is also partially explained by differences in the average SW reduction experienced by each crop. For maize and rice, for any given development stage perturbation is between 31-41%, but for wheat this is as much as 45-48%. Meanwhile, for maize and rice, we find that the percentage increase in diffuse fraction for the early vegetative stage is 4.4 and 7.9 times higher (respectively) than in the next highest development stage (the late vegetative stage). This results in larger yield increases for these simulations (seen in Figures 4.4.3.B.i and 4.4.3.C.i compared to 4.4.B.ii-iv and 4.4.C.ii-iv). The impacts of PM throughout wheat development are then greatly amplified by the relatively extended wheat development stages. In particular, the early vegetative stage takes place over a substantially longer period than might be expected. This is partly attributable to model artefacts, and should lend caution to any over-interpretation of the wheat results.

4.4 Discussion

4.4.1 PM deposition and development stage dependence

In deposition only simulations, the effects of PM deposition during the early vegetative stage are an order of magnitude greater for maize and rice than during any

other development stage. However, wheat suffers substantially greater yield losses than any other crop, and there is a less pronounced difference between the differently timed perturbations. The differences between wheat and the other crops are driven primarily by 1) the longer wheat development cycle, and 2) lower rainfall during wheat development at the most highly affected locations resulting in greater accumulation of PM to the leaf surface. The average simulated growing cycle for wheat post emergence is 67 days, versus 37 for maize and 41 for rice. By applying a constant perturbation for each development stage in turn, a crop spending a longer time in that development stage experiences a larger change in yield. The low precipitation across much of the wheat growing area then compounds the effects of PM deposition, with lower rates of PM removal by precipitation for wheat than for either maize or rice (an average 13.4% fewer PM removing rainfall events for wheat per affected grid cell than maize, and 11.6% fewer than rice). These areas are also likely to be those most affected by drought or other extreme weather in the future, suggesting that the effects of PM may compound on already reduced yields.

The substantially higher yield reductions in wheat than rice or maize strongly suggest that the effects of PM accumulate over time. With wheat experiencing PM deposition stress for a greater length of time, the effect appears to increase non-linearly with exposure period.

4.4.2 PM mediated light alterations and development stage dependence

When considering the impacts of PM-mediated changes in radiation, wheat is affected differently by PM across each development stage when compared to wheat and rice. Airborne PM associated perturbations reduce yields for wheat across the majority of locations for all simulations, while rice and maize yields mostly increase in all grid cells and perturbations. This is the result of the absolute change in average SW and diffuse fraction for the domain for the full vegetative stage in wheat.

The timing of the spring wheat growing season in this area compared to maize and rice means that changes to diffuse fraction changes applied (outlined in 2.2.2) reduce the average diffuse fraction over the crop's lifecycle instead of increasing it. The extended length of the wheat development cycle further compounds these effects of PM, resulting in the magnitude of change for wheat being considerably higher than that seen for maize or rice.

The increases in diffuse fraction for maize and rice outweigh the reductions in total SW reaching the canopy and result in increased yields across the full model domain. For wheat, however, there are much smaller differences between the increases to average diffuse fraction in early vegetative stage and in the perturbation with the next greatest influence (also the late vegetative stage). A different modelling approach that had not used a fixed fraction of diffuse light as outlined in 4.2.3 may have provided more useful and generalisable results for this crop. Further discussion of modelling revisions that could generate more useful wheat results is found in section 4.4.3.

Whilst the average change in diffuse fraction is greater for each development stage for wheat than for maize or rice, this varies dramatically across the model domain (with an average diffuse fraction of 0.25 across all simulated locations, but with a maximum average value of 0.39 and minimum of 0.16 for different locations across the region). For the grid cells where yields increase (see Fig. 2.A.i-iv), the change in diffuse fraction is up to 10 times higher for wheat than for maize or rice grid cells during the simulated time frame. However, where yields decrease, the increase in average diffuse fraction is only half that of maize or rice. Combined with a greater reduction in SW for these locations, this drives the yield losses seen in Figures 4.4.3.A and 4.4.A.

4.4.3 Implications for future pollution events

Whilst separate the effects of airborne and deposited PM are necessarily encoded separately in a mechanistic model, the combined impact is more important for understanding the real-world implications of future changes in PM concentrations. The results in Figure 4.6 suggest that the combined impact is additive, and yield losses from deposited PM can be offset by increases in yield due to the diffuse light fertilisation effect. This compensation occurs because deposited PM accumulates predominantly on the upper crop canopy, with lower levels shaded by upper layers. However, increases in diffuse fraction redistribute PAR from the upper canopy to lower canopy layers of crop plants to the benefit of both canopy sections. There does however appear to be a limit beyond which diffuse fertilisation is insufficient to recover yield lost due to PM deposition. For example, in the simulations described above, west Indian wheat yields, the deleterious effects of deposited PM are not outweighed by the diffuse light fertilisation effect.

The different outcomes from changed perturbation timing within the development cycle are found to be significant for all crops ($p < 0.05$). If losses are weighted by the relative length of the crop development cycle for which wheat is subjected to PM pollution, then late reproductive stage perturbations are most impactful. In rice and maize, the most impactful PM perturbations are those occurring in the early reproductive stage (in agreement with Wolffe et al (2021), see Chapter 2).

In Wolffe et al, 2023 (In preparation, see Chapter 3), PM composition is found to greatly change how PM deposition affects crops. The reduced levels of BC in future simulations compared to the present day results in deposited PM that is less light absorbing and has less impact on PAR availability for photosynthesis. If these future composition scenarios for BC concentration are replicated in reality, then this work implies that PM may even prove beneficial to maize and rice yields over India. This key role for BC is seen elsewhere in the literature, where yields are greatly reduced in environments with high levels of airborne and deposited carbonaceous aerosol (Bergin et al., 2001; Mina et al., 2017; 2021). If BC were to remain at current day levels or increase, for example if regulation or technological solutions are not put in place to reduce BC emissions from combustion processes, the effects of PM may be less positive in maize and rice, and even more negative in wheat.

4.4.4 Limitations and further work

Whilst this work presents an interesting insight into the possible development stage dependence of PM perturbations on cereal crop yields, further work is required to ensure that findings are robust and to supply policy makers with necessary tools to counter the resulting threats to food supply. Most critically, the changes to PAR and diffuse fraction here are underpinned by the relationship seen between present day PM concentrations, light intensity, and diffuse fraction. This relationship gives a useful average value for PM impacts on light that can be applied to simulated work, but relies upon a range of assumptions which do not capture the complexity of real-world processes. Particularly, PM concentrations and fluxes vary throughout a day, and therefore their effects on light will be more specific to time and place than the fixed value applied here. To determine a realistic effect of future PM, detailed process-based radiation modelling is essential.

The results observed in this study for maize and rice are likely useful for policy makers in visualising the extent of damage that can be done by PM pollution. Wheat simulations, however, provide substantially aberrant results compared to these other crops. Some of this difference is likely attributable to model artefacts – either from driving data choice, or from the limitations of wheat in simulating the impact of meteorological changes on end-point yield (Osborne et al., 2015). Further modelling studies incorporating a more nuanced depiction of the effects of PM on light would provide greater insight. For example, a radiation model that generates the available PAR at the surface and corresponding diffuse fraction of light given a specific particulate matter profile could be applied to generate bespoke time-varying radiation fields. These could then be applied to our simulations to depict a more realistic radiation scenario resulting from enhanced PM pollution.

Further modelling efforts must also be underpinned by more fundamental *in vivo* research into the effects of PM on crops. PM retention is known to vary significantly even between varieties of the same crop species (Mina et al., 2013; 2018; 2021). Leaf microstructure varies widely between species, and even between varieties of the same crop, with stomatal, leaf hair and micron scale ridge density all affecting PM retention. There is also likely a difference between the cereal crop species in their propensity to retain common PM species. Further experimental exploration of these differences would improve modelled estimates of PM retention under rainfall. Deposited PM also reduces leaf transpiration rates, and increases leaf temperature (Hatami et al., 2017, Mina et al., 2018), further reducing photosynthesis rates. Incorporating and implementing these effects within JULES or a similar model would enhance our understanding of PM deposition impacts. By doing so, models could better predict the outcome of future PM scenarios, and thus aid policy makers in avoiding threats to regional and global food supply.

Chapter 5: Conclusions

My simulations and sensitivity tests with JULES-Crop indicate that particulate matter (PM) may negatively affect global crop yields. Through the indirect and direct mechanisms postulated previously, airborne, and deposited PM reduce light availability for photosynthesis, thus reducing yields by a small amount across the whole planet. In Chapter 3, particularly substantial losses from PM deposition (up to 8%) are seen across two globally critical agricultural regions: the North China Plain (NCP) and Indo-Gangetic Plain (IGP). In combination with the simulated losses circa 3% attributed to airborne PM in chapter 2, this suggests a potentially sizeable role for PM in reducing regional crop production.

Whilst this work is underpinned by a range of generalisations and assumptions required to model these effects, the exploratory work here is indicative of an important phenomena that requires further research. The novel PM deposition model generated for this thesis can be utilised with JULES-crop as this model advances to project future impacts of PM deposition. It suggests, alongside the scant *in vivo* studies which have thus far been conducted, that this mechanism is important for the future global food supply. The discussion throughout this thesis highlights the important next steps that should be taken to further understand and quantify this phenomenon. The conclusions that can be drawn from this thesis, and the essential future work required to validate the results presented here, are summarised below.

5.1 The diffuse light fertilisation effect

The term “diffuse light fertilisation” describes the increase in carbon fixation by plants resulting from an increased diffuse fraction of PAR. In Chapters 2 and 4, the diffuse fertilisation effect is identified as playing an important role in crop productivity, increasing average yield substantially. However, the absolute reductions in total PAR which also result from PM pollution can counteract and overwhelm this effect, leading to an overall negative impact of airborne PM on crop yields. Chapter 2 estimates that NCP maize yields between 1981–2017 are reduced by an average of ~3% owing to airborne PM. In Chapter 4, however, we see a mixed effect of airborne PM on Indian maize yields at the average PM concentration expected later this decade. These differences arise from reduced levels of absorbing BC and relatively higher levels of scattering particles, driving a greater diffuse fertilisation effect. Whilst the studies in Chapter 4 are

more indicative of model sensitivity than directly transposable to the real world, they highlight the important factor of PM composition for understanding the outcomes from increased PM concentration. The compensatory nature of the diffuse light fertilisation effect and light attenuation, alongside the heterogeneity of PM in space and time, partially explains the somewhat conflicting literature surrounding the effects of PM on crops.

Chapter 4 explores the effects of airborne PM on wheat and rice. This outlines the boundaries of the diffuse light fertilisation effect, with an extreme elevation of diffuse light fraction and corresponding reduction in downward SW radiation. Under these conditions, rice is seen to benefit greatly under elevated PM levels during the early vegetative stage. Conversely, wheat appears to suffer from similarly increased levels of airborne PM, with the effects of reduced average PAR interception by the canopy outweighing the benefits of increased diffuse fraction. These results, however, can also be partly explained by modelling artefacts. Further studies are required to assess whether the model output differences seen for each crop are: 1) artefacts of study design – caused by growing season differences and sowing/harvest date; 2) functions of differing model skill in simulating each crop (see Introduction section 1.5); or 3) actual differences in crop susceptibility. Ideally, *in vivo* experimental work should be undertaken to assess the susceptibility of each crop to reduced PAR at different developmental stages, and to further establish whether this effect is as substantial as this thesis suggests.

5.2 PM deposition effects on crop yield

Particulate matter deposition affects crop photosynthesis rates by directly blocking PAR absorption. Chapter 3 presents the first global analysis of how PM deposition affects wheat, maize, and rice yields. This thesis finds small but significant yield reductions from PM deposition across the world (an average of ~1%), with more sizeable losses (up to 20%) at specific locations on the NCP and IGP. These losses were linked to the total amount of PM deposited, but also strongly determined by the composition of PM. Black carbon (BC) content was found to be the most significant predictor of total crop losses. BC accounted for over 50% of wheat yield losses and one third of rice and maize losses across the simulated area between 2015 and 2020.

Chapter 3 also highlights the dangers of increasing PM emissions, with projections of elevated PM in line with the worst levels already experienced in the

country resulting in average yield losses of 10%. However, whilst PM emissions are projected to rise across the region in coming decades, BC emissions are expected to reduce over this timespan. Given the results in Chapter 3 which highlight the importance of PM composition for yield losses, future PM composition changes may mean that larger PM concentrations coincide with a reduced overall effect on crop yields. In Chapter 4, much more sizeable yield losses are simulated across the IGP for wheat, but smaller losses for maize and rice. This is, however, a more artificial analysis than the simulations in Chapter 3, where meteorology, PM composition and PM flux vary spatiotemporally. Here, wheat is least impacted, while maize suffers most from PM deposition. As is noted throughout chapters 3 and 4, however, simulated wheat is least able of these three crops to replicate the results observed in reality for varying meteorology – the proxy measure here used to interpret model skill in simulating the effects of PM on crop yield. Further *in vivo* and *in silico* experimentation is required to refine these projections. This thesis suggests substantial crop losses could occur at high PM concentrations, but the effects on different crop species should be verified by field trials to confirm the magnitude of these yield reductions.

Furthermore, in Mina et al., 2018, different crop varieties are seen to respond differently to deposited PM. Whilst a substantial portion of these differences was attributable to relative PM retention rates, it may also have been partially due to differences in how rice varieties respond to PAR reduction. This would impact the scale of the indirect and direct effect of PM simulated here, and *in vivo* experimentation could allow further model refinement to represent this variable.

5.3 How the timing of PM perturbations within a crop development cycle affects yields

Chapters 2 and 3 demonstrated a relationship between the timing of PM perturbations relative to crop development state, and the final impact of these perturbations on cereal crop yield. In both studies, we find that changes in PM occurring during the early reproductive phase of crop development appeared most impactful. This is similar to results in a number of experimental studies investigating the effects of drought and temperature extremes, where the greatest yield losses for wheat were found when perturbations were applied during crop flowering (the early reproductive phase) (Chen et al., 2010; Farooq et al., 2014; Wollenweber et al., 2003). These results

prompted a more systematic investigation of the effect in Chapter 4, with interesting implications for the interpretation of earlier results.

The simulations performed in Chapter 4 indicate that within JULES-crop, PAR reductions during the early reproductive stage appear most impactful for wheat yields, whilst the early vegetative phase is most important for maize and rice yields (see Chapter 4, 4.1). While the timing of PAR reductions appears to have the greatest impact for carbon fixation, and thus crop yields, the difference in magnitude of the effect between different development stages appears to primarily be a function of the length of that development stage. This is, however, not the case for spring wheat, with the shorter development stages being most impactful on a per timestep basis. However, the degree to which this simulated effect is a reality, or merely a model artefact, is unclear. Whilst some evidence in the literature suggests this is a likely outcome (Chen et al., 2010; Farooq et al., 2014; Tsimba et al., 2013; Yang et al., 2020), this is not a well-researched area and requires further *in vivo* experimentation (see 5.4.1 below).

5.4 Future work

5.4.1 Experimental Validation

The differential sensitivity of crop yields to PM perturbations applied at different times throughout their development cycle is a key finding of this thesis, but one which requires further experimental work to validate. Though models are powerful scientific tools, they rely upon a range of assumptions and generalisations to draw conclusions. For example, ERA-5 reanalysis data is used to drive all simulations within this thesis. Whilst this data is best-in-class, and one of the best global high resolution meteorological datasets, it is not perfect. For example, a recent review identified underestimates in the diffuse light fraction in ERA-5 compared to some satellite retrievals (Jiang et al., 2020) over parts of China. There are sparse ground measurement sites within that region to compare to, necessitating the use of substantial infilling by ERA-5 using model data. This is the best available meteorological dataset for studying these areas, and yet substantial errors may yet exist within it. When we consider that a minimum of eight driving variables are obtained from ERA-5 for each simulation presented here, we can see that systematic error may be incorporated into these studies, and could affect their results. Furthermore, the JULES-crop model is based upon single varieties of each crop with a prescribed development cycle – in reality, the length of development stages can vary substantially between crop varieties.

Similarly, real world crops are not planted at fixed planting densities, or with fixed canopy densities, across the entire globe. We assume a fixed proportion of the carbon allocated to the harvestable portion is accounted for by the edible portion of the crop, and that a given fraction is always water to determine a final yield mass, but again, this can vary substantially within varieties of a given crop. Whilst the generalisations used in modelling are essential to ensuring a model can run smoothly and quickly at scale, they do embed a degree of artificiality within any results. The uncertainty generated through these assumptions could be vastly reduced by validating results against a range of *in vivo* examples.

Whilst there is some evidence to demonstrate the differential effects of environmental perturbations within a development cycle, to the best of my knowledge, this has never been explored *in vivo* for PM pollution. Furthermore, very little experimental research has explored the influence of the diffuse light fertilisation effect in crop canopies. To rectify this, a series of experimental studies should be conducted to explore how PM affects crops. Laboratory or field experiments to explore the degree to which diffuse light fertilisation can compensate for PM reductions are critical to further this field of research. This should be done systematically to confirm or refute the simulated findings within this thesis e.g., by directly measuring the effects of airborne PM on the level of PAR which reaches different crop canopies, and using vertical gradients in within-canopy PAR for different PM size distributions and compositions to calculate radiation use efficiency and net photosynthesis at heights corresponding to model levels. Following this model validation, a real-world dose-response relationship could be calculated and incorporated into land surface and crop models. The range of involved factors could then be explored to comprehensively characterise the response of a given crop to airborne PM. This would be compared to the responses simulated in Chapters 2 and 4, and the model further refined to improve its predictive capability.

Similar experiments should be conducted for PM deposition. By accurately measuring the retention of PM on crop leaves following different intensities of rainfall or wind, better understanding could be gained of accumulation to real-world surface morphologies. Through model tuning the skill of the model could then be increased, resulting in more accurate simulations of future pollution events and their impacts. This could broaden the model's use cases, making it useful for policy makers in understanding the impacts of pollution events on future food supply.

Ease of model interpretation could then be further aided through model development work. For example, enabling the output of each model variable (e.g., TPAR) for the crop development cycle could enable detailed comparison between model performance per timestep with *in vivo* crop development state.

5.4.2 Leaf Structure

To further understand the effects of PM deposition, and how these might be mitigated, a better understanding of leaf structure is required. In trees, it has been observed that differing leaf surfaces have widely varying capacities to retain deposited PM on their leaves (Lu et al., 2019). This is attributable to the differing leaf micro-morphology, with the levels of wax and surface grooves (Dzierżanowski et al., 2011) of such species contributing to the strength of particle adhesion. Leaves with deep grooves are most conducive for trapping PM_{2.5} and PM₁₀, whereas hairy leaves better retain large PM_{>10}, i.e., particles with diameters above 10 µm (Yan et al., 2022). Stomatal density (Mina et al., 2017) plays a similar role to surface ridges, trapping and retaining deposited PM particles. These enhance surface roughness, increasing the surface area over which adhesive forces can apply (Li et al., 2021). Furthermore, smaller PM particles may be absorbed into stomata and enter the leaf interior (Shahid et al., 2021). Absorbed heavy metal particles, or other toxic PM components, may cause damage to crops, even at low concentrations, exacerbating the detrimental effects of PM deposition. Better understanding of the relationships between leaf surface structures and PM accumulation and retention is therefore vital to understand the effects of future PM on crops. Exploring the effects of leaf structures in common wheat, maize, and rice varieties and their effects on particle capture could substantially improve model accuracy.

5.4.3 Wet Deposition to Crop Leaves

The dry deposition of PM which is discussed throughout Chapters 3 and 4 is not the only mechanism of PM deposition. Wet deposition occurs when pollutants are dissolved or carried within droplets of precipitation which fall to earth. Small PM particles dominate in wet deposition due to their role in cloud formation (Slanina, J., 2004). Fine PM particles between 0.1-2 µm in diameter are efficient cloud condensation nuclei (CCN) (Deshler, T., 2003), and are deposited to the surface during precipitation events alongside any other airborne particles. This process accounts for approximately half of all PM deposition to the earth's surface, depending on ambient meteorology (Slanina, J., 2004). Including a full parameterisation of this process in JULES-Crop simulations

would change the deposition flux experienced by different crop varieties and species, influencing the total reduction in PAR interception which crops are projected to experience. For example, by including wet deposition we may discover that at the end of any given precipitation event, the PM removal is lower than would be expected as newly wet deposited PM has replaced the PM which has been washed off. This could mean that PM accumulates more readily and is harder to remove from leaf surfaces, meaning that my simulations in Chapters 3 and 4 underestimate the effect of PM deposition on crop yield. Including this effect would create a more holistic and accurate model for the effects of PM on crop yields.

5.4.4 Particulate Matter and Ozone

PM is not the only prolific air pollutant which limits crop yields. Tropospheric ozone (O_3) is an important phytotoxin, and is predicted to increase across the globe throughout this century (Meul et al., 2018), presenting a clear threat to global food supply. Although the inclusion of ozone impacts was beyond the scope of this thesis, the interaction between PM and O_3 is potentially important in understanding the future evolution of this pollutant, and its effects on crops.

Whilst airborne, PM reduces the total level of medium wavelength shortwave radiation (including PAR) at the planet's surface through a combination of back-scattering and direct absorption of these wavelengths of light which is re-emitted as infra-red (see 1.3.1). Sunlight is vital to the formation of tropospheric O_3 , and so, reduced light at the surface reduces the ground-level O_3 formation rate. Recent evidence has also emerged that PM may in addition suppress O_3 formation in a similar manner to NO_x . NO_x is a catalyst for O_3 formation, but can act non-linearly to terminate photochemical reaction chains. NO_2 in particular can react reversibly with organic radicals to generate SOA. This sequestration of the radicals involved in O_3 formation can effectively suppress O_3 formation rates, with the recent global pandemic acting as a large-scale natural experiment demonstrating this phenomena. Numerous studies found that the NO_x decreases and reduced light interception caused by lower PM concentrations during COVID lockdowns drove increasing O_3 concentrations worldwide (Sicard et al., 2020). Aerosol-inhibition of O_3 formation is believed to occur in a similar manner (Ivatt, Evans, and Lewis, 2022). The uptake of HO_2 on particulate matter provides an alternative destination for these radical particles, preventing O_3 formation. It is estimated that tropospheric O_3 formation could be enhanced by as much as 30% over

the NCP and IGP if aerosol-inhibition were removed. Therefore, whilst PM reductions are critical for human and non-human animals, NO_x reductions must be simultaneous to prevent increasing tropospheric ozone pollution that could offset any and all benefits of reduced PM.

Furthermore, only a small number of studies have investigated the combined effects of ozone and deposited PM on crop yields. Deposited PM can block adaxial stomata and reduce gas exchange, limiting photosynthetic rate (Rahul et al, 2014, Moradi et al, 2017, Lee et al, 2017). However, in ozone polluted areas, this may in fact be a net positive for yields as the deposited PM may limit the stomatal absorption of ozone into the internal space of leaves (Sharma et al 2021), and so reduce the lifetime damage to a crop. To further complicate this interaction, partial blockage could prevent closure of stomata regardless of external conditions, which could instead enhance ozone uptake. It should also be noted that the blockage of stomata effectively insulates leaves, increasing internal leaf temperatures and potentially increasing temperatures above the optimum for photosynthesis. In northern India, for example, wheat is currently grown in locations where air temperatures approach the maximum viable wheat-growing temperature (Dubey et al., 2020). The detrimental combination of reduced stomatal conductance and increased leaf temperature may therefore outweigh the benefits of reduced ozone damage, reducing yield, when in another cooler region this may not be the case. Modelling studies could be used to indicate the scale of these interactions, and further experimental studies exploring how deposited PM affects ozone uptake for important crop species could be used to validate results. It is vital to understand how these pollutants may affect the global food supply over the 21st Century.

5. 5 Summary

Overall, I find that PM pollution could play an understudied role in contributing to crop yield losses across the world. The scale of crop losses would vary greatly by region, but this thesis suggests that over the NCP and IGP, current primary emissions and secondary formation of particles likely reduce cereal yields by circa 5%, with specific locations suffering yield losses up to 15%. PM dry deposition is found to contribute to an average global cereal yield reduction of circa 1%, but some highly polluted locations experience losses of up to 20%. Prior to this work, the contribution of PM deposition to yield losses had not been quantified or explored, leaving a potentially important gap in our understanding of how air pollution affects regional food supply.

Whilst substantial assumptions and generalisations are necessarily included within the modelling herein, this work does suggest that further *in vivo* research is essential to clarify the scope of damage caused by this pollutant.

Existing literature explores the effects of airborne PM in more detail, but the nature of this effect remains somewhat controversial. In line with existing literature, we find that under certain conditions airborne PM can positively influence cereal crop yields. If the properties of the PM do not substantially reduce total PAR whilst increasing the diffuse fraction, this leads to the diffuse light fertilisation effect, i.e., the enhancement of photosynthesis rates due to increased PAR penetration increased radiation use efficiency which outweighs the effects of lower total top-of-canopy PAR. However, over the present day NCP, I find the effects of airborne PM to be negative for maize production, and from the work contained in Chapter 4, it is likely that these impacts are additive with those of deposited PM.

One important factor for this effect is the black carbon (BC) content of bulk PM. Novelty, I identify that deposited BC is likely significantly more detrimental to crop yields than other PM components, and I have highlighted the importance of controlling this particular PM component for future crop yields. This is especially important over India, where BC contributes over 50% of the yield reductions attributed to bulk aerosol, and where the current research literature suggests that PM concentrations are likely to increase over the coming decades. If they continue to increase in an uncontrolled manner, i.e., with BC remaining a major component, then average yield losses from PM deposition alone could be as high as 10% for some crops, causing local economic damage and disrupting regional food exports.

The work contained within this thesis identifies crucial areas where further research is required, and provides novel modelling tools to conduct some of this work. Overall, the thesis highlights the potential extent of PM impacts on crop yields, and highlights areas for further research that would confirm or negate these conclusions. Particularly, this thesis highlights the potential impacts of highly light absorbing BC emissions – already known to contribute to climate change and now suggested to also have a direct effect on our food supply. Whilst further research is required to validate and confirm the findings of this thesis, it is hoped that the work herein highlights the importance of this line of inquiry, and provides tools which will aid in future investigation.

References

- Aas, W., Mortier, A., Bowersox, V., Cherian, R., Faluvegi, G., Fagerli, H., Hand, J., Klimont, Z., Galy-Lacaux, C., Lehmann, C. M. B., Myhre, C. L., Myhre, G., Olivié, D., Sato, K., Quaas, J., Rao, P. S. P., Schulz, M., Shindell, D., Skeie, R. B., ... Xu, X. (2019). Global and regional trends of atmospheric sulfur. *Scientific Reports* 2019 9:1, 9(1), 1–11. <https://doi.org/10.1038/s41598-018-37304-0>
- Abril, G. A., Wannaz, E. D., Mateos, A. C., & Pignata, M. L. (2014). Biomonitoring of airborne particulate matter emitted from a cement plant and comparison with dispersion modelling results. *Atmospheric Environment*, 82, 154–163. <https://doi.org/10.1016/J.ATMOENV.2013.10.020>
- Acevedo, M., Pixley, K., Zinyengere, N., Meng, S., Tufan, H., Cichy, K., Bizikova, L., Isaacs, K., Ghezzi-Kopel, K., & Porciello, J. (2020). A scoping review of adoption of climate-resilient crops by small-scale producers in low- and middle-income countries. *Nature Plants*, 6(10), 1231–1241. <https://doi.org/10.1038/s41477-020-00783-z>
- AgMIP. (n.d.). *Meerut, India - Impacts Explorer*. Retrieved October 1, 2022, from <https://agmip-ie.wenr.wur.nl/indo-gangetic-basin1>
- Aliyu, Y. A., & Botai, J. O. (2018). Reviewing the local and global implications of air pollution trends in Zaria, northern Nigeria. *Urban Climate*. <https://doi.org/10.1016/j.uclim.2018.08.008>
- Alton, P. B. (2008). Reduced carbon sequestration in terrestrial ecosystems under overcast skies compared to clear skies. *Agricultural and Forest Meteorology*, 148(10), 1641–1653. <https://doi.org/10.1016/J.AGRFORMET.2008.05.014>
- An, Z., Huang, R. J., Zhang, R., Tie, X., Li, G., Cao, J., ... Ji, Y. (2019). Severe haze in northern China: A synergy of anthropogenic emissions and atmospheric processes. *Proceedings of the National Academy of Sciences of the United States of America*. <https://doi.org/10.1073/pnas.1900125116>
- Ansari, K., Ramachandran, S., Aerosol characteristics over Indo-Gangetic Plain from ground-based AERONET and MERRA-2/CAMS model simulations, *Atmospheric*

Environment, Volume 293, 2023, 119434, ISSN 1352-2310,
<https://doi.org/10.1016/j.atmosenv.2022.119434>.

- Auffhammer, M., Ramanathan, V., & Vincent, J. R. (2006). Integrated model shows that atmospheric brown clouds and greenhouse gases have reduced rice harvests in India. *Proceedings of the National Academy of Sciences of the United States of America*, 103(52), 19668–19672. <https://doi.org/10.1073/pnas.0609584104>
- Aziz, R. M., Zabawi, A. G. M., Azdawiyah, A. T. S., & Fazlyzan, A. (2019). Effects of haze on net photosynthetic rate, stomatal conductance, and yield of Malaysian rice (*Oryza sativa* L.) varieties. *Journal of Agricultural and Food Science*, 47(1), 1–13.
- Bergin, M. H., Greenwald, R., Xu, J., Berta, Y., & Chameides, W. L. (2001). Influence of aerosol dry deposition on photosynthetically active radiation available to plants: A case study in the Yangtze Delta Region of China. *Geophysical Research Letters*, 28(18), 3605–3608. <https://doi.org/10.1029/2001GL013461>
- Best, M. J., Pryor, M., Clark, D. B., Rooney, G. G., Essery, R. L. H., Ménard, C. B., ... Harding, R. J. (2011). The Joint UK Land Environment Simulator (JULES), model description – Part 1: Energy and water fluxes. *Geoscientific Model Development*, 4(3), 677–699. <https://doi.org/10.5194/gmd-4-677-2011>
- Boman, J., Shaltout, A. A., Abozied, A. M., & Hassan, S. K. (2013). On the elemental composition of PM 2.5 in central Cairo, Egypt. *X-Ray Spectrometry*, 42(4), 276–283. <https://doi.org/10.1002/xrs.2464>
- Bora, S., Ceccacci, I., Delgado, C., & Townsend, R. (2011). *WORLD DEVELOPMENT REPORT 2011*. World Bank, Washington, DC.
- Briggs, N. L., & Long, C. M. (2016). Critical review of black carbon and elemental carbon source apportionment in Europe and the United States. *Atmospheric Environment*, 144, 409–427. <https://doi.org/10.1016/j.atmosenv.2016.09.002>
- Brodersen, C. R., & Vogelmann, T. C. (2010). Do changes in light direction affect absorption profiles in leaves? *Functional Plant Biology*, 37(5), 403. <https://doi.org/10.1071/FP09262>
- Browse, J., Carslaw, K. S., Arnold, S. R., Pringle, K., & Boucher, O. (2012). The scavenging processes controlling the seasonal cycle in Arctic sulphate and black carbon aerosol. *Atmospheric Chemistry and Physics*. <https://doi.org/10.5194/acp-12-6775-2012>

- Burney, J., & Ramanathan, V. (2014). Recent climate and air pollution impacts on Indian agriculture. *Proceedings of the National Academy of Sciences of the United States of America*, 111(46), 16319–16324. <https://doi.org/10.1073/pnas.1317275111>
- Cape, J. N., Coyle, M., & Dumitrean, P. (2012). The atmospheric lifetime of black carbon. *Atmospheric Environment*, 59, 256–263. <https://doi.org/10.1016/J.ATMOSENV.2012.05.030>
- Chameides, W. L., Yu, H., Liu, S. C., Bergin, M., Zhou, X., Mearns, L., ... Giorgi, F. (1999). Case study of the effects of atmospheric aerosols and regional haze on agriculture: An opportunity to enhance crop yields in China through emission controls? *Proceedings of the National Academy of Sciences of the United States of America*. <https://doi.org/10.1073/pnas.96.24.13626>
- Chandran Govindaraju, V. G. R., & Tang, C. F. (2013). The dynamic links between CO₂ emissions, economic growth and coal consumption in China and India. *Applied Energy*, 104, 310–318. <https://doi.org/10.1016/J.APENERGY.2012.10.042>
- Chapter 5 - Nucleation and Diffusional Growth, Editor(s): Judith A. Curry, Peter J. Webster, International Geophysics, Academic Press, Volume 65, 1999, Pages 129-158, ISSN 0074-6142, ISBN 9780121995706, [https://doi.org/10.1016/S0074-6142\(99\)80027-8](https://doi.org/10.1016/S0074-6142(99)80027-8). (<https://www.sciencedirect.com/science/article/pii/S0074614299800278>)
- Charlson, R. J., Schwartz, S. E., Hales, J. M., Cess, R. D., Coakley, J. A., Hansen, J. E., & Hofmann, D. J. (1992). Climate forcing by anthropogenic aerosols. *Science*. <https://doi.org/10.1126/science.255.5043.4232009>
- Chen, L., Liu, C., Zhang, L., Zou, R., & Zhang, Z. (2017). Variation in Tree Species Ability to Capture and Retain Airborne Fine Particulate Matter (PM_{2.5}). *Scientific Reports*, 7(1), 3206. <https://doi.org/10.1038/s41598-017-03360-1>
- Chen, Y., Zhi, G., Feng, Y., Liu, D., Zhang, G., Li, J., Sheng, G., & Fu, J. (2009). Measurements of black and organic carbon emission factors for household coal combustion in china: implication for emission reduction. *Environmental Science & Technology*, 43(24), 9495–9500. <https://doi.org/10.1021/es9021766>
- Chen, Y. (2010). Ecophysiological responses of winter wheat seedling to aerosol wet deposition of Xi'an area, China. *Journal of Environmental Sciences*, 22(11), 1786–1791. [https://doi.org/10.1016/S1001-0742\(09\)60320-X](https://doi.org/10.1016/S1001-0742(09)60320-X)

- Chen, W., Tong, D., Zhang, S., Dan, M., Zhang, X., & Zhao, H. (2015). Temporal variability of atmospheric particulate matter and chemical composition during a growing season at an agricultural site in northeastern China. *Journal of Environmental Sciences*, 38, 133–141. <https://doi.org/10.1016/J.JES.2015.05.023>
- Chen, W. W., Tong, D. Q., Dan, M., Zhang, S. C., Zhang, X. L., & Pan, Y. P. (2017). Typical atmospheric haze during crop harvest season in northeastern China: A case in the Changchun region. *Journal of Environmental Sciences*, 54, 101–113. <https://doi.org/10.1016/J.JES.2016.03.031>
- Cheng, Z., Wang, S., Jiang, J., Fu, Q., Chen, C., Xu, B., ... Hao, J. (2013). Long-term trend of haze pollution and impact of particulate matter in the Yangtze River Delta, China. *Environmental Pollution*. <https://doi.org/10.1016/j.envpol.2013.06.043>
- Cheng, S. J., Bohrer, G., Steiner, A. L., Hollinger, D. Y., Suyker, A., Phillips, R. P., & Nadelhoffer, K. J. (2015). Variations in the influence of diffuse light on gross primary productivity in temperate ecosystems. *Agricultural and Forest Meteorology*, 201, 98–110. <https://doi.org/10.1016/J.AGRFORMET.2014.11.002>
- China: Air Quality Standards | Transport Policy. (2013). Retrieved May 18, 2020, from <https://www.transportpolicy.net/standard/china-air-quality-standards/>
- Chinese Statistical Yearbook. (2008). [Http://www.Stats.Gov.Cn/Tjsj/Ndsj/2008/Indexeh.Htm](http://www.stats.gov.cn/tjsj/ndsj/2008/indexeh.htm).
- Clark, D. B., Mercado, L. M., Sitch, S., Jones, C. D., Gedney, N., Best, M. J., ... Cox, P. M. (2011). The Joint UK Land Environment Simulator (JULES), Model description – Part 2: Carbon fluxes and vegetation. *Geoscientific Model Development Discussions*, 4(1), 641–688. <https://doi.org/10.5194/gmdd-4-641-2011>
- Cohan, D. S., Xu, J., Greenwald, R., Bergin, M. H., & Chameides, W. L. (2002). Impact of atmospheric aerosol light scattering and absorption on terrestrial net primary productivity. *Global Biogeochemical Cycles*, 16(4), 37-1-37–12. <https://doi.org/10.1029/2001GB001441>
- Collins, J. W., Lamarque, J. F., Schulz, M., Boucher, O., Eyring, V., Hegglin, I. M., Maycock, A., Myhre, G., Prather, M., Shindell, D., & Smith, J. S. (2017). AerChemMIP: Quantifying the effects of chemistry and aerosols in CMIP6. *Geoscientific Model Development*, 10(2), 585–607. <https://doi.org/10.5194/gmd-10-585-2017>

- Copernicus Climate Change Service (C3S). (2017). ERA5: Fifth generation of ECMWF atmospheric reanalyses of the global climate . Copernicus Climate Change Service Climate Data Store (CDS).
- Costabile, F., Barnaba, F., Angelini, F., and Gobbi, G. P.: Identification of key aerosol populations through their size and composition resolved spectral scattering and absorption, *Atmos. Chem. Phys.*, 13, 2455–2470, <https://doi.org/10.5194/acp-13-2455-2013>, 2013.
- Crop Explorer - World Agricultural Production (WAP) Briefs - China and Taiwan. (n.d.). Retrieved February 25, 2022, from https://ipad.fas.usda.gov/cropexplorer/pecad_stories.aspx?regionid=che&ftype=prodbriefs
- Dalirian, M., Ylisirniö, A., Buchholz, A., Schlesinger, D., Ström, J., Virtanen, A., & Riipinen, I. (2018). Cloud droplet activation of black carbon particles coated with organic compounds of varying solubility. *Atmospheric Chemistry and Physics*. <https://doi.org/10.5194/acp-18-12477-2018>
- Das, M., Das, A., Ghosh, S., Sarkar, R., & Saha, S. (2021). Spatio-temporal concentration of atmospheric particulate matter (PM_{2.5}) during pandemic: A study on most polluted cities of Indo-Gangetic Plain. *Urban Climate*. <https://doi.org/10.1016/j.uclim.2020.100758>
- Deshmukh, D. K., Deb, M. K., & Mkoma, S. L. (2013). Size distribution and seasonal variation of size-segregated particulate matter in the ambient air of Raipur city, India. *Air Quality, Atmosphere & Health*, 6(1), 259–276. <https://doi.org/10.1007/s11869-011-0169-9>
- Din, S. A. M., Yahya, N. N.-H. N., & Abdullah, A. (2013). Fine particulates matter (pm_{2.5}) from coal-fired power plant in manjung and its health impacts. *Procedia - Social and Behavioral Sciences*, 85, 92–99. <https://doi.org/10.1016/J.SBSPRO.2013.08.341>
- Dhillon, B. S., Kataria, P., & Dhillon, P. K. (2010). National food security vis-à-vis sustainability of agriculture in high crop productivity regions. *CURRENT SCIENCE* (Vol. 98).
- Dubey, R., Pathak, H., Chakrabarti, B., Singh, S., Gupta, D. K., & Harit, R. C. (2020). Impact of terminal heat stress on wheat yield in India and options for adaptation. *Agricultural Systems*, 181, 102826. <https://doi.org/10.1016/j.agsy.2020.102826>
- Dzierzanowski, K., Popek, R., Gawrońska, H., Saebø, A., & Gawroński, S. W. (2011). Deposition of particulate matter of different size fractions on leaf surfaces and in waxes

of urban forest species. *International Journal of Phytoremediation*, 13(10), 1037–1046.
<https://doi.org/10.1080/15226514.2011.552929>

FAOSTAT. (n.d.-a). Retrieved April 2, 2020, from
<http://www.fao.org/giews/countrybrief/country.jsp?code=CHN>

FAOSTAT. (n.d.-b). FAOSTAT Crop Database. Retrieved November 30, 2018, from
<http://www.fao.org/faostat/en/#data/QC>

Farooq, M., Hussain, M., & Siddique, K. H. M. (2014). Drought Stress in Wheat during Flowering and Grain-filling Periods. *Critical Reviews in Plant Sciences*.
<https://doi.org/10.1080/07352689.2014.875291>

Gao, Y., Zhang, M., Liu, Z., Wang, L., Wang, P., Xia, X., ... Zhu, L. (2015). Modeling the feedback between aerosol and meteorological variables in the atmospheric boundary layer during a severe fog-haze event over the North China Plain. *Atmospheric Chemistry and Physics*. <https://doi.org/10.5194/acp-15-4279-2015>

Global Modeling and Assimilation Office (GMAO) (2015), tavg1_2d_adg_Nx: MERRA-2 3D IAU State, Meteorology Instantaneous 3-hourly (p-coord, 0.625x0.5L42), version 5.12.4, Greenbelt, MD, USA: Goddard Space Flight Center Distributed Active Archive Center (GSFC DAAC), Accessed 19-01-2022 at doi: 10.5067/HM00OHQBHKTP.

Gorai, A. K., Tchounwou, P. B., Biswal, S. S., & Tuluri, F. (2018). Spatio-temporal variation of particulate matter (pm2.5) concentrations and its health impacts in a mega city, delhi in india. *Environmental Health Insights*, 12. <https://doi.org/10.1177/1178630218792861>

Government of the Republic of China, Ministry of Energy (2012). *Energy Statistics*. China Statistical Yearbook.

Greenwald, R., Bergin, M. H., Xu, J., Cohan, D., Hoogenboom, G., & Chameides, W. L. (2006). The influence of aerosols on crop production: A study using the CERES crop model. *Agricultural Systems*. <https://doi.org/10.1016/j.agsy.2005.10.004>

Gu, L., Baldocchi, D., Verma, S. B., Black, T. A., Vesala, T., Falge, E. M., & Dowty, P. R. (2002). Advantages of diffuse radiation for terrestrial ecosystem productivity. *Journal of Geophysical Research Atmospheres*, 107(5–6), ACL 2-1.
<https://doi.org/10.1029/2001jd001242>

- Guenther, A. (2002). The contribution of reactive carbon emissions from vegetation to the carbon balance of terrestrial ecosystems. *Chemosphere*. [https://doi.org/10.1016/S0045-6535\(02\)00384-3](https://doi.org/10.1016/S0045-6535(02)00384-3)
- Gugamsetty, B., Wei, H., Liu, C.-N., Awasthi, A., Hsu, S.-C., Tsai, C.-J., Roam, G.-D., Wu, Y.-C., & Chen, C.-F. (2012). Source characterization and apportionment of pm10, pm2.5 and pm0.1 by using positive matrix factorization. *Aerosol and Air Quality Research*, *12*(4), 476–491. <https://doi.org/10.4209/aaqr.2012.04.0084>
- Gui, X., Wang, L., Su, X., Yi, X., Chen, X., Yao, R., & Wang, S. (2021). Environmental factors modulate the diffuse fertilization effect on gross primary productivity across Chinese ecosystems. *Science of the Total Environment*, *793*, 148443. <https://doi.org/10.1016/j.scitotenv.2021.148443>
- Guo, S., Hu, M., Zamora, M. L., Peng, J., Shang, D., Zheng, J., ... Zhang, R. (2014). Elucidating severe urban haze formation in China. *Proceedings of the National Academy of Sciences of the United States of America*, *111*(49), 17373–17378. <https://doi.org/10.1073/pnas.1419604111>
- Gupta, R. K., Majumdar, D., Trivedi, J. V., & Bhanarkar, A. D. (2012). Particulate matter and elemental emissions from a cement kiln. *Fuel Processing Technology*, *104*, 343–351. <https://doi.org/10.1016/J.FUPROC.2012.06.007>
- Hammer, M. S., van Donkelaar, A., Li, C., Lyapustin, A., Sayer, A. M., Hsu, N. C., Levy, R. C., Garay, M. J., Kalashnikova, O. v., Kahn, R. A., Brauer, M., Apte, J. S., Henze, D. K., Zhang, L., Zhang, Q., Ford, B., Pierce, J. R., & Martin, R. v. (2020). Global estimates and long-term trends of fine particulate matter concentrations (1998-2018). *Environmental Science and Technology*, *54*(13), 7879–7890. <https://doi.org/10.1021/acs.est.0c01764>
- Han, D., Wiesmeier, M., Conant, R. T., Kühnel, A., Sun, Z., Kögel-Knabner, I., ... Ouyang, Z. (2018). Large soil organic carbon increase due to improved agronomic management in the North China Plain from 1980s to 2010s. *Global Change Biology*, *24*(3), 987–1000. <https://doi.org/10.1111/gcb.13898>
- Han, D., Shen, H., Duan, W., & Chen, L. (2020). A review on particulate matter removal capacity by urban forests at different scales. *Urban Forestry & Urban Greening*, *48*, 126565. <https://doi.org/10.1016/J.UFUG.2019.126565>

- Han, S., Bian, H., Zhang, Y., Wu, J., Wang, Y., Tie, X., ... Yao, Q. (2012). Effect of aerosols on visibility and radiation in spring 2009 in Tianjin, China. *Aerosol and Air Quality Research*. <https://doi.org/10.4209/aaqr.2011.05.0073>
- Hatami, Z., Rezvani Moghaddam, P., Rashki, A., Nasiri Mahallati, M., & Habibi Khaniani, B. (2017). Effects of dust deposition from two major dust source regions of Iran on wheat (*Triticum aestivum* L.) production. *International Journal of Environmental Studies*, 1–10. <https://doi.org/10.1080/00207233.2017.1356630>
- Hatami, Z., Rezvani Moghaddam, P., Rashki, A., Mahallati, M. N., & Habibi Khaniani, B. (2018). Effects of desert dust on yield and yield components of cowpea (*Vigna unguiculata* L.). *Archives of Agronomy and Soil Science*, 64(10), 1446–1458. <https://doi.org/10.1080/03650340.2018.1440081>
- Haywood, J. M., & Shine, K. P. (1997). Multi-spectral calculations of the direct radiative forcing of tropospheric sulphate and soot aerosols using a column model. *Quarterly Journal of the Royal Meteorological Society*, 123(543), 1907–1930. <https://doi.org/10.1002/qj.49712354307>
- Hemming, S., Dueck, T., Janse, J., & van Noort, F. (2008). The effect of diffuse light on crops. *Acta Horticulturae*, 801, 1293–1300. <https://doi.org/10.17660/ActaHortic.2008.801.158>
- Hersbach, H., Bell, B., Berrisford, P., Biavati, G., Horányi, A., Muñoz Sabater, J., Nicolas, J., Peubey, C., Radu, R., Rozum, I., Schepers, D., Simmons, A., Soci, C., Dee, D., Thépaut, J-N. (2018): ERA5 hourly data on single levels from 1959 to present. Copernicus Climate Change Service (C3S) Climate Data Store (CDS). (Accessed on 14-APR-2021), [10.24381/cds.adbb2d47](https://doi.org/10.24381/cds.adbb2d47)
- Hirano, T., Kiyota, M., & Aiga, I. (1995). Physical effects of dust on leaf physiology of cucumber and kidney bean plants. *Environmental Pollution (Barking, Essex : 1987)*, 89(3), 255–261. <http://www.ncbi.nlm.nih.gov/pubmed/15091515>
- Horowitz, L. W., & Jacob, D. J. (1999). Global impact of fossil fuel combustion on atmospheric NO_x. *Journal of Geophysical Research: Atmospheres*, 104(D19), 23823–23840. <https://doi.org/10.1029/1999JD900205>
- Hu, X., & Zimmer, Y. (2013). China's Corn Production.
- Hua, S., Tian, H., Wang, K., Zhu, C., Gao, J., Ma, Y., Xue, Y., Wang, Y., Duan, S., & Zhou, J. (2016). Atmospheric emission inventory of hazardous air pollutants from China's cement

- plants: Temporal trends, spatial variation characteristics and scenario projections. *Atmospheric Environment*, 128, 1–9. <https://doi.org/10.1016/J.ATMOSENV.2015.12.056>
- Hua, Y., Cheng, Z., Wang, S., Jiang, J., Chen, D., Cai, S., ... Yu, J. (2015). Characteristics and source apportionment of PM_{2.5} during a fall heavy haze episode in the Yangtze River Delta of China. *Atmospheric Environment*. <https://doi.org/10.1016/j.atmosenv.2015.03.046>
- Huang, K., Wang, S., Zhou, L., Wang, H., Zhang, J., Yan, J., ... Shi, P. (2014). Impacts of diffuse radiation on light use efficiency across terrestrial ecosystems based on eddy covariance observation in China. *PLoS ONE*, 9(11), e110988. <https://doi.org/10.1371/journal.pone.0110988>
- Huang, R.-J., Zhang, Y., Bozzetti, C., Ho, K.-F., Cao, J.-J., Han, Y., ... Prévôt, A. S. H. (2014). High secondary aerosol contribution to particulate pollution during haze events in China. *Nature*, 514(7521), 218–222. <https://doi.org/10.1038/nature13774>
- Huang, T., Zhu, X., Zhong, Q., Yun, X., Meng, W., Li, B., Ma, J., Zeng, E. Y., & Tao, S. (2017). Spatial and temporal trends in global emissions of nitrogen oxides from 1960 to 2014. *Environmental Science and Technology*, 51(14), 7992–8000. https://doi.org/10.1021/ACS.EST.7B02235/ASSET/IMAGES/LARGE/ES-2017-02235U_0004.JPEG
- Huang, Y., Shen, H., Chen, Y., Zhong, Q., Chen, H., Wang, R., Shen, G., Liu, J., Li, B., & Tao, S. (2015). Global organic carbon emissions from primary sources from 1960 to 2009. *Atmospheric Environment*, 122, 505–512. <https://doi.org/10.1016/J.ATMOSENV.2015.10.017>
- Hueglin, C., Gehrig, R., Baltensperger, U., Gysel, M., Monn, C., & Vonmont, H. (2005). Chemical characterisation of PM_{2.5}, PM₁₀ and coarse particles at urban, near-city and rural sites in Switzerland. *Atmospheric Environment*, 39(4), 637–651. <https://doi.org/10.1016/J.ATMOSENV.2004.10.027>
- Indian Council of Agricultural Research (ICAR). (n.d.). Agriculture in India: A brief.
- Iizumi, T., Kim, W., & Nishimori, M. (2019). Modeling the global sowing and harvesting windows of major crops around the year 2000. *Journal of Advances in Modeling Earth Systems*, 11(1), 99–112. <https://doi.org/10.1029/2018MS001477>

- India: yield of rice 1991-2021 | Statista. Retrieved June 16, 2022, from <https://www.statista.com/statistics/764299/india-yield-of-rice/>
- IPCC - Pereira, J., Revi, A., Rose, S., Sanchez-Rodriguez, R., Lisa Schipper Sweden, E. F., Schmidt, D. U., ... Stringer, L. (2022). IPCC Summary for policy makers. <https://doi.org/10.1017/9781009325844.001>
- Jain, S., Aggarwal, P., Sharma, P., & Kumar, P. (2016). Vehicular exhaust emissions under current and alternative future policy measures for megacity Delhi, India. *Journal of Transport and Health*, 3(3), 404–412. <https://doi.org/10.1016/j.jth.2016.06.005>
- Jat, R., & Gurjar, B. R. (2021). Contribution of different source sectors and source regions of Indo-Gangetic Plain in India to PM_{2.5} pollution and its short-term health impacts during peak polluted winter. *Atmospheric Pollution Research*, 12(4), 89–100. <https://doi.org/10.1016/J.APR.2021.02.016>
- Jiang, Y., Lu, L., Ferro, A. R., & Ahmadi, G. (2018). Analyzing wind cleaning process on the accumulated dust on solar photovoltaic (PV) modules on flat surfaces. *Solar Energy*. <https://doi.org/10.1016/j.solener.2017.08.083>
- Jun Xu, Feng Han, Mingzhu Li, Zhongzhi Zhang, Du Xiaohui, Peng Wei, On the opposite seasonality of MODIS AOD and surface PM_{2.5} over the Northern China plain, *Atmospheric Environment*, Volume 215, 2019, 116909, ISSN 1352-2310, <https://doi.org/10.1016/j.atmosenv.2019.116909>.
- Just, A. C., Wright, R. O., Schwartz, J., Coull, B. A., Baccarelli, A. A., Tellez-Rojo, M. M., ... Kloog, I. (2015). Using high-resolution satellite aerosol optical depth to estimate daily pm_{2.5} geographical distribution in Mexico City. *Environmental Science & Technology*, 49(14), 8576–8584. <https://doi.org/10.1021/acs.est.5b00859>
- Kanniah, K. D., Beringer, J., North, P., & Hutley, L. (2012). Control of atmospheric particles on diffuse radiation and terrestrial plant productivity: A review. *Progress in Physical Geography*. <https://doi.org/10.1177/0309133311434244>
- Karanasiou, A., Querol, X., Alastuey, A., Perez, N., Pey, J., Perrino, C., ... Pascal, M. (2014). Particulate matter and gaseous pollutants in the Mediterranean Basin: Results from the MED-PARTICLES project. *Science of the Total Environment*. <https://doi.org/10.1016/j.scitotenv.2014.04.096>

- Kaur, R., & Pandey, P. (2021). Air pollution, climate change, and human health in Indian cities: a brief review. In *Frontiers in Sustainable Cities* (Vol. 3, p. 77). Frontiers Media S.A. <https://doi.org/10.3389/frsc.2021.705131>
- Kecorius, S., Ma, N., Teich, M., van Pinxteren, D., Zhang, S., Größ, J., Spindler, G., Müller, K., Iinuma, Y., Hu, M., Herrmann, H., & Wiedensohler, A. (2017). Influence of biomass burning on mixing state of sub-micron aerosol particles in the North China Plain. *Atmospheric Environment*. <https://doi.org/10.1016/j.atmosenv.2017.05.023>
- Khan, J. Z., Sun, L., Tian, Y., Dai, Q., Hu, T., & Feng, Y. (2021). Size distribution of ambient particulate matter and its constituent chemical species involving saccharides during early summer in a Chinese megacity. *Frontiers in Environmental Science*, 9, 85. <https://doi.org/10.3389/fenvs.2021.659329>
- Khan, S., Anwar, S., Ashraf, M. Y., Khaliq, B., Sun, M., Hussain, S., Gao, Z. Q., Noor, H., & Alam, S. (2019). Mechanisms and adaptation strategies to improve heat tolerance in rice. A review. In *Plants* (Vol. 8, Issue 11). MDPI AG. <https://doi.org/10.3390/plants8110508>
- Kim, K. H., Kabir, E., & Kabir, S. (2015). A review on the human health impact of airborne particulate matter. In *Environment International* (Vol. 74, pp. 136–143). Elsevier Ltd. <https://doi.org/10.1016/j.envint.2014.10.005>
- Kimball, B. A., Boote, K. J., Hatfield, J. L., Ahuja, L. R., Stockle, C., Archontoulis, S., ... Williams, K. (2019). Simulation of maize evapotranspiration: An inter-comparison among 29 maize models. *Agricultural and Forest Meteorology*. <https://doi.org/10.1016/j.agrformet.2019.02.037>
- Kimball, B. A., Boote, K. J., Hatfield, J. L., Ahuja, L. R., Stockle, C., Archontoulis, S., Baron, C., Basso, B., Bertuzzi, P., Constantin, J., Deryng, D., Dumont, B., Durand, J. L., Ewert, F., Gaiser, T., Gayler, S., Hoffmann, M. P., Jiang, Q., Kim, S. H., ... Williams, K. (2019). Simulation of maize evapotranspiration: An inter-comparison among 29 maize models. *Agricultural and Forest Meteorology*. <https://doi.org/10.1016/j.agrformet.2019.02.037>
- Kirchstetter, T. W., Novakov, T., & Hobbs, P. V. (2004). Evidence that the spectral dependence of light absorption by aerosols is affected by organic carbon. *Journal of Geophysical Research: Atmospheres*, 109(D21), n/a-n/a. <https://doi.org/10.1029/2004JD004999>

- Klimont, Z., Kupiainen, K., Heyes, C., Purohit, P., Cofala, J., Rafaj, P., Borcken-Kleefeld, J., & Schöpp, W. (2017). Global anthropogenic emissions of particulate matter including black carbon. *Atmospheric Chemistry and Physics*, 17(14), 8681–8723.
<https://doi.org/10.5194/acp-17-8681-2017>
- Kuhlmann, J., & Quaas, J. (2010). How can aerosols affect the Asian summer monsoon? Assessment during three consecutive pre-monsoon seasons from CALIPSO satellite data. *Atmospheric Chemistry and Physics*. <https://doi.org/10.5194/acp-10-4673-2010>
- Langner, J., Rodhe, H., Crutzen, P. J., & Zimmermann, P. (1992). Anthropogenic influence on the distribution of tropospheric sulphate aerosol. *Nature*.
<https://doi.org/10.1038/359712a0>
- LEI, H.-M., & YANG, D.-W. (2009). Seasonal and interannual variations in carbon dioxide exchange over a cropland in the North China Plain. *Global Change Biology*, 16(11), no-no. <https://doi.org/10.1111/j.1365-2486.2009.02136.x>
- Li, H., Jiang, D., Wollenweber, B., Dai, T., & Cao, W. (2010). Effects of shading on morphology, physiology, and grain yield of winter wheat. *European Journal of Agronomy*, 33(4), 267–275. <https://doi.org/10.1016/J.EJA.2010.07.002>
- Li, J. (2009). Production, breeding and process of maize in china. In *handbook of maize: its biology* (pp. 563–576). Springer New York. https://doi.org/10.1007/978-0-387-79418-1_28
- Li, J., Cao, L., Gao, W., He, L., Yan, Y., He, Y., Pan, Y., Ji, D., Liu, Z., and Wang, Y.: Seasonal variations in the highly time-resolved aerosol composition, sources, and chemical processes of background submicron particles in the North China Plain, *Atmos. Chem. Phys.*, 21, 4521–4539, <https://doi.org/10.5194/acp-21-4521-2021>, 2021.
- Li, K., Jacob, D. J., Liao, H., Shen, L., Zhang, Q., & Bates, K. H. (2019). Anthropogenic drivers of 2013–2017 trends in summer surface ozone in China. *Proceedings of the National Academy of Sciences of the United States of America*.
<https://doi.org/10.1073/pnas.1812168116>
- Li, T., & Yang, Q. (2015). Advantages of diffuse light for horticultural production and perspectives for further research. *Frontiers in Plant Science*, 6, 704.
<https://doi.org/10.3389/fpls.2015.00704>

- Li, X., Mauzerall, D. L., & Bergin, M. H. (2020). Global reduction of solar power generation efficiency due to aerosols and panel soiling. *Nature-Sustainability*.
- Lindberg, S. E., & Garten, C. T. (1988). Sources of sulphur in forest canopy throughfall. *Nature*. <https://doi.org/10.1038/336148a0>
- Lindberg, S. E., & Garten, C. T. (1988). Sources of sulphur in forest canopy throughfall. *Nature*. <https://doi.org/10.1038/336148a0>
- Liu, J., Tong, D., Zheng, Y., Cheng, J., Qin, X., Shi, Q., Yan, L., Lei, Y., & Zhang, Q. (2021). Carbon and air pollutant emissions from China's cement industry 1990-2015: Trends, evolution of technologies, and drivers. *Atmospheric Chemistry and Physics*, 21(3), 1627–1647. <https://doi.org/10.5194/acp-21-1627-2021>
- Liu, Y., Wang, E., Yang, X., & Wang, J. (2010). Contributions of climatic and crop varietal changes to crop production in the North China Plain, since 1980s. *Global Change Biology*, 16(8), 2287–2299. <https://doi.org/10.1111/j.1365-2486.2009.02077.x>
- Lohmann, U., Feichter, J., Chuang, C. C., & Penner, J. E. (1999). Prediction of the number of cloud droplets in the ECHAM GCM. *Journal of Geophysical Research Atmospheres*, 104(D8), 9169–9198. <https://doi.org/10.1029/1999JD900046>
- Lu, C., & Fan, L. (2013). Winter wheat yield potentials and yield gaps in the North China Plain. *Field Crops Research*, 143, 98–105. <https://doi.org/10.1016/j.fcr.2012.09.015>
- López-Caravaca, A., Crespo, J., Galindo, N., Yubero, E., Castañer, R., & Nicolás Aguilera, J. F. (2022). Characterization of aerosol absorption properties and PM1 at a mountain site located in the southeast of the Iberian Peninsula. *Atmospheric Pollution Research*, 13(10), 101559. <https://doi.org/10.1016/j.apr.2022.101559>
- Lu, X., Zhang, S., Xing, J., Wang, Y., Chen, W., Ding, D., Wu, Y., Wang, S., Duan, L., & Hao, J. (2020). Progress of air pollution control in china and its challenges and opportunities in the ecological civilization era. *Engineering*, 6(12), 1423–1431. <https://doi.org/10.1016/J.ENG.2020.03.014>
- Lu, Z., Zhang, Q., & Streets, D. G. (2011). Sulfur dioxide and primary carbonaceous aerosol emissions in China and India, 1996–2010. *Atmospheric Chemistry and Physics*, 11(18), 9839–9864. <https://doi.org/10.5194/acp-11-9839-2011>

- Malm, W. C., Day, D. E., Kreidenweis, S. M., Collett, J. L., & Lee, T. (2003). Humidity-dependent optical properties of fine particles during the Big Bend Regional Aerosol and Visibility Observational Study. *Journal of Geophysical Research: Atmospheres*. <https://doi.org/10.1029/2002jd002998>
- Mathison, C., Challinor, A. J., Deva, C., Falloon, P., Garrigues, S., Moulin, S., Williams, K., & Wiltshire, A. (2021). Implementation of sequential cropping into JULESv5.2 land-surface model. *Geoscientific Model Development*, 14(1), 437–471. <https://doi.org/10.5194/gmd-14-437-2021>
- Mcgrath, J. M., Betzelberger, A. M., Wang, S., Shook, E., Zhu, X., & Long, S. P. (2015). An analysis of ozone damage to historical maize and soybean yields in the United States. <https://doi.org/10.1073/pnas.1509777112>
- Mehmood, T., Ahmad, I., Bibi, S., Mustafa, B., & Ali, I. (2020). Insight into monsoon for shaping the air quality of Islamabad, Pakistan: Comparing the magnitude of health risk associated with PM 10 and PM 2.5 exposure. *Journal of the Air & Waste Management Association (1995)*, 70(12), 1340–1355. <https://doi.org/10.1080/10962247.2020.1813838>
- Meng, Q., Sun, Q., Chen, X., Cui, Z., Yue, S., Zhang, F., & Romheld, V., (2012). Alternative cropping systems for sustainable water and nitrogen use in the North China Plain. *Agriculture, Ecosystems and Environment*. <https://doi.org/10.1016/j.agee.2011.10.015>
- Mercado, L. M., Bellouin, N., Sitch, S., Boucher, O., Huntingford, C., Wild, M., & Cox, P. M. (2009). Impact of changes in diffuse radiation on the global land carbon sink. *Nature*, 458(7241), 1014–1017. <https://doi.org/10.1038/nature07949>
- Meul, S., Langematz, U., Kröger, P., Oberländer-Hayn, S., & Jöckel, P. (2018). Future changes in the stratosphere-to-troposphere ozone mass flux and the contribution from climate change and ozone recovery. *Atmospheric Chemistry and Physics*, 18(10), 7721–7738. <https://doi.org/10.5194/acp-18-7721-2018>
- Mills, G., Pleijel, H., Malley, C. S., Sinha, B., Cooper, O. R., Schultz, M. G., ... Xu, X. (2018). Tropospheric ozone assessment report: Present-day tropospheric ozone distribution and trends relevant to vegetation. *Elementa*. <https://doi.org/10.1525/elementa.302>
- Mina, U., Chandrashekara, T. K., Kumar, S. N., Meena, M. C., Yadav, S., Tiwari, S., Singh, D., Kumar, P., & Kumar, R. (2018). Impact of particulate matter on basmati rice varieties

grown in Indo-Gangetic Plains of India: Growth, biochemical, physiological and yield attributes. *Atmospheric Environment*, 188, 174–184.

<https://doi.org/10.1016/j.atmosenv.2018.06.015>

Mina, U., Singh, B. C. (2013). Agricultural production and air quality: an emerging challenge. *International Journal of Environmental Science: Development and Monitoring*, 4(2231), 81–88.

Mogno, C., Palmer, P. I., Knote, C., Yao, F., & Wallington, T. J. (2021). Seasonal distribution and drivers of surface fine particulate matter and organic aerosol over the Indo-Gangetic Plain. *Atmos. Chem. Phys*, 21, 10881–10909. <https://doi.org/10.5194/acp-21-10881-2021>

Moosmüller, H., Chakrabarty, R. K., & Arnott, W. P. (2009, July 1). Aerosol light absorption and its measurement: A review. *Journal of Quantitative Spectroscopy and Radiative Transfer*. Pergamon. <https://doi.org/10.1016/j.jqsrt.2009.02.035>

Motai, A., Yamazaki, M., Muramatsu, N., Watanabe, M., & Izuta, T. (2018). Submicron ammonium sulfate particles deposited on leaf surfaces of a leafy vegetable (*Komatsuna*, *Brassica rapa* L. var. *perviridis*) are taken up by leaf and enhance nocturnal leaf conductance. *Atmospheric Environment*, 187, 155–162.
<https://doi.org/10.1016/J.ATMOSENV.2018.05.064>

Nagpure, A. S., Gurjar, B. R., Kumar, V., & Kumar, P. (2016). Estimation of exhaust and non-exhaust gaseous, particulate matter and air toxics emissions from on-road vehicles in Delhi. *Atmospheric Environment*, 127, 118–124.
<https://doi.org/10.1016/J.ATMOSENV.2015.12.026>

Naidoo, G., & Chirkoot, D. (2004). The effects of coal dust on photosynthetic performance of the mangrove, *Avicennia marina* in Richards Bay, South Africa. *Environmental Pollution*, 127(3), 359–366. <https://doi.org/10.1016/J.ENVPOL.2003.08.018>

Nguy-Robertson, A., Suyker, A., & Xiao, X. (2015). Modeling gross primary production of maize and soybean croplands using light quality, temperature, water stress, and phenology. *Agricultural and Forest Meteorology*, 213, 160–172.
<https://doi.org/10.1016/J.AGRFORMET.2015.04.008>

Niyogi, D., Chang, H., Saxena, V. K., Holt, T., Alapaty, K., Booker, F., Chen, F., Davis, K. J., Holben, B., Matsui, T., Meyers, T., Oechel, W. C., Pielke, R. A., Wells, R., Wilson, K., &

- Xue, Y. (2004). Direct observations of the effects of aerosol loading on net ecosystem CO₂ exchanges over different landscapes. *Geophysical Research Letters*, 31(20), L20506. <https://doi.org/10.1029/2004GL020915>
- OECD-FAO *Agricultural Outlook 2021-2030*. (2021). OECD. <https://doi.org/10.1787/19428846-en>
- Ojha, N., Sharma, A., Kumar, M., Girach, I., Ansari, T. U., Sharma, S. K., ... Gunthe, S. S. (2020). On the widespread enhancement in fine particulate matter across the Indo-Gangetic Plain towards winter. *Scientific Reports*, 10(1), 1–9. <https://doi.org/10.1038/s41598-020-62710-8>
- Oliver, R. J., Mercado, L. M., Clark, D. B., Huntingford, C., Taylor, C. M., Vidale, P. L., McGuire, P. C., Todt, M., Folwell, S., Shamsudheen Semeena, V., and Medlyn, B. E.: Improved representation of plant physiology in the JULES-vn5.6 land surface model: photosynthesis, stomatal conductance and thermal acclimation, *Geosci. Model Dev.*, 15, 5567–5592, <https://doi.org/10.5194/gmd-15-5567-2022>, 2022.
- Ortega, A. M., Day, D. A., Cubison, M. J., Brune, W. H., Bon, D., de Gouw, J. A., & Jimenez, J. L. (2013). Secondary organic aerosol formation and primary organic aerosol oxidation from biomass-burning smoke in a flow reactor during FLAME-3. *Atmospheric Chemistry and Physics*. <https://doi.org/10.5194/acp-13-11551-2013>
- Osborne, T., Gornall, J., Hooker, J., Williams, K., Wiltshire, A., Betts, R., & Wheeler, T. (2015). JULES-crop: a parametrisation of crops in the Joint UK Land Environment Simulator. *Geoscientific Model Development*, 8(4), 1139–1155. <https://doi.org/10.5194/gmd-8-1139-2015>
- Peltier, R. E., Cromar, K. R., Ma, Y., Fan, Z. H., & Lippmann, M. (2011). Spatial and seasonal distribution of aerosol chemical components in New York City: (2) Road dust and other tracers of traffic-generated air pollution. *Journal of Exposure Science and Environmental Epidemiology*. <https://doi.org/10.1038/jes.2011.15>
- Peng, J., Hu, M., Guo, S., Du, Z., Zheng, J., Shang, D., Zamora, M. L., Zeng, L., Shao, M., Wu, Y. S., Zheng, J., Wang, Y., Glen, C. R., Collins, D. R., Molina, M. J., & Zhang, R. (2016). Markedly enhanced absorption and direct radiative forcing of black carbon under polluted urban environments. *Proceedings of the National Academy of Sciences of the United States of America*. <https://doi.org/10.1073/pnas.1602310113>

- Penner, J. E., & J.E. (1994). Carbonaceous aerosols influencing atmospheric radiation: Black and organic carbon. <https://doi.org/10.2172/10118242>
- Petzold, A., Ogren, J. A., Fiebig, M., Laj, P., Li, S. M., Baltensperger, U., Holzer-Popp, T., Kinne, S., Pappalardo, G., Sugimoto, N., Wehli, C., Wiedensohler, A., & Zhang, X. Y. (2013). Recommendations for reporting black carbon measurements. *Atmospheric Chemistry and Physics*. <https://doi.org/10.5194/acp-13-8365-2013>
- Pinto, M. A. B., Parfitt, J. M. B., Timm, L. C., Faria, L. C., Concenço, G., Stumpf, L., & Nörenberg, B. G. (2020). Sprinkler irrigation in lowland rice: Crop yield and its components as a function of water availability in different phenological phases. *Field Crops Research*, 248, 107714. <https://doi.org/10.1016/j.fcr.2020.107714>
- Pommier, Matthieu, et al. "Impact of regional climate change and future emission scenarios on surface O₃ and PM_{2.5} over India." *Atmospheric Chemistry and Physics* 18.1 (2018): 103-127.
- Pradhan, G. P., Prasad, P. V. V., Fritz, A. K., Kirkham, M. B., & Gill, B. S. (2012). Effects of drought and high temperature stress on synthetic hexaploid wheat. *Functional Plant Biology*. <https://doi.org/10.1071/FP11245>
- Proctor, J., Hsiang, S., Burney, J., Burke, M., & Schlenker, W. (2018). Estimating global agricultural effects of geoengineering using volcanic eruptions. *Nature*, 560(7719), 480–483. <https://doi.org/10.1038/s41586-018-0417-3>
- Qin, G., Niu, Z., Yu, J., Li, Z., Ma, J., & Xiang, P. (2021). Soil heavy metal pollution and food safety in China: Effects, sources and removing technology. In *Chemosphere* (Vol. 267, p. 129205). Elsevier Ltd. <https://doi.org/10.1016/j.chemosphere.2020.129205>
- Qin, K., Zou, J., Guo, J., Lu, M., Bilal, M., Zhang, K., ... Zhang, Y. (2018). Estimating PM₁ concentrations from MODIS over Yangtze River Delta of China during 2014–2017. *Atmospheric Environment*, 195, 149–158. <https://doi.org/10.1016/J.ATMOENV.2018.09.054>
- Qin, Weihua, et al. "Variation, sources and historical trend of black carbon in Beijing, China based on ground observation and MERRA-2 reanalysis data." *Environmental Pollution* 245 (2019): 853-863.
- Qu, W., Wang, J., Zhang, X., Sheng, L., & Wang, W. (2016). Opposite seasonality of the aerosol optical depth and the surface particulate matter concentration over the north

- China Plain. *Atmospheric Environment*, 127, 90–99.
<https://doi.org/10.1016/j.atmosenv.2015.11.061>
- Quan, J., Zhang, Q., He, H., Liu, J., Huang, M., & Jin, H. (2011). Analysis of the formation of fog and haze in North China Plain (NCP). *Atmospheric Chemistry and Physics*.
<https://doi.org/10.5194/acp-11-8205-2011>
- Raes, F., Dingenen, R. van, Vignati, E. h gatfohat., Wilson, J., Putaud, J.-P., Seinfeld, J. H., & Adams, P. (2000). Formation and cycling of aerosols in the global troposphere. *Atmospheric Environment*, 34(25), 4215–4240. [https://doi.org/10.1016/S1352-2310\(00\)00239-9](https://doi.org/10.1016/S1352-2310(00)00239-9)
- Ramanathan, V., Crutzen, P. J., Kiehl, J. T., & Rosenfeld, D. (2001). Atmosphere: Aerosols, climate, and the hydrological cycle. *Science*. <https://doi.org/10.1126/science.1064034>
- Rap, A., Scott, C. E., Reddington, C. L., Mercado, L., Ellis, R. J., Garraway, S., ... Spracklen, D. V. (2018). Enhanced global primary production by biogenic aerosol via diffuse radiation fertilization. *Nature Geoscience*, 11(9), 640–644. <https://doi.org/10.1038/s41561-018-0208-3>
- Rap, A., Spracklen, D. V., Mercado, L., Reddington, C. L., Haywood, J. M., Ellis, R. J., ... Butt, N. (2015). Fires increase Amazon Forest productivity through increases in diffuse radiation. *Geophysical Research Letters*, 42(11), 4654–4662.
<https://doi.org/10.1002/2015GL063719>
- Ray, D. K., West, P. C., Clark, M., Gerber, J. S., Prishchepov, A. v., & Chatterjee, S. (2019). Climate change has likely already affected global food production. *PLOS ONE*, 14(5), e0217148. <https://doi.org/10.1371/journal.pone.0217148>
- Raza, A., Razzaq, A., Mehmood, S., Zou, X., Zhang, X., Lv, Y., & Xu, J. (2019). Impact of Climate Change on Crops Adaptation and Strategies to Tackle Its Outcome: A Review. *Plants*, 8(2), 34. <https://doi.org/10.3390/plants8020034>
- Roderick, M. L., Farquhar, G. D., Berry, S. L., & Noble, I. R. (2001). On the direct effect of clouds and atmospheric particles on the productivity and structure of vegetation. *Oecologia*, 129(1), 21–30. <https://doi.org/10.1007/s004420100760>
- Sacks, W. J., Deryng, D., Foley, J. A., & Ramankutty, N. (2010). Crop planting dates: An analysis of global patterns. *Global Ecology and Biogeography*.
<https://doi.org/10.1111/j.1466-8238.2010.00551.x>

- Saxena, P., Sonwani, S., & Kulshrestha, U. C. (2017). Impact of tropospheric ozone and particulate matter on plant health. In *Sustaining Future Food Security in Changing Environments*.
- Schiferl, L. D., & Heald, C. L. (2018). Particulate matter air pollution may offset ozone damage to global crop production. *Atmospheric Chemistry and Physics*, 18(8), 5953–5966. <https://doi.org/10.5194/acp-18-5953-2018>
- Schuhmacher, M., Domingo, J. L., & Garreta, J. (2004). Pollutants emitted by a cement plant: health risks for the population living in the neighborhood. *Environmental Research*, 95(2), 198–206. <https://doi.org/10.1016/J.ENVRES.2003.08.011>
- Sembhi, H., Wooster, M., Zhang, T., Sharma, S., Singh, N., Agarwal, S., Boesch, H., Gupta, S., Misra, A., Tripathi, S., N. (2020). Post-monsoon air quality degradation across Northern India: assessing the impact of policy-related shifts in timing and amount of crop residue burnt. *Environmental Research Letters*, 15 104067. <https://doi.org/10.1088/1748-9326/aba714>
- Sen, A., Ahammed, Y. N., Banerjee, T., Chatterjee, A., Choudhuri, A. K., Das, T., ... Vachaspati, C. V. (2016). Spatial variability in ambient atmospheric fine and coarse mode aerosols over Indo-Gangetic plains, India, and adjoining oceans during the onset of summer monsoons, 2014. *Atmospheric Pollution Research*, 7(3), 521–532. <https://doi.org/10.1016/J.APR.2016.01.001>
- Sen, A., Abdelmaksoud, A. S., Nazeer Ahammed, Y., Alghamdi, M. ., Banerjee, T., Bhat, M. A., Chatterjee, A., Choudhuri, A. K., Das, T., Dhir, A., Dhyani, P. P., Gadi, R., Ghosh, S., Kumar, K., Khan, A. H., Khoder, M., Maharaj Kumari, K., Kuniyal, J. C., Kumar, M., ... Mandal, T. K. (2017). Variations in particulate matter over Indo-Gangetic Plains and Indo-Himalayan Range during four field campaigns in winter monsoon and summer monsoon: Role of pollution pathways. *Atmospheric Environment*, 154, 200–224. <https://doi.org/10.1016/J.ATMOSENV.2016.12.054>
- Shen, J., Liu, X., Zhang, Y., Fangmeier, A., Goulding, K., & Zhang, F. (2011). Atmospheric ammonia and particulate ammonium from agricultural sources in the North China Plain. *Atmospheric Environment*. <https://doi.org/10.1016/j.atmosenv.2011.02.031>
- Sharma, R., Sachdeva, K., & Sharma, A. R. (2021). Assessment of synergistic impact of ambient surface ozone and fine particulate matter on experimentally grown wheat crop.

Asian Journal of Atmospheric Environment, 15(1), 1–14.
<https://doi.org/10.5572/AJAE.2020.080>

Shen, R., Schäfer, K., Schnelle-Kreis, J., Shao, L., Norra, S., Kramar, U., ... Emeis, S. (2018). Seasonal variability and source distribution of haze particles from a continuous one-year study in Beijing. *Atmospheric Pollution Research*.
<https://doi.org/10.1016/j.apr.2017.12.013>

Shi, J., Feng, Y., Ren, L., Lu, X., Zhong, Y., Han, X., & Ning, P. (2021). Mass Concentration, Chemical Composition, and Source Characteristics of PM_{2.5} in a Plateau Slope City in Southwest China. *Atmosphere*, 12(5), 611. <https://doi.org/10.3390/atmos12050611>

Shihuang, Z., & Kaijian, H. (2010). Maize and the formal agricultural research and development system: evolution, challenges, and alternatives. In *Seeds and Synergies* (pp. 13–28). Practical Action Publishing. <https://doi.org/10.3362/9781780440330.002>

Shim, Sungbo, et al. "Regional features of long-term exposure to pm_{2.5} air quality over Asia under SSP scenarios based on CMIP6 models." *International journal of environmental research and public health* 18.13 (2021): 6817. Singh, B. P., Singh, D., Kumar, K., & Jain, V. K. (2021). Study of seasonal variation of PM_{2.5} concentration associated with meteorological parameters at residential sites in Delhi, India. In *Journal of Atmospheric Chemistry* (Vol. 78, Issue 3, pp. 161–176). Springer Science and Business Media B.V. <https://doi.org/10.1007/s10874-021-09419-8>

Sicard, P., de Marco, A., Agathokleous, E., Feng, Z., Xu, X., Paoletti, E., Rodriguez, J. J. D., & Calatayud, V. (2020). Amplified ozone pollution in cities during the COVID-19 lockdown. *Science of the Total Environment*, 735, 139542.
<https://doi.org/10.1016/j.scitotenv.2020.139542>

Singh, G. K., Choudhary, V., Rajeev, P., Paul, D., & Gupta, T. (2021). Understanding the origin of carbonaceous aerosols during periods of extensive biomass burning in northern India. *Environmental Pollution*, 270, 116082. <https://doi.org/10.1016/j.envpol.2020.116082>

Slanina, J. (2004). Air pollution from energy production and use. In *Encyclopedia of Energy*.
<https://doi.org/10.1016/b0-12-176480-x/00387-9>

Slater, J., Coe, H., Mcfiggans, G., Tonttila, J., & Romakkaniemi, S. (2022). The effect of BC on aerosol-boundary layer feedback: Potential implications for urban pollution episodes.

Atmospheric Chemistry and Physics, 22(4), 2937–2953. <https://doi.org/10.5194/acp-22-2937-2022>

Song, C., Ma, C., Zhang, Y., Wang, T., Wu, L., Wang, P., Liu, Y., Li, Q., Zhang, J., Dai, Q., Zou, C., Sun, L., & Mao, H. (2018). Heavy-duty diesel vehicles dominate vehicle emissions in a tunnel study in northern China. *Science of the Total Environment*. <https://doi.org/10.1016/j.scitotenv.2018.04.387>

Song, X., Hao, Y., & Zhu, X. (2019). Air pollutant emissions from vehicles and their abatement scenarios: a case study of Chengdu-Chongqing urban agglomeration, China. *Sustainability*, 11(22), 6503. <https://doi.org/10.3390/su11226503>

Sreenivas, A., & Bhosale, K. (2013). Black and Dirty: The real challenges facing India's coal sector. *Prayas Energy Group*.

Sridevi V, & Chellamuthu V. (n.d.). *Impact of weather on rice – A review*, 2015

Statista (Accessed 08-08-23), <https://www.statista.com/statistics/690823/china-annual-pm25-particle-levels-beijing/>

Statista (Accessed 11-08-22), <https://www.statista.com/statistics/1183370/china-population-density-by-region-province/>

Steinparzer, M., Schaubmayr, J., Godbold, D., L., Rewald, B. (2023). Particulate matter accumulation by tree foliage is driven by leaf habit types, urbanization- and pollution levels., *Environmental Pollution*, Volume 335, 15 October 2023, 122289. <https://doi.org/10.1016/j.envpol.2023.122289>.

Steckel, J. C., Edenhofer, O., & Jakob, M. (2015). Drivers for the renaissance of coal. *Proceedings of the National Academy of Sciences*. <https://doi.org/10.1073/pnas.1422722112>

Steinfeld, J. I. (2012). Atmospheric chemistry and physics: from air pollution to climate change. *Environment: Science and Policy for Sustainable Development*. <https://doi.org/10.1080/00139157.1999.10544295>

Strada, S., Unger, N., & Yue, X. (2015). Observed aerosol-induced radiative effect on plant productivity in the eastern United States. *Atmospheric Environment*, 122, 463–476. <https://doi.org/10.1016/J.ATMOENV.2015.09.051>

- Sun, D., & Wang, Q. (2018). Linear relationships between photosynthetic rate and photochemical energy expressed by PAR x Fv/Fm. *American Journal of Plant Sciences*, 09(02), 125–138. <https://doi.org/10.4236/ajps.2018.92011>
- Tai, A. P. K., & Val Martin, M. (2017). Impacts of ozone air pollution and temperature extremes on crop yields: Spatial variability, adaptation, and implications for future food security. *Atmospheric Environment*, 169. <https://doi.org/10.1016/j.atmosenv.2017.09.002>
- Tai, A. P. K., Martin, M. V., & Heald, C. L. (2014). Threat to future global food security from climate change and ozone air pollution. July 2–6. <https://doi.org/10.1038/NCLIMATE2317>
- Tang, L., Qu, J., Mi, Z., Bo, X., Chang, X., Anadon, L. D., Wang, S., Xue, X., Li, S., Wang, X., & Zhao, X. (2019). Substantial emission reductions from Chinese power plants after the introduction of ultra-low emissions standards. *Nature Energy* 2019 4:11, 4(11), 929–938. <https://doi.org/10.1038/s41560-019-0468-1>
- Tao, S., Xu, H., Ren, Y., Zhang, W., Meng, W., Yun, X., Yu, X., Li, J., Zhang, Y., Shen, G., Ma, J., Li, B., Cheng, H., Wang, X., & Wan, Y. (2021). Updated global black carbon emissions from 1960 to 2017: Improvements, trends, and drivers. *Environmental Science and Technology*, 55(12), 7869–7879. https://doi.org/10.1021/ACS.EST.1C03117/SUPPL_FILE/ES1C03117_SI_002.XLSX
- Teixeira, E. I., Fischer, G., van Velthuisen, H., Walter, C., & Ewert, F. (2013). Global hot-spots of heat stress on agricultural crops due to climate change. *Agricultural and Forest Meteorology*, 170, 206–215. <https://doi.org/10.1016/J.AGRFORMET.2011.09.002>
- Textor, C., Schulz, M., Guibert, S., Kinne, S., Balkanski, Y., Bauer, S., Berntsen, T., Berglen, T., Boucher, O., Chin, M., Dentener, F., Diehl, T., Easter, R., Feichter, H., Fillmore, D., Ghan, S., Ginoux, P., Gong, S., Grini, A., ... Tie, X. (2006). Analysis and quantification of the diversities of aerosol life cycles within AeroCom. *Atmospheric Chemistry and Physics*, 6(7), 1777–1813. <https://doi.org/10.5194/acp-6-1777-2006>
- Timsina, J. (2012). Review of rice-wheat in IGP- *Advances in Agronomy* (Vol. 117). Elsevier Inc. Retrieved from https://www.academia.edu/9776292/Review_of_rice-wheat_in_IGP-_Advances_in_Agronomy
- Turpin, B. J., & Huntzicker, J. J. (1991). Secondary formation of organic aerosol in the Los Angeles basin: A descriptive analysis of organic and elemental carbon concentrations.

Atmospheric Environment. Part A. General Topics, 25(2), 207–215.
[https://doi.org/10.1016/0960-1686\(91\)90291-E](https://doi.org/10.1016/0960-1686(91)90291-E)

UNICEF. (2021). *Malnutrition in Children - UNICEF DATA*.
<https://data.unicef.org/topic/nutrition/malnutrition/>

USDA, India - Area, Yield and Production, Retrieved June 16, 2022, from
https://ipad.fas.usda.gov/cropexplorer/util/new_get_psd_data.aspx?regionid=sasia

USDA, *FoodData Central*. (n.d.). Retrieved January 7, 2023, from <https://fdc.nal.usda.gov/fdc-app.html#/food-details/169761/nutrients>

van Donkelaar, A., Martin, R. V., Spurr, R. J. D., Drury, E., Remer, L. A., Levy, R. C., & Wang, J. (2013). Optimal estimation for global ground-level fine particulate matter concentrations. *Journal of Geophysical Research: Atmospheres*, 118(11), 5621–5636.
<https://doi.org/10.1002/jgrd.50479>

Vohra, K., Marais, E. A., Suckra, S., Kramer, L., Bloss, W. J., Sahu, R., ... Coheur, P. F. (2021). Long-Term trends in air quality in major cities in the UK and India: A view from space. *Atmospheric Chemistry and Physics*. <https://doi.org/10.5194/acp-21-6275-2021>

Wang, J., Wang, S., Jiang, J., Ding, A., Zheng, M., Zhao, B., Wong, D. C., Zhou, W., Zheng, G., Wang, L., Pleim, J. E., & Hao, J. (2014). Impact of aerosol-meteorology interactions on fine particle pollution during China's severe haze episode in January 2013. *Environmental Research Letters*. <https://doi.org/10.1088/1748-9326/9/9/094002>

Wang, L., Gong, H., Liao, W., & Wang, Z. (2015). Accumulation of particles on the surface of leaves during leaf expansion. *Science of the Total Environment*, 532, 420–434.
<https://doi.org/10.1016/j.scitotenv.2015.06.014>

Wang, X., Tian, G., Yang, D., Zhang, W., Lu, D., & Liu, Z. (2018). Responses of PM_{2.5} pollution to urbanization in China. *Energy Policy*, 123, 602–610.
<https://doi.org/10.1016/J.ENPOL.2018.09.001>

Wang, Y., Li, W., Gao, W., Liu, Z., Tian, S., Shen, R., Ji, D., Wang, S., Wang, L., Tang, G., Song, T., Cheng, M., Wang, G., Gong, Z., Hao, J., & Zhang, Y. (2019). Trends in particulate matter and its chemical compositions in China from 2013–2017. *Science China Earth Sciences*. <https://doi.org/10.1007/s11430-018-9373-1>

- Weerakkody, U., Dover, J. W., Mitchell, P., & Reiling, K. (2018). Evaluating the impact of individual leaf traits on atmospheric particulate matter accumulation using natural and synthetic leaves. *Urban Forestry and Urban Greening*, 30, 98–107.
<https://doi.org/10.1016/j.ufug.2018.01.001>
- WHO. (2015). WHO | Ambient (outdoor) air quality and health. Retrieved from <https://web.archive.org/web/20160104165807/http://www.who.int/mediacentre/factsheets/fs313/en/>
- Wickens, G. E., & Horn, H. S. (1972). The adaptive geometry of trees. *Kew Bulletin*.
<https://doi.org/10.2307/4109478>
- Williams, K., Gornall, J., Harper, A., Wiltshire, A., Hemming, D., Quaife, T., ... Scoby, D. (2017). Evaluation of JULES-crop performance against site observations of irrigated maize from Mead, Nebraska. *Geoscientific Model Development*, 10(3), 1291–1320.
<https://doi.org/10.5194/gmd-10-1291-2017>
- Winiger, P., Andersson, A., Eckhardt, S., Stohl, A., & Gustafsson, O. (2016). The sources of atmospheric black carbon at a European gateway to the Arctic. *Nature Communications*, 7(1), 1–8. <https://doi.org/10.1038/ncomms12776>
- Wolffe, M. C., Wild, O., Long, S. P., & Ashworth, K. (2021). Temporal variability in the impacts of particulate matter on crop yields on the North China Plain. *Science of the Total Environment*. <https://doi.org/10.1016/j.scitotenv.2021.145135>
- Wollenweber, B., Porter, J. R., & Schellberg, J. (2003). Lack of Interaction between Extreme High-Temperature Events at Vegetative and Reproductive Growth Stages in Wheat. *Journal of Agronomy and Crop Science*, 189(3), 142–150.
<https://doi.org/10.1046/j.1439-037X.2003.00025.x>
- Wu, C., Wu, D., & Yu, J. Z. (2018). Quantifying black carbon light absorption enhancement with a novel statistical approach. *Atmospheric Chemistry and Physics*, 18(1), 289–309.
<https://doi.org/10.5194/acp-18-289-2018>
- Wu, R., Fei Liu, Dan Tong, Yixuan Zheng, Yu Lei, Chaopeng Hong, Meng Li, Jun Liu, Bo Zheng, Yu Bo, Xiaoting Chen, Xin Li and Qiang Zhang (2019). Variation in tree species ability to capture and retain airborne fine particulate matter (PM_{2.5}). *Environmental Research Letters* **14**, 094016. DOI 10.1088/1748-9326/ab3bae

- Xie, X., Wang, T., Yue, X., Li, S., Zhuang, B., & Wang, M. (2020). Effects of atmospheric aerosols on terrestrial carbon fluxes and CO₂ concentrations in China. *Atmospheric Research*, 237, 104859. <https://doi.org/10.1016/J.ATMOSRES.2020.104859>
- Xu, J., Bergin, M. H., Yu, X., Liu, G., Zhao, J., Carrico, C. M., & Baumann, K. (2002). Measurement of aerosol chemical, physical and radiative properties in the Yangtze delta region of China. *Atmospheric Environment*, 36(2), 161–173. [https://doi.org/10.1016/S1352-2310\(01\)00455-1](https://doi.org/10.1016/S1352-2310(01)00455-1)
- Xu, X., Yu, X., Mo, L., Xu, Y., Bao, L., & Lun, X. (2019). Atmospheric particulate matter accumulation on trees: A comparison of boles, branches, and leaves. *Journal of Cleaner Production*, 226, 349–356. <https://doi.org/10.1016/j.jclepro.2019.04.072>
- Xu, X., Zhang, Z., Bao, L., Mo, L., Yu, X., Fan, D., & Lun, X. (2017). Influence of rainfall duration and intensity on particulate matter removal from plant leaves. *Science of The Total Environment*, 609, 11–16. <https://doi.org/10.1016/J.SCITOTENV.2017.07.141>
- Yan, G., Liu, J., Zhu, L., Zhai, J., Cong, L., Ma, W., Wang, Y., Wu, Y., & Zhang, Z. (2018). Effectiveness of wetland plants as biofilters for inhalable particles in an urban park. *Journal of Cleaner Production*, 194, 435–443. <https://doi.org/10.1016/j.jclepro.2018.05.168>
- Yang, L., Shen, X., Yang, Q., Liu, J., Wu, W., Li, D., Du, J., Zhang, B., & Fan, S. (2021). Fabrication of biomimetic anisotropic super-hydrophobic surface with rice leaf-like structures by femtosecond laser. *Optical Materials*, 112, 110740. <https://doi.org/10.1016/J.OPTMAT.2020.110740>
- Yang, S., & Chen, B. (2017). Driving forces of particulate matter emissions in China. *Energy Procedia*, 105, 4601–4606. <https://doi.org/10.1016/j.egypro.2017.03.995>
- Yang, S., Duan, F., Ma, Y., Li, H., Ma, T., Zhu, L., ... He, K. (2020). Mixed and intensive haze pollution during the transition period between autumn and winter in Beijing, China. *Science of the Total Environment*. <https://doi.org/10.1016/j.scitotenv.2019.134745>
- Yao, L., Yang, L., Yuan, Q., Yan, C., Dong, C., Meng, C., Sui, X., Yang, F., Lu, Y., & Wang, W. (2016). Sources apportionment of PM_{2.5} in a background site in the North China Plain. *Science of the Total Environment*. <https://doi.org/10.1016/j.scitotenv.2015.09.123>

- Yao, Wenrui, et al. "Can MERRA-2 reanalysis data reproduce the three-dimensional evolution characteristics of a typical dust process in East Asia? A case study of the dust event in May 2017." *Remote Sensing* 12.6 (2020): 902.
- Yin, Z. C., Wang, H. J., & Guo, W. L. (2015). Climatic change features of fog and haze in winter over North China and Huang-Huai Area. *Science China Earth Sciences*, 58(8), 1370–1376. <https://doi.org/10.1007/s11430-015-5089-3>
- Yu, S., Dennis, R. L., Bhave, P. v., & Eder, B. K. (2004). Primary and secondary organic aerosols over the United States: estimates on the basis of observed organic carbon (OC) and elemental carbon (EC), and air quality modeled primary OC/EC ratios. *Atmospheric Environment*, 38(31), 5257–5268. <https://doi.org/10.1016/J.ATMOSENV.2004.02.064>
- Yuan, J., Na, C., Lei, Q., Xiong, M., Guo, J., & Hu, Z. (2018). Coal use for power generation in China. *Resources, Conservation and Recycling*. <https://doi.org/10.1016/j.resconrec.2016.03.021>
- Yue, X., & Unger, N. (2017). Aerosol optical depth thresholds as a tool to assess diffuse radiation fertilization of the land carbon uptake in China. *Atmospheric Chemistry and Physics*, 17(2), 1329–1342. <https://doi.org/10.5194/acp-17-1329-2017>
- Zeng, Y., Cao, Y., Qiao, X., Seyler, B. C., & Tang, Y. (2019). Air pollution reduction in China: Recent success but great challenge for the future. *Science of the Total Environment*. <https://doi.org/10.1016/j.scitotenv.2019.01.262>
- Zhai, S., Jacob, D. J., Wang, X., Shen, L., Li, K., Zhang, Y., Gui, K., Zhao, T., & Liao, H. (2019). Fine particulate matter (PM_{2.5}) trends in China, 2013-2018: separating contributions from anthropogenic emissions and meteorology. *Atmospheric Chemistry and Physics*. <https://doi.org/10.5194/acp-19-11031-2019>
- Zhao, Y., Wang, S., Duan, L., Lei, Y., Cao, P., & Hao, J. (2008). Primary air pollutant emissions of coal-fired power plants in China: Current status and future prediction. *Atmospheric Environment*. <https://doi.org/10.1016/j.atmosenv.2008.08.021>
- Zhang, H., Wang, S., Hao, J., Wang, X., Wang, S., Chai, F., & Li, M. (2016). Air pollution and control action in Beijing. In *Journal of Cleaner Production*. <https://doi.org/10.1016/j.jclepro.2015.04.092>

- Zhang, Y., Zhang, Q., Cheng, Y., Su, H., Kecorius, S., Wang, Z., Wu, Z., Hu, M., Zhu, T., Wiedensohler, A., & He, K. (2016). Measuring the morphology and density of internally mixed black carbon with SP2 and VTDMA: New insight into the absorption enhancement of black carbon in the atmosphere. *Atmospheric Measurement Techniques*. <https://doi.org/10.5194/amt-9-1833-2016>
- Zhang, S., Worrell, E., Crijns-Graus, W., Krol, M., de Bruine, M., Geng, G., Wagner, F., & Cofala, J. (2016). Modeling energy efficiency to improve air quality and health effects of China's cement industry. *Applied Energy*, 184, 574–593. <https://doi.org/10.1016/J.APENERGY.2016.10.030>
- Zhao, L., Wang, W., Hao, T., Qu, W., Sheng, L., Luo, C., ... Zhou, Y. (2020). The autumn haze-fog episode enhanced by the transport of dust aerosols in the Tianjin area. *Atmospheric Environment*. <https://doi.org/10.1016/j.atmosenv.2020.117669>
- Zheng, G., & Li, P. (2019). Resuspension of settled atmospheric particulate matter on plant leaves determined by wind and leaf surface characteristics. *Environmental Science and Pollution Research*. <https://doi.org/10.1007/s11356-019-05241-8>
- Zhou, Li, Chen, X., & Tian, X. (2018). The impact of fine particulate matter (PM_{2.5}) on China's agricultural production from 2001 to 2010. *Journal of Cleaner Production*, 178, 133–141. <https://doi.org/10.1016/J.JCLEPRO.2017.12.204>
- Zhou, Luxi, Schwede, D. B., Wyat Appel, K., Mangiante, M. J., Wong, D. C., Napelenok, S. L., ... Zhang, B. (2019). The impact of air pollutant deposition on solar energy system efficiency: An approach to estimate PV soiling effects with the Community Multiscale Air Quality (CMAQ) model. *Science of The Total Environment*, 651, 456–465. <https://doi.org/10.1016/J.SCITOTENV.2018.09.194>
- Zhou, S., Yan, G., Wu, Y., Zhai, J., Cong, L., & Zhang, Z. (2020). The PM removal process of wetland plant leaves with different rainfall intensities and duration. *Journal of Environmental Management*, 275, 111239. <https://doi.org/10.1016/J.JENVMAN.2020.111239>
- Zhu, Y., Huang, L., Li, J., Ying, Q., Zhang, H., Liu, X., Liao, H., Li, N., Liu, Z., Mao, Y., Fang, H., & Hu, J. (2018). Sources of particulate matter in China: Insights from source apportionment studies published in 1987–2017. *Environment International*, 115, 343–357. <https://doi.org/10.1016/J.ENVINT.2018.03.037>

Zhuang, H., Chan, C. K., Fang, M., & Wexler, A. S. (1999). Size distributions of particulate sulfate, nitrate, and ammonium at a coastal site in Hong Kong. *Atmospheric Environment*, 33(6), 843–853. [https://doi.org/10.1016/S1352-2310\(98\)00305-7](https://doi.org/10.1016/S1352-2310(98)00305-7)

Zia-Khan, S., Spreer, W., Pengnian, Y., Zhao, X., Othmanli, H., He, X., & Müller, J. (2015). Effect of dust deposition on stomatal conductance and leaf temperature of cotton in Northwest China. *Water (Switzerland)*, 7(1), 116–131. <https://doi.org/10.3390/w7010116>